INFORMATION TO USERS

This manuscript has been reproduced from the microfilm master. UMI films the text directly from the original or copy submitted. Thus, some thesis and dissertation copies are in typewriter face, while others may be from any type of computer printer.

The quality of this reproduction is dependent upon the quality of the copy submitted. Broken or indistinct print, colored or poor quality illustrations and photographs, print bleedthrough, substandard margins, and improper alignment can adversely affect reproduction.

In the unlikely event that the author did not send UMI a complete manuscript and there are missing pages, these will be noted. Also, if unauthorized copyright material had to be removed, a note will indicate the deletion.

Oversize materials (e.g., maps, drawings, charts) are reproduced by sectioning the original, beginning at the upper left-hand corner and continuing from left to right in equal sections with small overlaps. Each original is also photographed in one exposure and is included in reduced form at the back of the book.

Photographs included in the original manuscript have been reproduced xerographically in this copy. Higher quality 6" x 9" black and white photographic prints are available for any photographs or illustrations appearing in this copy for an additional charge. Contact UMI directly to order.

UMI®

Bell & Howell Information and Learning
300 North Zeeb Road, Ann Arbor, MI 48106-1346 USA
800-521-0600

MAGMATIC EVOLUTION AND GEOCHEMISTRY OF THE PIEDRAS VERDES DEPOSIT, SONORA, MEXICO.

by

Victor Javier Espinosa Perea

A thesis Submitted to the Faculty of the

DEPARTMENT OF GEOSCIENCES

In Partial Fulfillment of the Requirements for the Degree of

MASTER OF SCIENCE

In the Graduate College

THE UNIVERSITY OF ARIZONA

1999

UMI
300 North Zeeb Road
Ann Arbor, MI 48103

STATEMENT BY AUTHOR

This thesis has been submitted in partial fulfillment of requirements for an advanced degree at the University of Arizona and is deposited in the University Library to be made available to borrowers under rules of the Library.

Brief quotations from this thesis are allowable without special permission, provided that accuarate acknowledgement of source is made. Requests for permission for extended quotation from or reproduction of this manuscript in whole or in part may be granted by the head of the major department or the Dean of the Graduate College when in his or her judgment the proposed use of the material is in the interests of scholarship. In all other instances, however, permission must be obtained from the author.

SIGNED 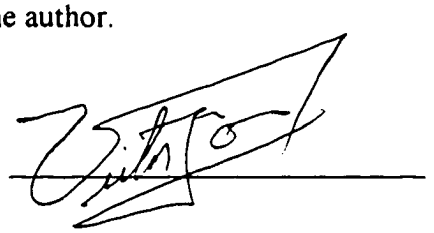

APPROVAL BY THESIS DIRECTOR

This thesis has been approved on the date shown below:

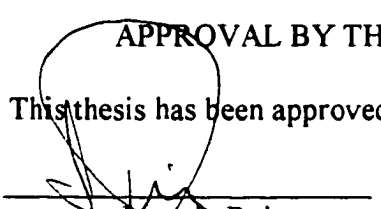

Joaquin Ruiz
Department Head
Geosciences

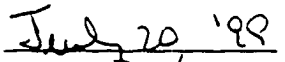

Date

ACKNOWLEDGEMENTS

I am indebted to Phelps Dodge Mining Company for providing the necessary support to conduct my studies at the University of Arizona. I am especially grateful to Gary Heinemeyer and Marty Wiggins for their confidence and patience throughout this project. I wish to thank Dr. Joaquin Ruiz for giving me advice, and research freedom. I also thank Dr Spencer Titley, who contributed with important ideas and suggestions, and Tom McCandless, who contributed with interesting ideas and performed Re-Os analyses on molybdenite and sulfide samples. This work benefited from critical reviews by Mark Thoman and Lukas Zurcher. Finally, thanks to Sergio Castro for his support in the ore minerals petrography.

For Natalia Maria and Javier Alberto with love

TABLE OF CONTENTS

LIST OF FIGURES

LIST OF TABLES

ABSTRACT

Piedras Verdes is a supergene-enriched porphyry-copper deposit. It contains 290 Mt at a total copper grade of 0.37%. The average thickness of the chalcocite blanket is 110 m. It is 400-500 m wide in a north-south direction and approximately 4 km long. The oxide-sulfide interface ranges from 80 m to 340 m in depth. The country rocks are a Triassic-Jurassic or Paleozoic meta-sedimentary sequence and a Tertiary intrusive porphyry suite.

Geochemical studies define six principal intrusive phases of volcanic arc affinity, from quartz monzodiorite to granodiorite in composition. The first magmatic event at Piedras Verdes, was the emplacement of the Sinaloa-Sonora batholith at 67.3 ± 1.4 Ma. This was followed by the emplacement of quartz monzodiorite, "tall" biotite granodiorite, quartz-feldspar and biotite-hornblende granodiorite porphyries, fractionated from a less evolved magma than the preceding batholith. The latest magmatic activity at Piedras Verdes originated andesitic dikes (48.4 ± 1.2 Ma).

Mineragraphic studies indicate three mineralizing pulses. A first pulse, related to emplacement of the batholith and the quartz monzodiorite, produced skarns. The second event was associated with the "tall" biotite granodiorite porphyry, introducing sulfides. The third pulse, related to the quartz-feldspar porphyry introduced quartz-molybdenite-chalcopyrite veins.

Neodymium isotopic analyses, indicate that the four main intrusive phases at Piedras Verdes were formed by a mixture of primitive and crustal materials. Re-Os

isotopic analyses on sulfides yield no considerable amount of Re. It is assumed that the sulfides suffered Re loss during alteration after primary mineralization.

INTRODUCTION

The Piedras Verdes porphyry-copper system is 21 km north-northwest of the town of Alamos, in southern Sonora, Mexico (Fig 1). Piedras Verdes has an exploration history dating back to 1909-1920. Drilling, geological and geophysical studies were realized by Cominco in1969, Minera Trion in 1975, and AZCO Inc in 1991-1995. The regional geology has not been extensively studied. Published work on the region of Piedras Verdes include those of Robert E. King (1939) who provided the first reconnaissance- level map, covering an area limited by Tonichi to the North, Empalme to the West, Alamos to the South and Minaca to the East; a Master's thesis on the Alamos Mining District by A.Vazquez Perez (1975) who presented a geologic description and mineral resource of the Alamos district. An additional description of the geology of the Alamos Mining District was published by the Consejo de Recursos Minerales de Mexico (Cardenas Vargas J. ed. 1992). Isotopic age determination for the batholithic rocks in Sonora-Sinaloa have been made by Damon et al. (1962-1983). Publications of the Piedras Verdes deposit include those of Pearce (1910), and Dreir and Braun (1994). From 1996 to1998, Minera Phelps Dodge Mexico, extended the geologic mapping and core drilling within and around the known mineralized zone. The exploration effort provided a better understanding of the geology and an allowed for the generation of a more detailed evolutionary model of the PiedrasVerdes deposit.

This study integrates geology, alteration and mineralization facts acquired sofar,

and presents new reults from geochemical studies performed on the intrusive phases at Piedras Verdes and Re-Os isotopic data obtained from sulfide (pyrite, chalcopyrite and molybdenite) veins, collected from drill-core samples.

Based on this information interpretations of the chronology of magmatic events, as well as a possible age and mixing model of crustal versus mantle influences for the metals of the deposit, are given.

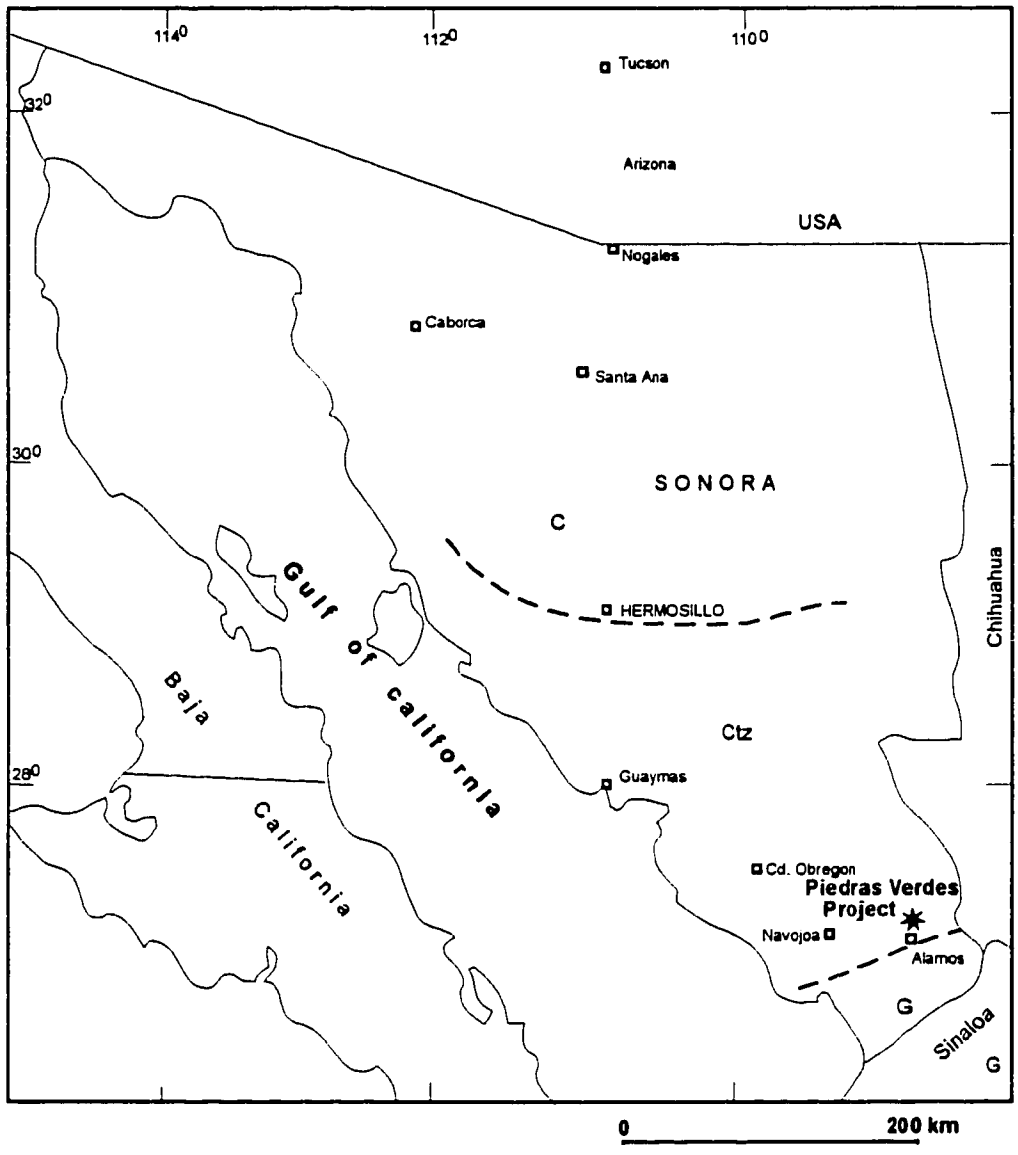

Fig. 1 . Piedras Verdes Project location map. Dashed lines represent tecnostratigraphic terranes approximate limits. Caborca terrane (C), Cortez terrane (Ctz) and Guerrero terrane (G).

REGIONAL GEOLOGY

The Piedras Verdes project is within the limits of the southernmost part of the late Tertiary Basin and Range Province with the valley and ridges subprovince of the Sierra Madre Occidental Tertiary volcanic sequence. In the Piedras Verdes region, exposed rocks range in age from Paleozoic (?) or Triassic-Jurassic to recent. A meta-sedimentary sequence, crops out at Presa Mocuzari, consisting of limestone, quartzite and slate, and small outcrops of limestone around Piedras Verdes, was assigned to the upper Paleozoic by King (1939). A second meta-sedimentary sequence formed by gneissic units, schists, phyllites, meta-silstones, metaquartzites, and meta-arkoses, and in some places recrystallized calcareous units, was assigned to the Triassic-Jurassic Barranca Group (King,1939; Vazquez,1975; Wilkins,1995). This correlation was based on graphite occurrences at San Bernardo area (20 km northeast of Piedras Verdes) similar to the graphite occurrences hosted within the Barranca Group sequence located in central Sonora. This sequence has been subjected to various deformational events; folding, regional greenschist facies metamorphism, and contact metamorphism associated with the intrusion of the batholithic rocks (Sinaloa-Sonora Batholith), and Tertiary quartz monzodiorite intrusive bodies. Middle Cretaceous massive and bedded gray limestone, often recrystallized occurs as ridges or isolated outcrops and discordantly overlays the meta-sedimentary units. Various andesitic to dacitic rather pyroclastic are considered also of Cretaceous age (Vazquez, 1975). Outcrops of volcanic rocks in the area were assigned to the upper Cretaceous (i.e. Tarahumara group of Roldan Quintana, 1994).

A varied sequence of intrusive rocks of Late Cretaceous to early Tertiary age (Laramide) occurs in the region. Some are phases of the Sinaloa-Sonora Batholith (Roldan-Quintana and Stewart, 1994), and consist of coarse and medium-grained biotite-hornblende granodiorites, quartz-diorites, quartz-monzodiorites, granodiorite porphyry, granite porphyry, and aplite. The biotite-hornblende granodiorites are considered the earliest phases of the batholith and have K-Ar dates of 67-72 Ma (Damon et al., 1983). Volcanic rocks around Piedras Verdes range from Oligocene to Pliocene in age. Oligocene flows, agglomerates and tuffs, all of andesitic composition, crop out in the Sierra de Alamos (Vazquez, 1975) and elsewhere. Younger rhyolitic flows and tuffs are probably of Miocene age. Extensive outcrops of the Miocene-Oligocene Baucarit Formation (King, 1939), consisting of volcaniclastic conglomerates, dacitic to andesitic flows, and felsic tuffs, have been recognized.

Structurally, the earliest deformational event in the region is the polyphase folding of the meta-sedimentary rocks. These units show at least three major folding events the first two of them probably occurred during the Jurasic-Cretaceous Nevadan Orogeny and late Cretaceous-early Tertiary Laramide Orogeny. These, larger and small folds show east-west oriented axis indicating a north-south to northeast-southwest compression (Mullan, 1978). The third deformational event, affected the metasediments and locally the early porphyry phase in the Late Laramide and is represented by an E-NE oriented shear with associated fault-drag folds, observed out side of the deposit area.

The region was intensely affected by faulting events, possibly as old as the Jurassic

(Nevadan Orogeny). Although the ages of the deformational events that produced these faults are not well constrained until now, at least three different fault systems could be interpreted, which have been reactivated during subsequent deformational events after their formation. The earliest faulting event is represented by two prominent northeast-oriented regional lineaments (≥100 km long) that are recognized on Landsat Images (this work). The Piedras Verdes deposit is located along the trend of one of these lineaments. The other lineament is projected to pass southeast from Piedras Verdes. Although references about the attitudes of this lineaments are not well known, they may have been formed during the late Jurassic-early Cretaceous Nevadan orogeny, as it was explained for similar structures in northern Sinaloa by Mullan, 1978. A younger system of E-NE striking faults (N75-80°E) is indicated by many smaller structures, shear zones, and the orientation of the porphyry intrusion at Piedras Verdes. Therefore, they are most likely Laramide in age. They are approximately parallel to the trend of two major interpreted structures that bound the region (Stewart and Roldan-Quintana, 1994). This structural orientation is also suggested by an interpreted east-west trending boundary between the Seri terrane in northwestern and central Sonora and the Tahue terrane in southernmost Sonora and northern Sinaloa, (Sedlock, et al, 1992). This boundary lies close to 27° N latitude, which is the approximate latitude of Piedras Verdes. Some of these faults show ductile regimes with strike-slip movement. The youngest faulting event is a pronounced northwest normal system (N45–70°W) that offsets the east-northeast faults and the supergene mineralization at Piedras Verdes. This latest fault system could be related to the beginning of extensional events after the Laramide Orogeny.

The most notable mineralization in the region is a system of silver-rich polymetallic (lead, zinc, copper, silver, and gold) epithermal veins in the Aduana, Minas Nuevas, and Los Tanques areas. Most of these veins strike northeast or northwest and are mid-Tertiary in age. Other mineral occurrences are small Laramide skarn bodies distributed throughout the region. Some of these skarn bodies are cut by structures that host copper oxides. Other porphyry-style occurrences of interest, located north of Piedras Verdes are Las Salvias, which has copper oxides exposed in a strong quartz-sericite alteration zone along a north orientation that is cut by east-northeast-striking faults. The other, La Reforma, is an east-northeast trending, brecciated granodiorite intruded by a quartz-feldspar porphyry that carries molybdenite and very little amounts of gold.

ORE DEPOSIT GEOLOGY

LITHOLOGY

Triassic-Jurassic Piedras Verdes meta-sedimentary sequence

The oldest rocks at Piedras Verdes consist of a meta-sedimentary sequence, siliceous to argillaceous in composition, which have been affected by tectono-magmatic events. The meta-sedimentary sequence consists of greenschist facies, mudstone, shale/phyllite, silstone, meta-quartzite, meta-arkoses, and biotite/muscovite schist (Mpvs). This unit has been transformed to hornfels along the contact with the batholith imparting locally "gneissic" texture (Mgn). The meta-sedimentary units generally strike northwest, with steep dips mainly to the northeast and southwest. Variations from this general trend are minor, striking to northeast, which are the result of isometric and asymmetric folds that occurred during regional metamorphism.

(Mpvs): These units crop out mainly in the eastern part of the deposit, and surround the main granodiorite porphyry stock. The units are truncated to the west by the northwest-striking Tepustete Fault, which places them in contact with their gneissic equivalents. The estimated thickness for this unit is 520 meters. It is constituted by an intercalation of meta-arkose, thick-bedded impure quartzite, and thin-bedded chloritic to biotitic schist (*Mqst*). All three rock types are fine to medium grained. They are believed to constitute the upper part of the meta-sedimentary sequence. The middle part of the

sequence consists of very fine grained, siliceous to argillaceous sericitic schist (Mmsh). The protoliths are likely to have been interlayered mudstone and shales. They show foliation, including kink-bands. Occasionally coarse muscovite is present in the schist. Chlorite or sericite has affected the biotite. Some of the chlorite may be primary and not after biotite. The schistocity and metamorphic grade increase with depth and grade into the gneissic unit.

The "Gneissic" (hornfels) unit **(Mgn)**: crops out mainly in the western part of the deposit. They exhibit a fine to medium grained gneissic structure, constituted by irregular 1 mm to 1 cm banding of alternating quartz and feldspar-biotite-bands. The rocks of this unit have foliation with dips generally 30° or more to the drill core axis. This unit locally shows ptygmatic to irregular chevron and open folding and is 200 meters thick.

The presence of andalucite (Dreir and Braun, 1994), a mineral common to hornfels, raises the possibility that the gneiss-hornfels were formed by thermal metamorphism related to the emplacement of the Alamos batholith.

Intrusive rocks

The intrusive rocks show a quartz diorite-quartz monzodiorite to granodiorite composition. The largest exposure consists of a batholitic-sized Cretaceous granodiorite. Various phases of an intrusive suite are recognized, but only the principal phases are described here (see Figs. 4, 5 and 6).

Granodiorite Batholith (Kgd)

The Cretaceous granodiorite at Piedras Verdes is batholithic in character and is believed to be a portion of the Alamos Batholith. K/Ar dated on biotite from fresh granodiorite yielded an age of 67.3 ± 1.4 to 72 Ma (Damon et al., 1983). It crops out mainly in the northeastern part of the deposit. It is light gray, equigranular and medium to fine-grained. The granodiorite consists of 50-70% euhedral to anhedral zoned plagioclase with andesine-oligoclase composition; 10-12% subhedral to anhedral weakly chloritized biotite, mostly as fine-grained disseminated aggregates surrounding ragged hornblende; 4-10% ragged and corroded hornblende with replacement by biotite/chlorite; 12-15% anhedral-interestitial quartz, and 2% fine-grained orthoclase. The texture of the batholith changes from north to south, becoming coarser grained to the south of the deposit. Two samples of the Alamos batholith were taken, one over a cut along the Alamos- El Tabelo road, and the other one from the Cretaceous granodiorite (Kgd) at Piedras Verdes. The most important difference between them is that the former shows a coarser texture with 5-8 mm biotite and feldspar fenocrysts and with an equigranular texture. Otherwise, both of them have very similar mineralogical and geochemical composition. Table 1, presents representative chemical and normative determinations for these samples. The Streckeisen diagram of figure 21 shows the compositional range of this unit.

Tertiary Quartz Diorite to Quartz Monzodiorite (Tqd)

Quartz diorite phase is the predominat rock in the southwestern portion of the map

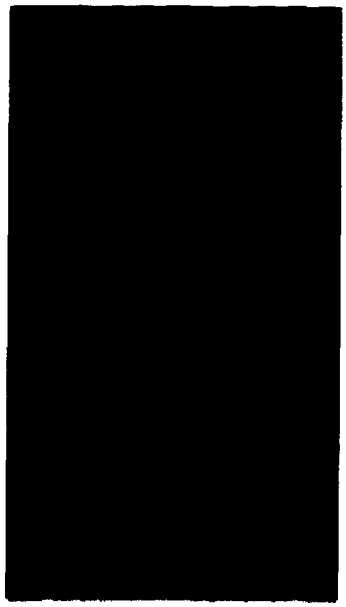

(a)

(b)

Fig. 2. a) The quartz monzodiorite to quartz diorite (Tqd). b) A xenolith of Tqd in a fine-medium grained quartz monzodiorite to granodiorite phase (MDChato). The MDchato is probably , a pre-granodiorite porphyry suite phase.

area. Intrusive phases vary from equigranular-hornblende quartz diorite to hornblende-biotite quartz monzodiorite (Fig. 2). These rocks are dark gray to green. The biotitic phase has a fine to medium-grained hypidiomorphic texture. The hornblende quartz diorite is similar to the biotite quartz monzodiorite, but has 10% coarse euhedral to subhedral hornblende partially resorbed by biotite. These rocks consist of 55-75% subhedral plagioclase, 6-8% anhedral quartz interstitial to plagioclase, 10-12% anhedral to euhedral biotite that is generally corroded, , 4-5% orthopyroxene (hypersthene), and less than 2% apatite, and magnetite. Several thin granodiorite porphyry dikes (20-40 cm thick) with as much as 3% disseminated pyrite and, a small finger-like dike containing copper oxides, intrude quartz monzodiorite in the western limits of the deposit. These relationships indicate that the diorite was emplaced before the ore related granodiorite porphyries. K/Ar dated on biotite yielded 60.3 ± 1.5 Ma and 61.7 ± 1.6 Ma ages (PD internal report, 1996). Table 1, lists representative quartz monzodiorite major elements normative determinations. Figure 21 illustrates its petrologic composition. The QMBuffel and QMChato are rocks taken within the quartz monzodiorite-quartz diorite stock. QMChato plots in the limit between granodiorite and quartz monzodiorite fields, whereas QMBuffel falls within the granodiorite field. Nevertheless, they are considered part of the quartz monzodiorite-quartz diorite unit.

Granodiorite Porphyry phases (Tgdp)

The granodiorite porphyry phases (Tgdp) unit is constituted by various intrusive

phases, which where no differentiated on the simplified geologic map of figure No. 4. The main intrusive body of this unit is the "tall biotite" granodiorite porphyry (**$Tgdp_{tb}$**) that crops out in a dike-like fashion along the main east-northeast fault occupying the center of the Piedras Verdes deposit. It is a gray rock with weak porphyry texture containing medium-grained phenocrysts (1-4mm) in a very fine-grained crystalline groundmass (Fig.3). This rock is constituted of 55% euhedral to subhedral, some resorbed, plagioclase phenocrysts (oligoclase-andesine composition), 5% rounded to anhedral, some resorbed, quartz phenocrysts, and 10-15% euhedral to anhedral biotite phenocrysts. Biotite phenocrysts are characteristically "tall" with "c" axis greater than "a", and "b" axes. Some biotite crystals have been replaced by chlorite. There are a few crystals (2-3%) of hornblende with their borders replaced by biotite. The 30% by volume groundmass is composed of 60% quartz, 35% orthoclase and minor biotite (5%, probably secondary). A core sample was dated by the K-Ar method on biotite yielding an age of 62.2 ± 1.6 Ma (PD internal report, 1996). A special phase of this porphyritic unit is a biotite granodiorite with seriate texture (i. e. crowded porphyry) constituted of 70-80% (rock volume) medium-grained phenocrysts (1-4 mm); 60% plagioclase, 5% biotite and 5-10% quartz. The groundmass consists mainly of quartz-orthoclase. This seriate phase is restricted to the contacts with the metasedimentary rocks. It is considered either as a precursor, but may represent the "chilled" margin of the tall biotite granodiorite. Figure 21 shows the composition of the "tall" biotite granodiorite.

Intrusion Breccias (Tibx)

Intrusion breccias associated with the "tall" biotite granodiorite crop out along the southern contact between this unit and the meta-sedimentary sequence. They are heterolithic and generally fragment-supported breccias. They are constituted mainly by large metasedimentary and porphyry clast as large as 2-3 meters across, but most clasts are 0.5 meters and less in diameter. The porphyritic matrix is quartz-rich and contains minor hematite. The matrix contains abundant clay, alunite, calcite and gypsum in veinlets as well. The granodiorite porphyry fragments are rounded to sub-rounded and the metasedimentary fragments are angular to sub-angular.

Quartz-Feldspar Porphyry (Tqfp)

This unit is a porphyrytic siliceous light gray dike and/or plug with phenocrysts of feldspar and quartz, texturally much like the "tall" biotite granodiorite porphyry, but with little to no biotite (Fig. 3). In places, this porphyry has coarse rounded quartz phenocrysts from 5 to 8mm across. In outcrop, is restricted to a very small area south and southeast of the village of Piedras Verdes. It occurs as a 10m wide dike trending east-northeast; is not extensive and crosscut the "tall" biotite granodiorite porphyry. This porphyry becomes much more voluminous at depth where it has been intersected with diamond drill holes.

Biotite-hornblende Granodiorite dikes ($Tgdp_x$)

Latest biotite-hornblende granodiorite porphyry dikes crop out along the central

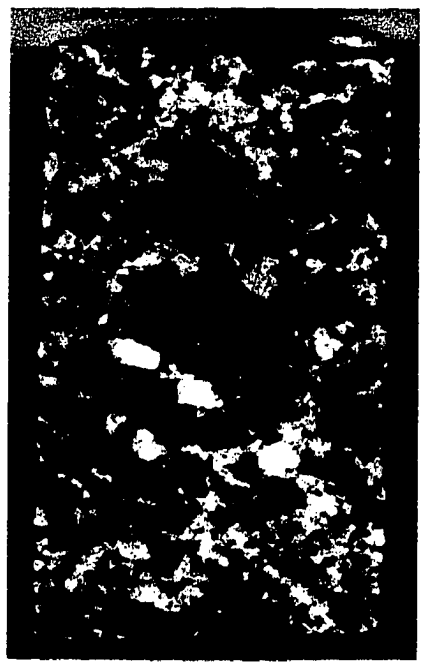

(a)

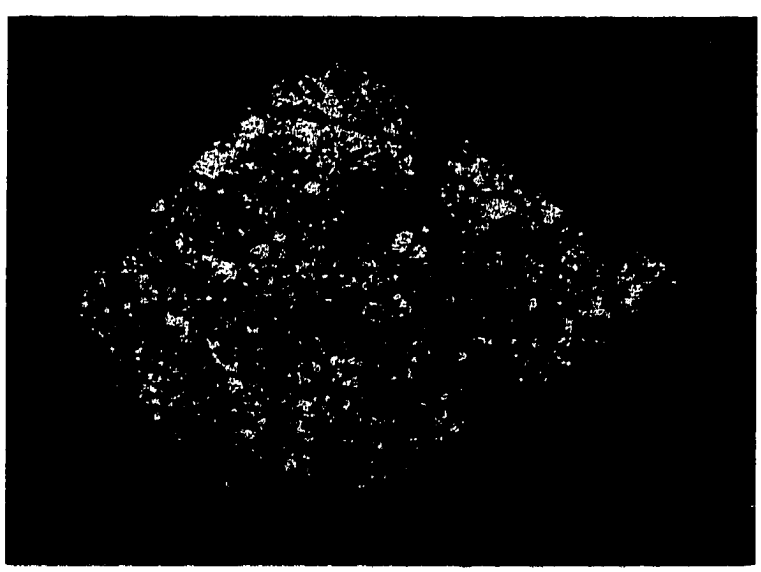

(b)

Fig.3. a) 'Tall" biotite Granodiorite Porpyry (Tgdp$_{tb}$). Note the 'tall" biotite crystalls (black). b) Quartz - feldspar porphyry (Tqfp). Note the big quartz-eyes (dark gray) and more obvious porphyritic texture than Tgdp$_{tb}$.

axis of the "tall" biotite porphyry, and along east-northeast structures. They cut the main "tall" biotite granodiorite porphyry. Crosscutting relationships with the quartz-feldspar porphyry are less clear. On the western side they intrude biotite "gneiss" and are displaced by northwest-striking faults. The biotite-hornblende granodiorite dikes are gray rocks with 40% fine to medium-grained plagioclase phenocrysts, 30% commonly shreddy, biotite, 10% quartz and 5-10% hornblende. They are considered as a late stage dikes due to they have exotic, not hypogene copper mineralization. Figure 21shows the petrologic composition of this rock.

Porphyritic andesitic dikes (Tpa)

Plagioclase-hornblende andesite dikes are postmineral and form narrow dikes. Outcrops of these dikes are found in the east and west portions of the deposit. Their orientation is mainly northwest and less often northeast. They contain euhedral plagioclase and hornblende phenocrysts, which exhibit trachitic texture in an aphanitic gray groundmass. They retain their original texture with argillic alteration (deuteric). A sample of these rocks was dated at 48.4 ± 1.2 Ma (K-Ar on biotite, Pd internal report, 1996). Due to strong alteration, they plot in a wrong composition field according to the normative classification. Additionally they had a high loss on ignition number, which indicates a strong alteration as well.

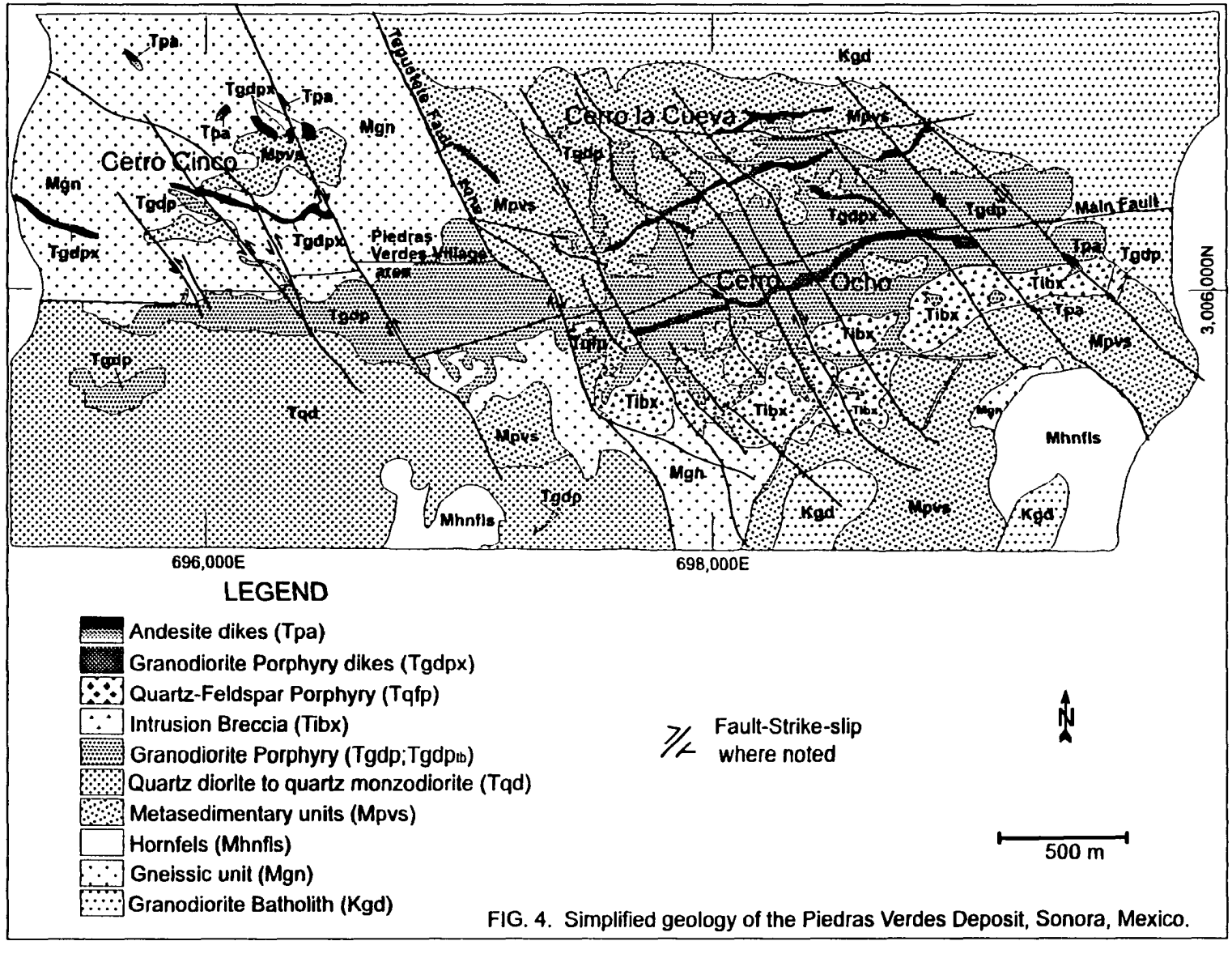

FIG. 4. Simplified geology of the Piedras Verdes Deposit, Sonora, Mexico.

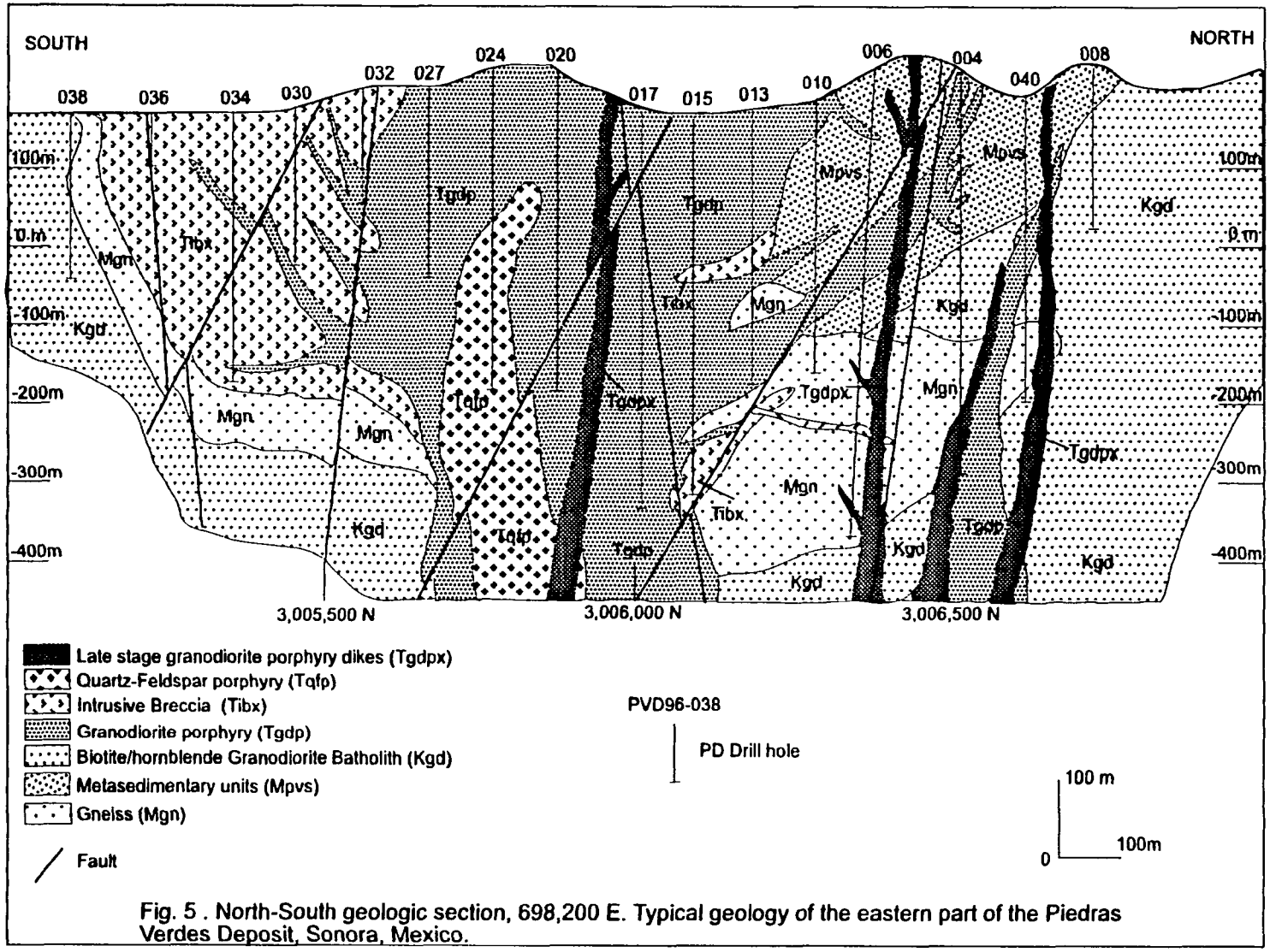

Fig. 5 . North-South geologic section, 698,200 E. Typical geology of the eastern part of the Piedras Verdes Deposit, Sonora, Mexico.

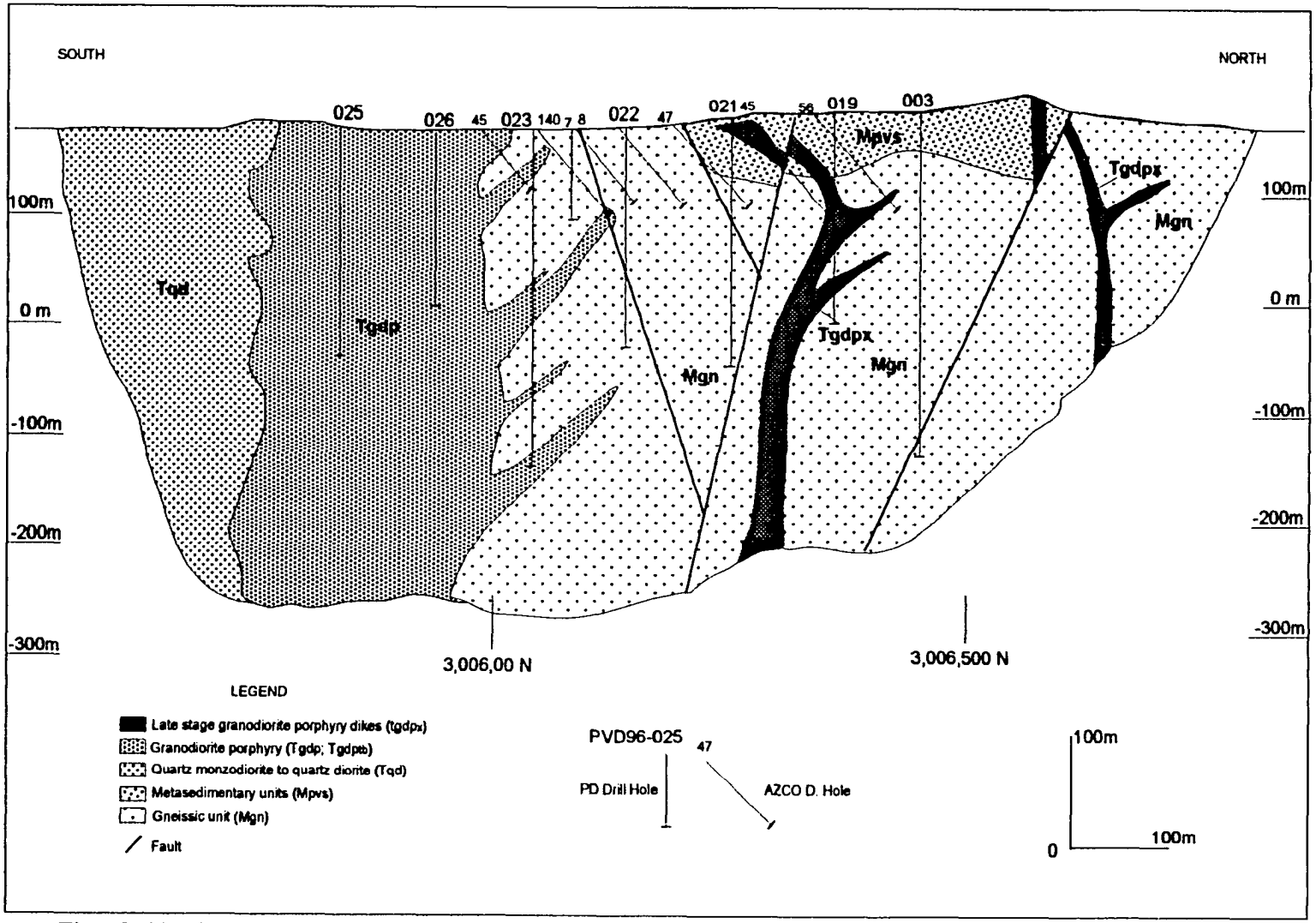

Fig. 6. North-south geologic section, 696,400 East. Typical geology of the western part of the Piedras Verdes Deposit, Sonora, Mexico.

STRUCTURE

The Piedras Verdes area has been affected by several faulting events. Premineral, intramineral and postmineral faults are recognized. Preexisting Mesozoic faults were reactivated during porphyry emplacement and again in the Tertiary, generating a highly fractured environment.

Premineral Faulting

The earliest faulting event at Piedras Verdes deposit is indicated by premineral faults mainly of N50°E. This episode is likely upper Cretaceous in age or older, and is well defined regionally around the Piedras Verdes deposit (PD internal reports).

Intramineral Faulting

A N70°E shear zone was generated previous and during the early stage of porphyry emplacement. The main E-NE elongated granodiorite porphyry and related mineralization are controlled by this direction (main fault zone in figure 4). Small N10°E oriented faults in the west side of the deposit, near the town of Piedras Verdes, are also considered to be part of the major shearing event. Good exposures of east-northeast mineralized slikensided shear surfaces and ductile fabric are confined to the western part of the deposit. These structures show a component of subhorizontal strike-slip movement. However, this E-NE major fault zone is ill defined in the east side of the deposit . Nevertheless in any case, a possible continuation of this major structure is an

east-west-striking fault, which crops out in a wash approximately three kilometers east of the deposit, and projects along strike from the Piedras Verdes deposit. The fault only affects granodioritc rocks in this locality. Small east-northeast-striking copper-oxide mineralized fractures exposed on the eastern limits of the deposit suggest continuity of the east-northeast fault zone, as well.

Post- primary mineralization Faults

High-angle (>50°) mainly N35-50°W, and minor N60-70°W and N10°W-striking faults and fractures, mostly southwestern dipping truncate premineral faults. The latest movements along these faults postdate supergene events. Nevertheless, an initial movement before significant oxidation and supergene enrichment is suggested by a 48.4±1.2 Ma old andesite porphyry dike, which intruded along a northwest striking quartz-hematite zone. The largest northwest structure is the Tepustete fault zone, which practically divides the geology and ore characteristics in the east and west sides of the deposit. It is interpreted as a Riedel fault. The fault directions resemble the shear model proposed by Wilcox, et al., (Davis, 1994,1996). Like the premineral faults, the northwest faults show sub-horizontal strike-slip displacement. Faults with right-lateral and left-lateral movements have been observed within and around the deposit, which suggest the possibility that left-lateral movement was active before to the porphyry complex emplacement and associated or later reactivated with right-lateral displacement. A preliminary interpretation suggests that cumulative right-lateral displacement of the northwest faults along the strike length of the deposit may be as much as 650 meters.

Owing to the continuous right-lateral displacement of the abundant parallel northwest-striking faults, the former northeast orientation of the deposit, was changed to the present overall east-west orientation (Fig. 7). However, the initial northeast orientation is indicated by the northeast trend of individual porphyries, dikes and mineralized structures.

E-W local low-angle faults mostly occur in the eastern portion of the deposit, with dips of ±20° south, and show right-lateral movements, as indicated by slickensides. They are restricted in lateral extent. These faults have juxtaposed meta-sedimentary units against porphyry, and porphyry against porphyry. Any of these fault types has not been intersected with core drilling. The relationships between these faults and the former systems are not well constrained, but they are interpreted as a young faulting event (PD internal reports, 1996).

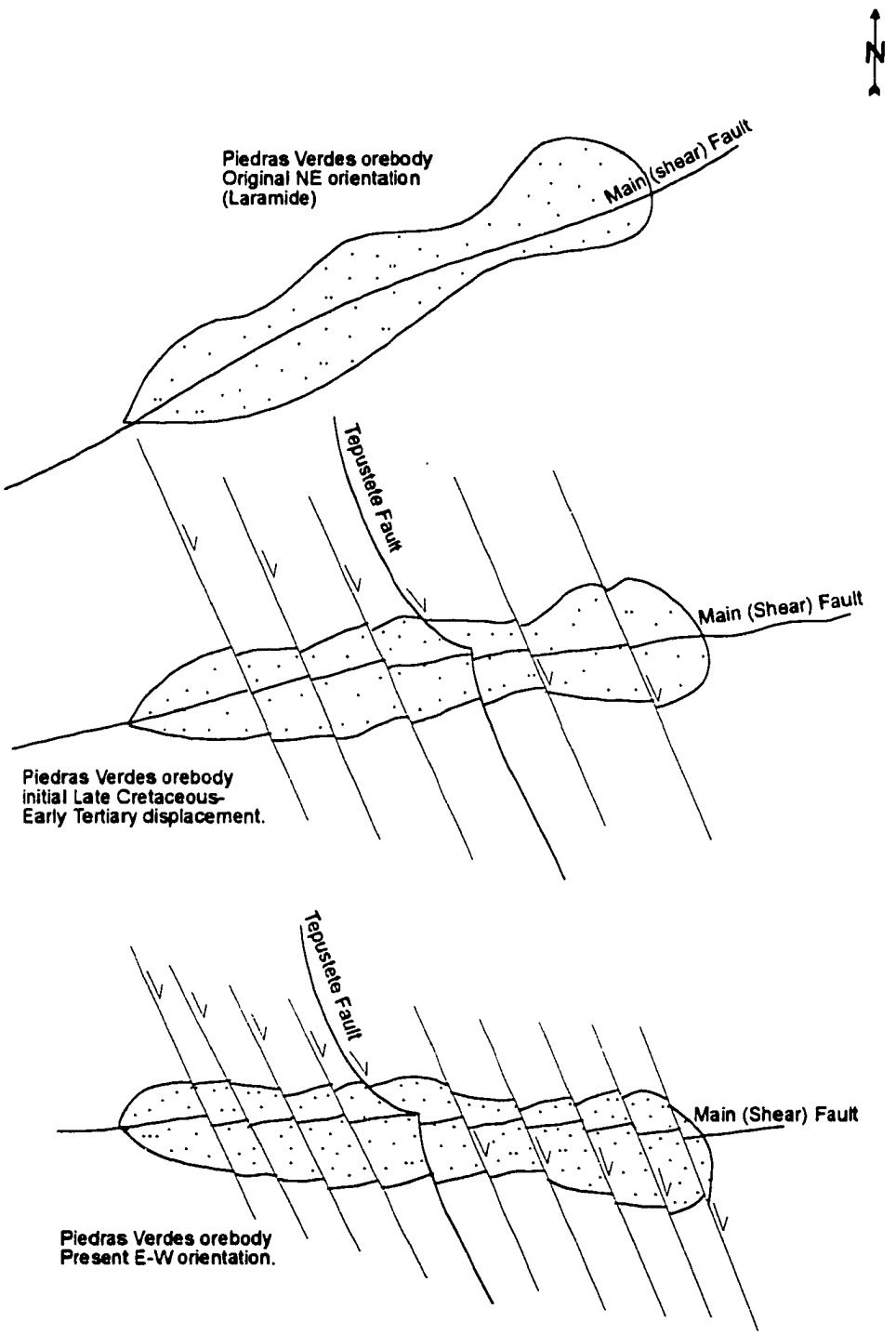

Fig. 7. Plan view of the interpreted original NE and present E-W orientation of the Piedras Verdes deposit by countinous right-lateral displacement of North-west striking faults.

ALTERATION

Hypogene alteration

Hypogene alteration consists of a potassic core surrounded by a phyllic shell, capped by advanced argillic, which fades out into a very weak propylitic alteration. The phillic shell is capped by advanced argillic alteration. These alteration associations occur as bands that roughly parallel the East-West elongation of the porphyry system (Fig. 8). Quartz-sericite alteration overprints Kspar-biotite and supergene clays in the center of the system. Propylitic alteration, where observed, appears weak and selective. Other supergene alteration consists of silica-hematite (jasperoid) developed along structures. Contact metamorphic alteration, including garnet skarn and diopside hornfels, occur mainly to the west and south of the porphyry system.

Pre-porphyry suite emplacement: Skarn alteration

Skarns, consisting of garnet, diopside, quartz and magnetite, occur south of the mineralized area. Epidote, actinolite and specularite are also found here. In a few drill holes on the western side of Cerro la Cueva, garnet, magnetite, chlorite, and epidote, locally replace meta-sediments. Most skarn occurrences are proximal to the granodiorite batholith and the quartz monzodiorite-quartz diorite stock, and are therefore considered to be an earlier event. Formation of hornfels is also associated to the granodiorite batholith. Skarn type alteration was encountered at the bottom of the drill hole PVD-96-22 (420m depth), which consists in an assemblage of calc-silicate minerals including

serpentine, humite, and pennine in a bearing-Ca-Mg (probably dolomitic) thin bed within the gneissic-hornfels unit, and they are cut by graphite veinlets.

Alteration associated with the porphyry stocks

Potassic alteration

Replacement and vein-veinlets of secondary biotite and quartz-orthoclase characterize potassic alteration . Within the granodiorite porphyry stock this is expressed as biotite replacement of igneous hornblende and biotite. Plagioclase phenocrysts are replaced by potassium feldspar. Potassic alteration of the hornfelsed biotite-rich meta-sedimentary rocks is defined by biotite recrystallization followed by tourmaline. Quartz-orthoclase veining also occurs within the porphyry, and around meta-sedimentary units-porphyry contacts. Within the granodiorite porphyry, in the core of the system, minor amounts of light-purpure anhydrite occur in association with quartz-pyrite-molybdenite veinlets. Overall, potassic alteration is weak in the main Piedras Verdes system.

Tourmaline is present along fractures and very fine fibrous patches and in disseminations. A tourmaline zone coincides with the central core of the porphyry, where in some places it is also associated with chalcopyrite-magnetite and minor arsenopyrite veinlets. Elsewhere, tourmaline is found within the gneissic unit associated with quartz-pyrite veining.

Propylitic alteration

The propylitic alteration zone, is weak, selective, and restricted. Where present it consists of quartz-chlorite-sulfides veinlets, vein selvages, and chlorite replacing biotite. It is accompanied by minor amounts of epidote. Chloritization is also seen within the biotite "gneiss" and after feldspar and mafic phenocrysts in intrusive rocks. Around the deposit weak propylitic alteration affects the granodiorite of the Alamos batholith and the quartz monzodiorite (Fig. 8). Much of this chloritization may be deuteric.

Phyllic alteration

Sericite+pyrite+quartz defines the phyllic alteration zone. It is the most widespread and pervasive hypogene alteration adjacent and within the central potassic elongate zone (Fig. 8). Its distribution is very strongly controlled by structures. It occurs as sericite-quartz pervasive (>50%) flooding, as quartz in veins with sericite selvages. Sericite also replaces biotite selectively. It affects both the meta-sedimentary and porphyry units. There is abundant chlorite associated with this alteration as well, wich can be seen particularly well in deep holes. Silicification is pervasive in places within the gneissic unit and the porphyry, but mostly occurs as veining and stockworks. Strong quartz stockworks are found in porphyry under Cerro Ocho. It is interpreted that this represents a late-stage event in the evolution of the porphyry system, possibly associated with the quartz-feldspar porphyry, which is moderately to strongly altered to quartz-sericite. Extensive silica flooding is associated with quartz-feldspar porphyry under

Piedras Verdes Village. Probably, as a second stage tourmaline was also observed associated with quartz-sericite veins related to the quartz-feldspar porphyry intrusion.

Argillic alteration

The argillic zone is defined by strong clay development with clays replacing feldspar, biotite , and sericite. It is difficult to distinguish hypogene from supergene clays. Clays include kaolinite, and locally alunite present at depth as veinlets associated with gypsum and some times montmorillonite. The fragments of the intrusion breccia show weak argillic alteration, but many of them are not altered. Argillic alteration is interpreted as almost all supergene in origin.

Silicification

High-silica-hematite jasperoids occur replacing fault breccias and along high-angle faults, and in the form of almost circular breccias with hematitic matrix. These small circular breccias cut granodiorite porphyry and metasediments. The jasperoid-bearing faults crop out principally in the southeastern part of the deposit with both northwest and northeast orientations (Fig. 8). They are also displaced by late northwest striking faults. These jasperoidal-bearing faults cut relatively unaltered rocks, and argillic and phyllically altered rocks. The jasperoids occur in late supergene alteration zones and they are considered a late Tertiary, post-supergene alteration event (Wilkins, 1996). Nevertheless they contain anomalous copper values (1767-1300 ppm, range), probably

from copper remobilization due to leaching of deep chalcocite veins. It is possible that the quartz-chalcocite vein of probably, primary origen, located very close to the east limit of the Piedras Verdes deposit, could be associated with these silica-hematite veins. If this latter observation is correct, then the jasperoids are pre-supergene alteration, and the associated hematite formed after chalcocite.

Supergene Alteration

Supergene alteration effects are intense ubiquitous throughout the porphyry system. The deposit is moderately to strongly stained and veined with limonites. Iron oxides include hematite, jarosite, and goethite, in variable concentrations. "Live" limonites, derived from oxidized chalcocite are common. On the eastern side of the deposit, limonites are predominantly jarosite and hematite, suggesting a higher original content of sulfides. On the west side, where copper oxides occur near surface, limonites are dominantly goethite and hematite, indicating lesser amounts of original sulfides. This may also indicate, more neutral conditions (i.e. influence of biotite hornfels). In drill core, limonites are observed as fracture coatings, as pervasive and selective stainings, and as veinlets. Near structures and above the enrichment, limonites continue to depths in excess of 300 meters. Here, changes in limonite ratios correspond roughly to increases in copper grades. It is argued that not all limonites in the deposit are due to sulfides destruction. Some iron oxides stem from in situ oxidation of mafic minerals, since hematite staining is also present in areas where the sulfide content was insufficient. In addition, copper oxides have also remobilized, particularly along structures.

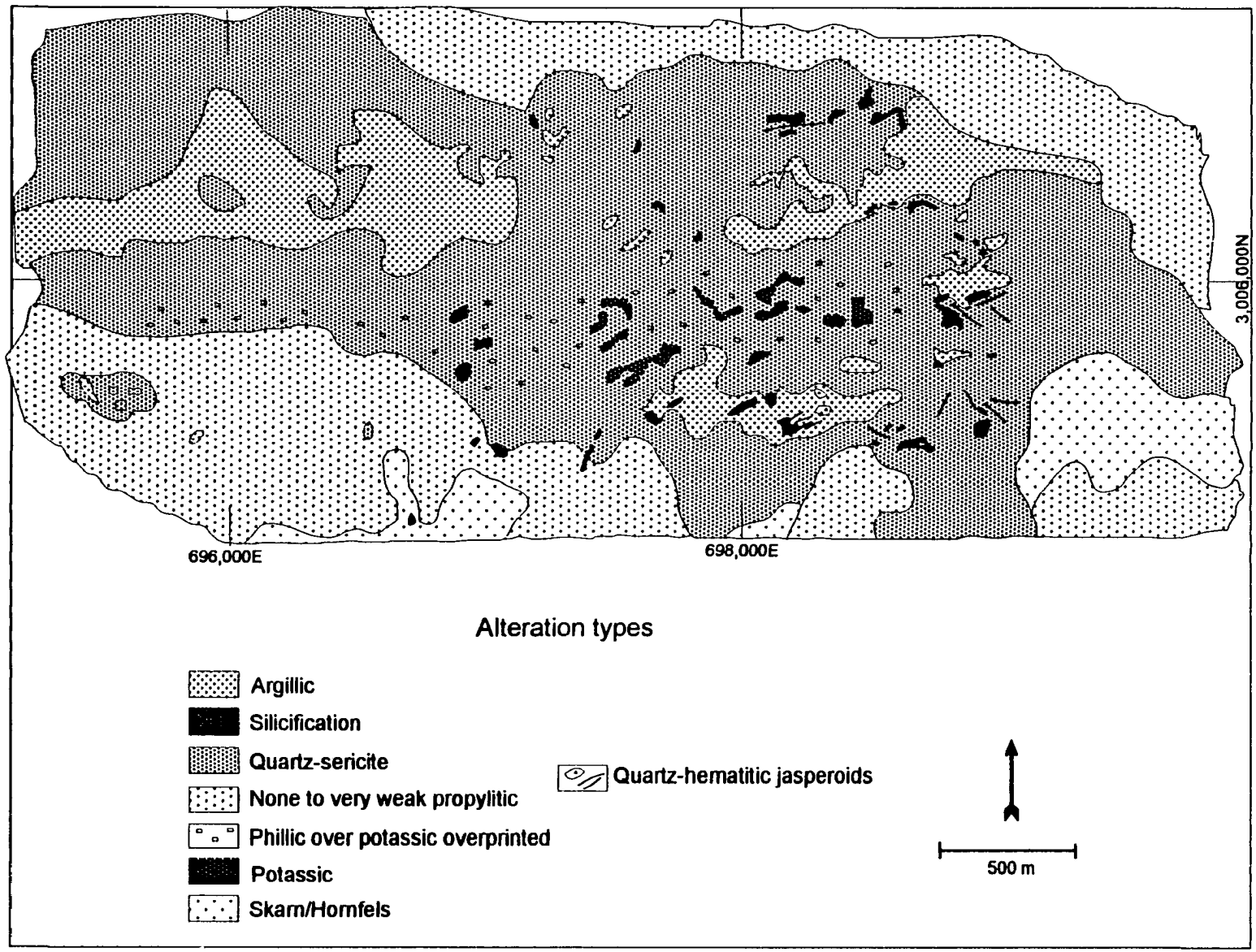

Fig. 8 . Alteration distribution of Piedras Verdes Deposit, Sonora, Mexico.

MINERALIZATION AND ORE TYPES

Hypogene mineralization

The only place where primary sulfides crop out abundantly, is at the eastern part of the Cerro Chato, located approximately 600m west of the deposit. Here pyrite is abundant with minor chalcopyrite (observed in drill chips). Elsewhere within the deposit area, a leached cap or copper oxides, are present. Primary copper grades average 0.10 to 0.15% in chalcopyrite, cupriferous pyrite, and minor amounts of bornite and possible covellite. Total sulfides constitute as much as 4-5% volume per cent. Pyrite content in the core of the system is 2-4% by volume, increasing outward to 5-7% in the quartz-sericite zone. Pyrite-chalcopyrite ratios are commonly in excess of 10:1. Chalcopyrite- pyrite occur as disseminations, veinlets, and bleblike aggregates predominantly near the contacts of the porphyry and meta-sedimentary units. Molybdenite is concentrated (200-300 ppm) mainly within the core of the system and at the contact with the meta-sedimentary units. It occurs in quartz-veinlets, quartz-chalcopyrite-pyrite veinlets, and anhydrite-calcite-pyrite veinlets. Additional pyrite, molybdenite, and minor chalcopyrite were introduced by a latter episode of mineralization associated with the intrusion of a quartz- feldspar porphyry. Locally, associated with pyrite-chalcopyrite veinlets at depth in the core of the system, there is some very fine-grained magnetite, pyrrhotite and minor arsenopyrite. It is probably that some of this assemblage is of hornfels-skarn type mineralization, associated with the batholith intrusion.

Paragenesis

The sequence of the mineralization events that formed the Piedras Verdes deposit is depicted schematically in the figure 9. Twenty polished sections of sulfide veinlets taken from drill core samples were studied. The samples were taken at depths of 150 to 450m. Only one sample was taken at a depth of 65m. The location of these samples and their corresponding drill holes are shown in the table No. 7. Only the sulfide mineral paragenesis of the hypogene mineralization period is described. Three main pulses of hypogene mineralization have been recorded. The three pulses of mineralization are associated with different sulfide and alteration assemblages related to different intrusive phases in the deposit. It is important to say that the samples are representative of the deposit and therefore they cannot accurately portray all the possible processes taking place during mineralization.

Skarn-type mineralization (period I)

Early, possibly, skarn-type mineralization is characterized by the presence of magnetite- hematite, in a calc-silicate gangue constituted mainly by tremolite, serpentine, and a humite mineral group as chlorites, which includes pennine, and secondary biotite (Fig.10a). The host rock is likely a Mg-Ca carbonate rock (dolomite). It is believed that this stage of mineralization is related to the intrusion of the Cretaceous Alamos Batholith (Sinaloa-Sonora Batholith, R. Quintana et al., 1994) which affect to the Paleozoic or Triassic-Jurassic sedimentary sequences. Regionally this type of mineralization is broadly

distributed in the region. A good example of calc-silicate alteration developed on these rocks is the sample PVPS-14. This sample was taken close the contact of the Cretaceous granodiorite batholith (Kgd) with the contact metamorphosed, gnessic unit (Mgn) (depth of 419 m).

The paragenetic relationships between the sulfide minerals on this sample are: early formation of magnetite (Period I) followed by introduction of pyrrhotite, chalcopyrite, and ± molybdenite (Period II) into the calc-silicate as well as in the Ca-Mg rich gangue (Figs. 12e,12f). Deposition of sulfides takes place along cleavage plains and grain and spaces between crystals in the calc-silicate aggregates as well as intergranular space in the host rock (Figs. 11a,11b and 12e,12f)). In some cases, however there is evidence of exsolution or mixing. Presence of chalcopyrite inclusions in different pyrrhotite decomposition intergrowths support a common origin (Fig.11c,11d). It appears that formation of elongated marcasite with subordinated magnetite aggregates,with magnetite in the center of two adjoining marcasite blades oriented along cleavage planes of pyrrhotite is the earliest decomposition product of the early magnetite, presumably under hydrothermal conditions. Pyrrhotite is also destroyed by graphic intergrowh of pyrite and magnetite (Fig. 11c,11d). Isolated pyrrhotite in the gange and preserved pyrrhotite enclaves are replaced by pyrite alone, forming coarse grained rather homogenous aggregates. Late veinlets formed by a white, acicular or sheet-like mineral, possibly anhydrite, containing an association of what appears to be graphite and molybdenite was observed. It cuts trough earlier calc-silicate assemblages and seems to belong to the Period II (Fig. 11g, 11h).

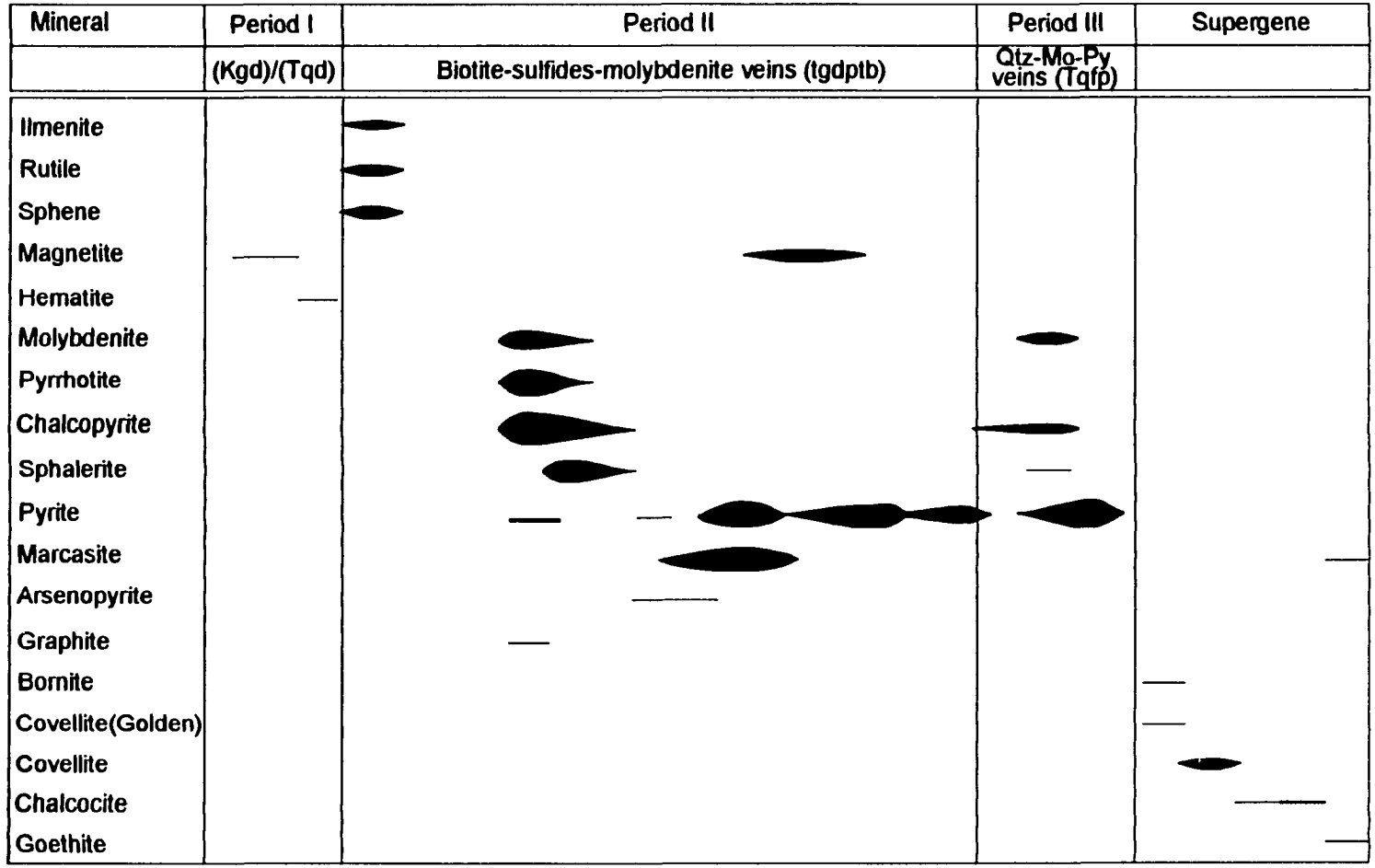

Fig. 9. Diagram showing the paragenesis and paragenetic sequence for the hypogene ore minerals associated with the porphyries of the Piedras Verdes deposit. The Period I corresponds to one sample taken very close to the batholith intrusion (sample PVPS-14).

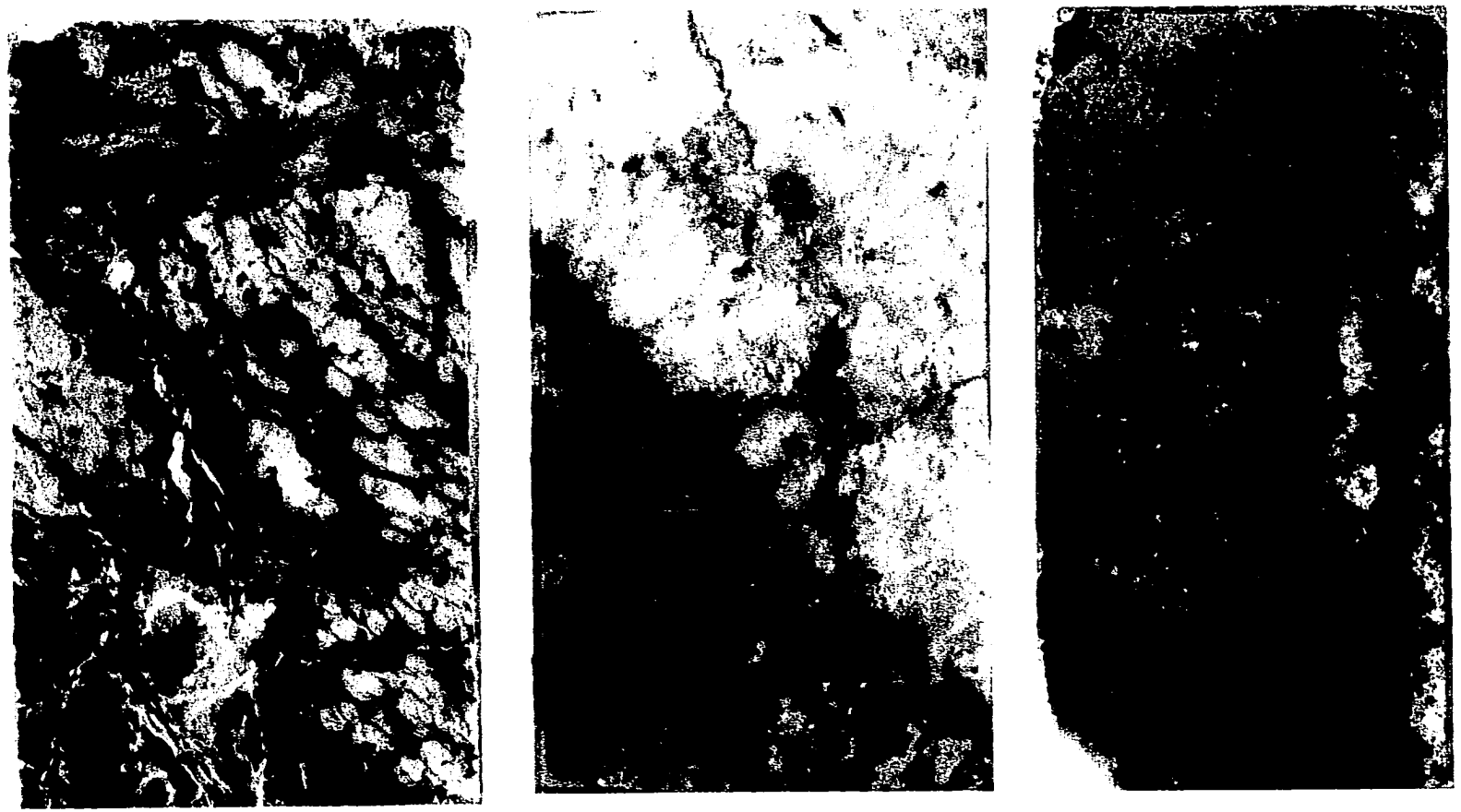

Fig. 10. a) Calc-silicate altered rock , chlorite, pennine-humite-magnetite veins (light green) of the mineralizing Period I, with chalcopyrite (yellow-gray)-biotite (brown) of Period II,(sample Pvps-14).b) Pyrrhotite+chalcopryrite+ sphalerite+magnetite veinlet cutting the Mgn unit. Strong quartz-sericite (white) and biotite (brown) alteration of the Period II in Mgn. c) Chalcopyrite+magnetite+pyrrhotite+pyrite veinlet in porphyry (Tgdp). Strong biotite and sericite alteration. Pyrite is replacing pyrrothite in this case.

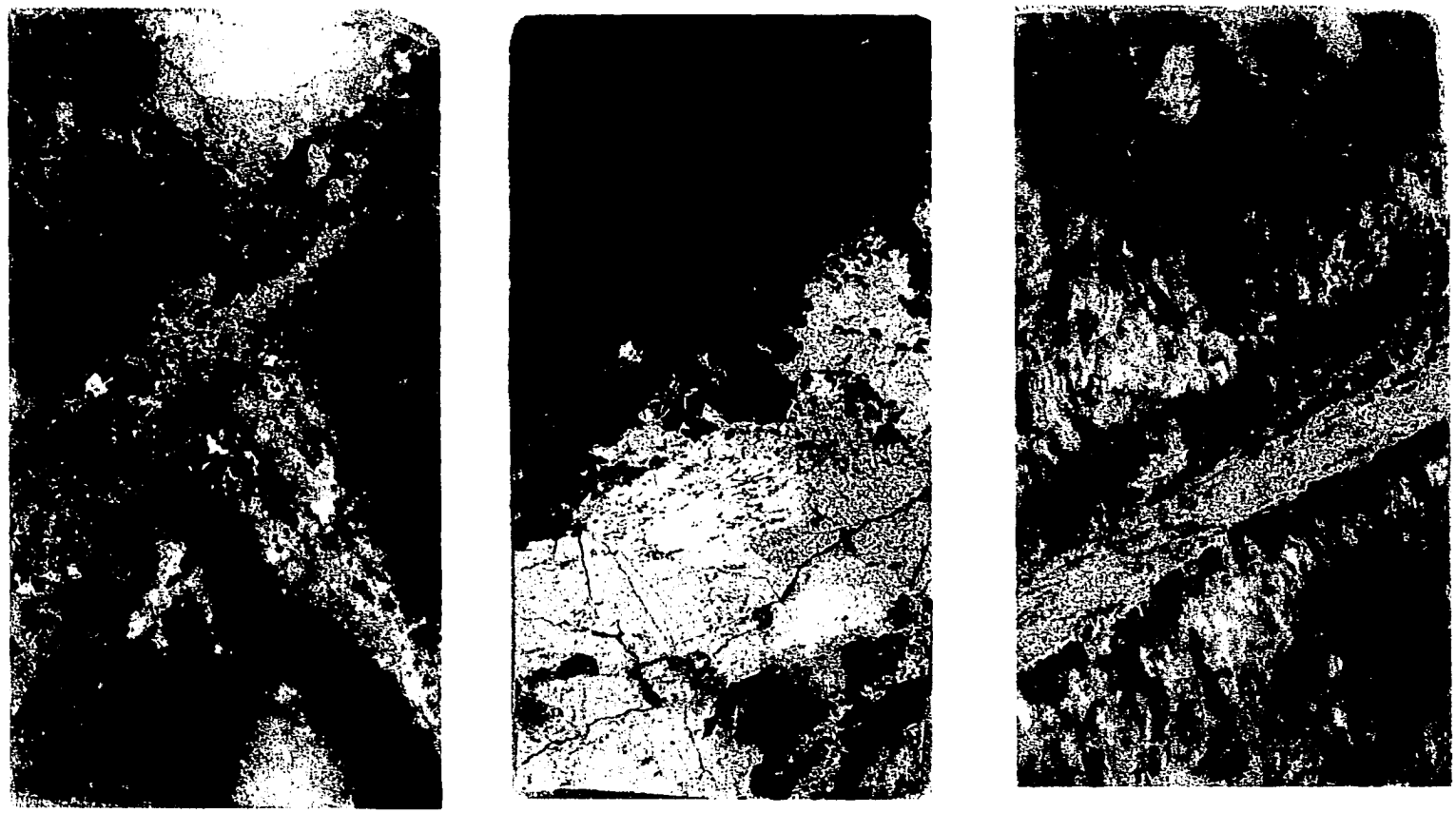

(d) (e) (f)

Fig. 10 continuation. Three sulfide-biotite veinlets examples of the Period II. d) Chalcopyrite+sphalerite+pyrrhotite+ magnetite+pyrite+molybdenite and minor biotite veinlet . Pyrite is replacing pyrrhotite. e) Arsenopyrite+pyrrhotite+ chalcopyrite+pyrrhotite+pyrite and minor sphalerite with strong chlorite halo (dark green). f) Pyrrhotite+chalcopyrite +pyrite and minor marcasite vein, chloritic halo (green) after biotite (brown). All of the three cases are in Mgn. Note the aggregated deposition of sulfides (white disseminated spots) preferentially along the biotite bands.

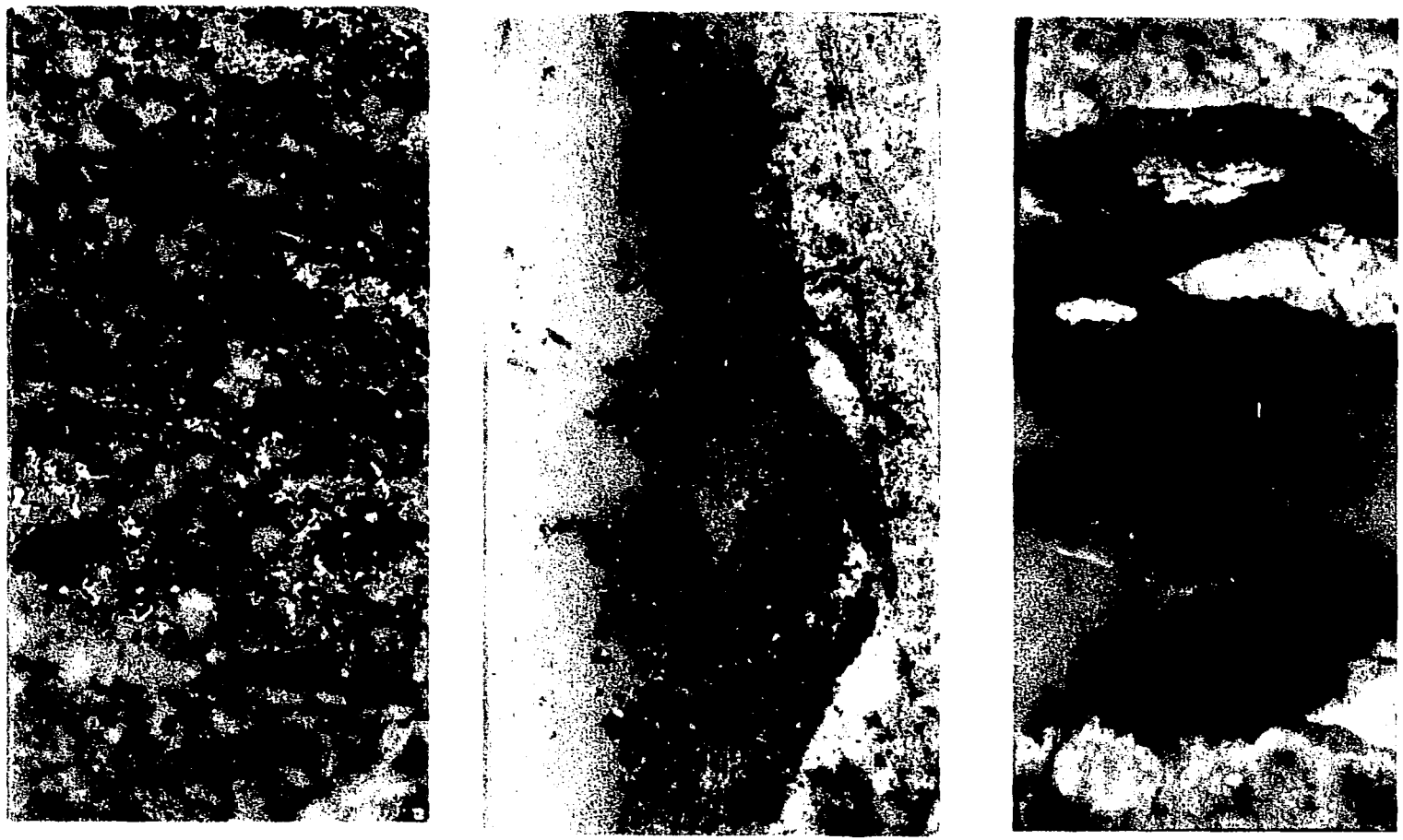

Fig.10 continuation. g) Deposition of sulfides principally along the biotite bands in an aggregated form, Period II, and two, h) and i) quartz-molybdenite+pyrite and minor chalcopryrite veins of the Period III (Second mineralizing event associated with the quartz-feldspar porphyry at the Piedras Verdes deposit). Note in h) the molybdenite-sulfides are deposited in an aggregated form within biotite-chlorite sites, and in i) the molybdenite-sulfides are deposited in chlorite-biotite sites, and also filling fractures in the quartz vein. Note the strong quartz-sericite alteration (white) of the granodiorite porphyry. Also note disseminated sulfides in biotite sites within the granodiorite porphyry.

Figure 11. Mineragraphic textures observed in hornfels-skarn type mineralization, from the polished sections of the figure 10. Sample PVPS-14. Period I and Period II as it is indicated.

a) Interlayered aggregate of chalcopyrite and chlorite within the chloritic zone of alteration (PP, 20X). Period II.

b) Impregnation aggregate of sulfide, most likely pyrrhotite, in the dolomite gangue. This is derived from the fact that the complex intergrowth of marcasite-magnetite and pyrite-magnetite resulting from the decomposition of pyrrhotite does not replace or exert any crystallization pressure on the gangue minerals. (PP, 20X). Period II.

c) Complex aggregate of pyrite, marcasite and magnetite in contact with a magnetite grain. This complex texture is the result of the decomposition of pyrrhotite first to marcasite blades with magnetite forming in the intermediate space and than to a reticulate intergrowth of magnetite and pyrite. Pyrite forming from pyrrhotite also replaces the adjoining magnetite. (PP, 40X). Period I-II, superimposed.

d) Intergrowth between chalcopyrite and the complex marcasite-magnetite/pyrite-magnetite decomposition texture (PP, 40X). Period I-II.

e) Aggregate of medium gray, poorly polished magnetite near or in contact with pyrite. Notice the beginning of replacement of magnetite by pyrite. (PP, 20X). Period II.

f) Cluster of xenomorphic chalcopyrite crystals around a cluster of alteration in the dolomite gangue. The soft mineral with the very low reflectivity and orange colored irregular reflection anisotropy is graphite, which appears associated with chlorite. (PP, 20X). Period I-II.

g). The strong anisotropy of graphite under crossed nicols is revealed by its orange-golden colors and is in contrast to the clear and almost transparent nature of the chlorite into which the graphite appears to interfinger. (XP, 20X). Period II or I.

h) Aggregate of very low reflecting graphite sheets displaying characteristic fine and irregular reflection pleochroism effects in orange, interleaved between chlorite crystals. (PP, 20X). Period II.

(a)

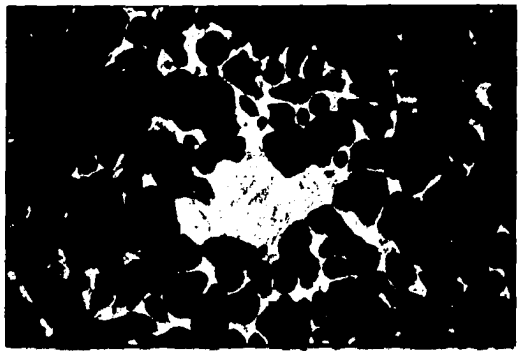

(b)

(c)

(d)

(e)

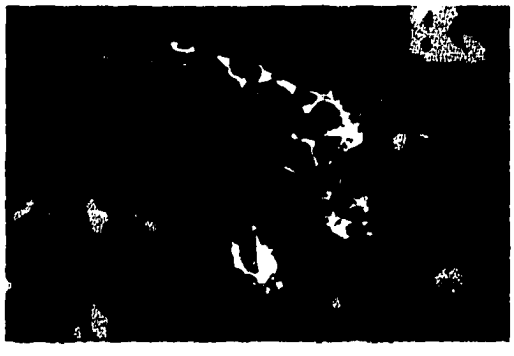

(f)

(g)

(h)

Biotite-sulfides-molybdenite veinlets (Period II)

All the samples of sulfide veinlets that are believed to correspond to a second pulse of mineralization (principal event of Cu mineralization, related to the tall biotite granodiorite porphyry phase) were taken from veinlets within the meta-sedimentary Piedras Verdes sequence and the gneissic units (Mvps and Mgn) as country rocks. Most of them are at or near granodiorite porphyries (Tgdp phases)-meta-sedimentary units contact. These sulfide veinlets are constituted of chalcopyrite, pyrrhotite, pyrite, magnetite, marcasite, with or without molybdenite and minor sphalerite. Rutile was observed as well, mainly following the biotite bands of the host rocks and replacing ilmenite. In nearly all the samples the sulfides are closely related in space to the presence of biotite alteration both pervasive and in veinlets. The biotite- sulfide veinlets were observed, principally, cutting the biotite-quartz-feldspar banding of the gneiss and schist of the meta-sedimentary units (Figs. 10c to 10f) and the granodiorite phases. From the veinlets the mineralizing fluids infiltrated into the country rocks and deposited the sulfides preferentially in the biotite bands, where they were observed replacing biotite showing chlorite alteration (Figs. 10g; 12). This suggests that biotitization is followed by chlorite alteration and deposition of sulfides. The chlorite alteration of biotite occurs in the vecinity of crosscutting sulfide veinlets but rarely penetrate more than 5 mm into the host rocks (Figs 10e to 10f). In the sample PVPS-12 and PVPS-13 tourmaline in coescistence or being replaced by sulfides was also observed (Fig. 13e, 13f). This suggests that a first tourmalinization event formed close in time either before or

contemporaneously with the sulfide mineralization.

Broadly speaking the paragenetic relationships in the biotite-sulfide veinlets are: early deposition of pyrrhotite, chalcopyrite, magnetite, molybdenite and arsenopyrite; exsolution of sphalerite in chalcopyrite, and possibly formation of sphalerite in the host rock; partial decomposition of pyrrhotite to marcasite-pyrite in the form of a "bird eyes" like-texture (Fig. 13d); and to pyrite-magnetite (Fig. 11c;11d); replacement of marcasite and magnetite by pyrite (Fig. 11e) and formation of pyrite veinlets. Presence of pyrite as moderate to coarse aggregates with relict cleavage, appears to indicate formation of a pyrite+marcasite intergrow subsequently replaced by pyrite (Fig. 13b). In the sample PVPS-4, pyrite-marcasite intergrows showing the same orientation as early arsenopyrite, suggest the formation of early arsenopyrite after pyrrhotite (Fig. 13c). Sphalerite was observed as isolated grains in the gangue and as inclusions within pyrite at the edge of the gangue (Fig. 13f). Sphalerite within pyrite at the edge of the gangue indicates that pyrite might have replaced chalcopyrite (Fig. 13a).

In the samples PVPS-1, PVPS-16, pvps-19 and PVPS-21, minerals of supergene origin were encountered. In the sample PVPS-1, chalcopyrite is replaced by bornite and covellite wich are in turn replaced by chalcocite (Fig.15e,15g,15h). In the sample PVPS-16, covellite is replaced by chalcocite. In The sample PVPS-19 a quartz vein with presence of sulfates (possibly brochantite) were observed in interstices around fractured a pyrite (Fig. 15f), however no chalcopyrite was identified in the sample.. In the sample PVPS-21, chalcopyrite is replaced by covellite and chalcocite. It is no clear if the

Figure 12. Sulfides and molybdenite textures in biotite. Period II.

a) Poorly polished aggregate of chalcopyrite deposited in the interstices of biotite (PP, 10X). From polished section of figure 10b. Period II.

b) Poorly polished aggregates of chalcopyrite deposited in the interstices of biotite crystals (PP, 10X) From Sample PVPS-3 (Fig 10b). Period II.

c) Moderately polished aggregate of chalcopyrite deposited in the interstices of biotite crystals (PP, 10X) From polished section of figure 10b (PVPS-3). Period II.

d) Molybdenite and chalcopyrite deposited in the interstices of biotite crystals. A molybdenite crystal shows splitting along the cleavage plain and the possible presence of biotite in the space between. (PP, 10X). Polished section PVPS-3 (Fig. 10b). Period II.

e) Small cluster of adjoining or twinned molybdenite crystals in a biotite aggregate within the silicate gangue. (PP, 20X). Polished section PVPS-11. Period II.

f) Cluster of molybdenite crystals within calc-silicate gangue apparently without signs of alteration in or near the cluster. (PP, 20X). Polished section PVPS-14 (Fig. 10a). Period II.

g) Incompletely crossed nicol view of a chlorite's halo penetrating finger from a sulfide vein into its silicate host rock. The greenish color of the chlorite can be recognized, further the presence of some preserved biotite crystals within the chlorite halo and the deposition of pyrite at the core of the finger (incomplete XP, 5X). Polished section PVPS-5. Period II.

h) Aggregate of chalcopyrite crystals in a biotite cluster within the silicate gangue. (PP, 10X). Polished section PVPS-11. Period II.

(a)

(b)

(c)

(d)

(e)

(f)

(g)

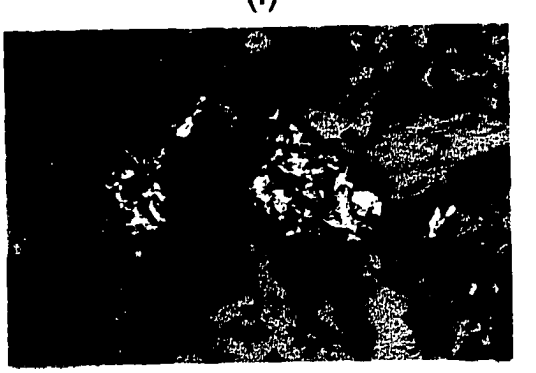

(h)

Figure 13. Mineragraphic textures and assemblages of the mineralization period II.

a) Inclusion of brownish-pinkish pyrrhotite and chalcopyrite in pyrite (PP, 40X). Polished section PVPS-2 (Fig. 10d). Period II.

b) Colloform-looking aggregate of porous pyrite formed from the decomposition of pyrrhotite. The development of concentric rings in the fine grained porous pyrite around what appears to be an idiomorphic crystal of quartz is clearly recognizable and seems to indicate a relatively fast decomposition of pyrrhotite. (PP, 10X). P. section PVPS-13 (Fig. 10g). Period II.

c) Complex sequence of destruction textures of pyrrhotite can be observed in this slide. Early decomposition of pyrrhotite with the formation of marcasite blades can be deduced from the presence of preserved pyrrhotite (yellow-light green) enclosed between a large grain of pyrite (white) with magnetite inclusions (gray) and the marcasite blades (light blue). This is followed by destruction of remaining pyrrhotite to a characteristicly reticulated intergrowth of magnetite and pyrite (rugged surface, right). Relict pyrrhotite preserved between marcasite blades is replaced by pyrite, which shows a finely porous surface. (PP, 40X). P. section PVPS-4 (Fig. 10e). Period II.

d) Inclusion of chalcopyrite and "birds eyes" intergrowth of bluish-white marcasite and yellowish-white pyrite (upper-central part) resulting from the decomposition of pyrrhotite, within pyrite. (PP, 40X). Polished section PVPS-17. Periods I-II.

e) Differences in the anisotropy colors under crossed nicols between pyrrhotite inclusion (brownish-pinkish inclusion), the first generation of arsenopyrite (bluish white inner domain) and a later arsenopyrite generation which constitutes the rim (purple-violet colored outer shell). (PP, 5X). Polished section PVPS-4. (Fig. 10e). Period II.

f) Example of chalcopyrite exsolution along crystallographic directions in sphalerite. The shape of the inclusions seems to be controlled by crystallographic directions as well. (PP, 40X). P. section PVPS-4 (Fig. 10e). Period II

g) Almost completely enclosed aggregate of chalcopyrite and pyrrhotite in late arsenopyrite. The enclosed chalcopyrite shows replacement by finely granular arsenopyrite. (PP, 40X). P. section PVPS-4. Period II.

h) Inclusion of medium gray sphalerite and chalcopyrite in silicate gangue. The more or less right angle contact between the two minerals and straight nature of the boundary between them suggests their unmixing or exsolution. (PP, 40X). PVPS-12. Period II.

(a)

(b)

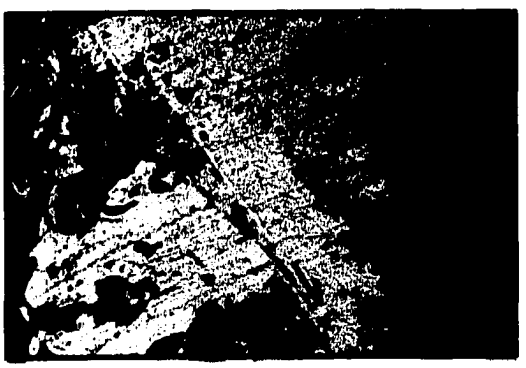

(c)

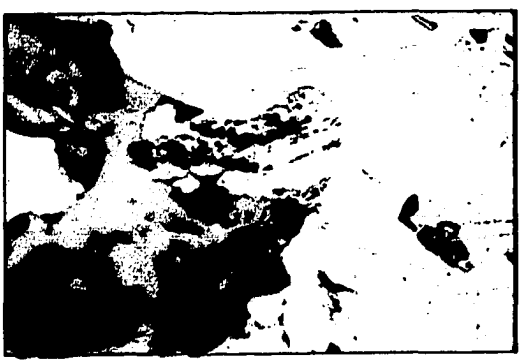

(d)

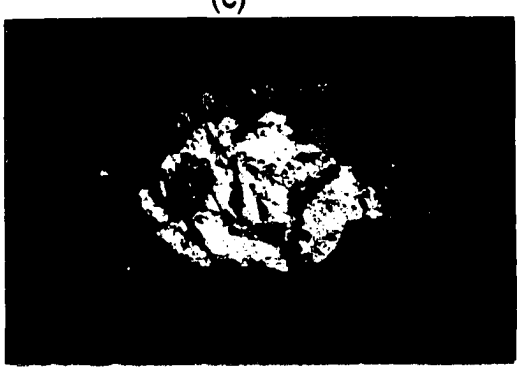

(e)

(f)

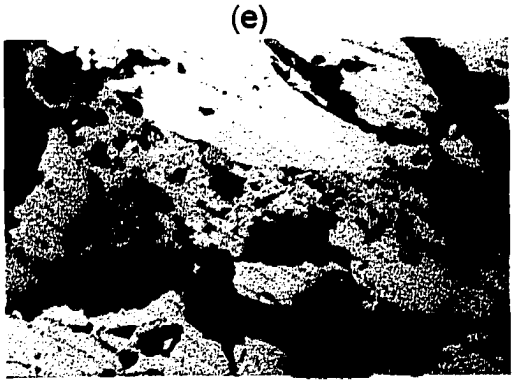

(g)

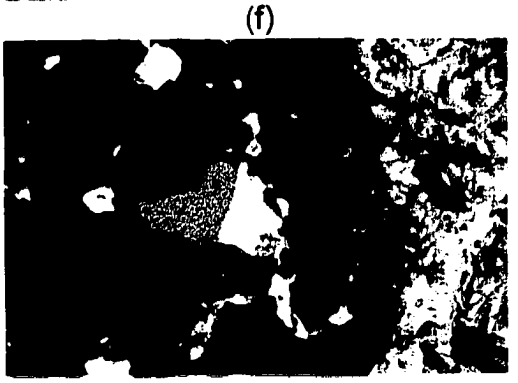

(h)

covellite is primary and related with the chalcopyrite mineralization or it is of supergene origin. However the relatively scarcity of covellite (in this sample) occurring principally in fractures suggest that it is a mineral of secondary origin.

Qtz-Py-Mo veins (period III)

The samples PVPS-7 and PVPS-8 consist of a quartz-molybdenite vein that cut to moderately to strongly quartz-sericite altered granodiorite phase, with local chlorite in the cores of possibly former plagioclase crystals (Fig. 10h, 10i). Chalcopyrite, pyrrhotite and sphalerite occur preferentially in the altered rock, whereas chalcopyrite, pyrite and molybdenite are present together in close proximity to chlorite in the quartz vein. Locally late pyrite has been observed filling up cracks in the gangue. A chalcopyrite vein, possibly associated with this late pulse of sulfide mineralization was encountered cutting to a sulfide vein in the sample PVSP- 5 (Fig.15a). This third period of sulfide mineralization is related, probably, to the intrusion of the quartz-feldspar porphyry (Tqfp). It is believed that part of the chalcopyrite associated with the quartz-molybdenite vein belongs, probably, to the former mineralizing events and was remobilized by this late quartz-molybdenite mineralizing pulse.

Supergene mineralization

Secondary copper mineralization at Piedras Verdes shows successive cycles of in-situ oxidation-leaching as well as chalcocite enrichment. Supergene copper oxide minerals

include chalcocite, chrysocolla, neotocite/tenorite, copper limonites, cuprite, native copper, and minor amounts of malachite, brochantite, libethenite, and azurite. The thickest chalcocite blanket was produced over the strongest pyirte concentrations and copper oxides formed in the central weak potassic and biotite stable zones (Fig. 16). More than one episode of leaching is suggested by overlapping of predominantly oxide over mixed oxide-chalcocite mineralization and enriched chalcocite zones at depth. In addition multiple episodes of enrichment are inferred from drill core where high-grade intervals alternate with low-grade to unenriched intervals. Subsequent episodic oxidation and mobilization of copper oxides and chalcocite occurred in densely fractured zones, principally at the intersections of major faults.

Age of mineralization

Age of mineralization associated with the granodiorite porphyries

Two pulses of hypogene copper mineralization occurred at Piedras Verdes. The age of the first event of hypogene mineralization is constrained by the Laramide age of the "tall" biotite granodiorite porphyry ($Tgdp_{tb}$) of 62 ± 1.6 Ma, obtained by K/Ar on biotite concentrate. Shortly after the first event of hypogene mineralization a second mineralizing pulse took place. This pulse was associated with the quartz-feldspar porphyry (Tqfp), which is also of Laramide age, based in that the latest magmatic event at Piedras Verdes was the emplacement of the andesitic dikes (48 ± 1.2 Ma), late Laramide time, which cut to the precedent porphyries.

Age of supergene enrichment

The age of the first stage of supergene enrichment at Piedras Verdes, is constrained by the age of andesitic dikes (48 ± 1.2 Ma), which show clay alteration, to Middle Eocene. It is well known that the first stage of supergene enrichment in most of the porphyry copper deposits of southwestern North America occurred during Eocene time. K/Ar dating of alunite, jarosite, and illite support this conclusion (Cook, 1994). Like the enriched blankets across the American southwest, the supergene enrichment at piedras Verdes was buried by Oligocene volcanic rocks and weathered again since the Paleocene time (Cook, op cit). At Piedras Verdes this event was related to Oligocene-Miocene voluminous explosion of ignimbrites that built most of the Sierra Madre Occidental (Coney, 1977; McDowell and Clabaugh, 1979). Cook (1994), also postulated that two post-volcanic stages of supergene activity occurred in the southwestern North America. The first stage of supergene enrichment was initiated by mid-Tertiay crustal extension which culminated with the formation of the metamorphic core complexes (Spencer and Reynolds, 1989). The second cicle of supergene activity was initiated by the late Miocene to Quaternary block faulting, the Basin and Range formation. Both of these tectonic events occurred also in Northwestern Sonora. At Piedras Verdes the latter event could be represented by the latest northwest striking faults that are widespread in the region (Wilkins, 1996). According to these events, it could be postulated that at least three stages of supergene enrichment have occurred at piedras Verdes deposit.

Figure 14. Mo-Cp, and Cp-Sph, and Cp replacing tourmaline. Period II and III.

a) Aggregate of molybdenite and chalcopyrite in silicate gangue. Notice a sliver of chalcopyrite at the edge of one of the molybdenite crystals. The illusion of a convex boundary on the side of the chalcopyrite is to an extent the result of the contact between the adjacent and partially enclosing silicate grain and the molybdenite crystal. More likely the two sulfides coexist, as has been observed in other samples. (PP, 20X). Sample PVPS-13(Fig 10g), Period II.

b) Aggregate of pinkish-tan , poorly polished pyrrhotite, medium to light gray molybdenite and minor chalcopyrite in a silicate gangue. The curved shape of the softer and better polished molybdenite crystals stands in contrast to the harder and poorly polished pyrrhotite and chalcopyrite. (PP, 10X). Sample PVPS-11. Period II.

c) Bluish medium gray crystal of molybdenite accompanied by medium gray rutile in silicate gangue with pyrite. The difference in the polishing hardness between molybdenite and rutile can be observed. (PP, 20X) Sample PVPS-2 (Fig. 10d), Period II.

d) Aggregate of chalcopyrite and sphalerite formed within the intrusive host rock of a quartz-molybdenite vein. (PP, 20X). Sample PVPS-8a (Fig. 10h), Period II.

e) Radiate aggregate of dark gray tourmaline with poorly polished aggregates of chalcopyrite and minor pyrrhotite in the interstices of the tourmaline. (PP, 5X). Sample PVPS-12, Period II.

f) Close up view of acicular the tourmaline. This slide and 14e suggest the formation of tourmaline probably in the presence of biotite during or prior to what is considered to be early mineralization, rather than formation during late quartz-sericite-pyrite alteration. (PP, 10X). Sample PVPS-12. Period II.

g) Contrasting view of molybdenite crystals at the contact between intrusive host rock and a pyrite-anhydrite ± quartz veinlet, and within the intrusive host away from the contact, here accompanied by chalcopyrite and pyrite. The observed differences in the appearance of molybdenite can be attributed to alteration caused by the fluids responsible for the formation of the veinlet, however this image presents a relatively fresh, if only splayed molybdenite crystal in contact with vein quartz on one side, and more dulled and irregular molybdenite in contact with anhydrite on the other side of the vein. (PP, 10X). Sample PVPS-11. Period III.

h) Late pyrite-anhydrite ± quartz veinlet. Observe the dull gray and irregular aggregate of molybdenite in contact with the late pyrite, which stands in sharp contrast to better crystallized molybdenite seen in other samples within the intrusive host rock. This suggest the possibility of a second generation of molybdenite. (PP, 20X). Sample PVPS-1. Period III.

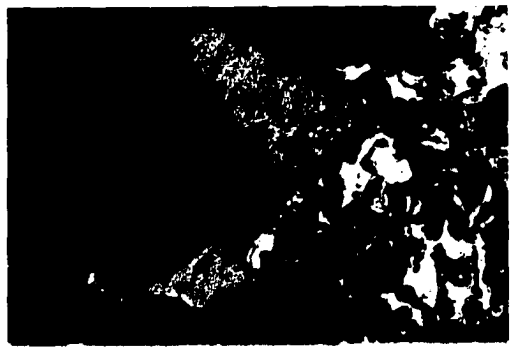

(a)

(b)

(c)

(d)

(e)

(f)

(g)

(h)

Figure 15. Qtz-Mo veins, Period III, and some supergene alteration textures.

a) Late chalcopyrite veinlet cutting pyrite within the sulfide vein. (PP, 20X). Polished section PVPS-5 (Fig. 10f), Period III.

b) Aggregate of molybdenite in a quartz gangue. In this image it can be seen that molybdenite forms preferentially following cracks within the quartz vein, in contrast with the following sample where molybdenite appears to form around chlorite clusters. (XP, 5X). PVPS-8b (Fig. 10I), Period III.

c) Aggregate of molybdenite crystals formed around a silicate (possibly chlorite) within the quartz molybdenite vein. (incomplete XP, 5X). Sample PVPS-8a (Fig. 10h), Period III.

d) Aggregate of molybdenite crystals formed around a former mafic site within the intrusive host rock to a quartz-molybdenite vein, indicated by the presence of chlorite (incomplete XP, 10X). Sample PVPS-8a (Fig. 10h), Period III>

e) Light bluish gray chalcocite replacing orange-colored, tarnished chalcopyrite under supergene conditions, also visible is a medium-dark gray radiated aggregate of goethite (PP, 20X). Sample PVPS-1. Supergene alteration.

f) View under partially crossed nicols of reflecting yellowish-white pyrite and the bluish inner reflections of supergene copper sulfate, possibly brochantite, easier to observe under crossed nicols. (partially XP, 20X). Sample PVPS-19. Supergene alteration.

g) View of an intergrowth of chalcopyrite, bornite, covellite and chalcocite formed at the edge of a large fractured pyrite aggregate. It appears that the formation of these supergene minerals is accompanied by the formation of small idiomorphic crystals of pyrite within more or less clear quartz in the gangue. (PP, 40X). Sample PVPS-1. Supergene alteration.

h) Detailed view of the intergrowth between chalcopyrite, bornite, covellite and chalcocite between chlorite blades. Bornite seems to form exclusively in sites between chlorite crystals in comparison to covellite, which forms at those sites but also in contact with the exterior quartz gangue. (PP, 40X). Sample PVPS-1. Supergene alteration.

(a)

(b)

(c)

(d)

(e)

(f)

(g)

(h)

Ore type distribution

The characteristics of the supergene copper mineralization change from West to East across the Piedras Verdes deposit, depending on structural preparation, rock type and the original amount of sulfides at depth. For this purpose the deposit can be broken down into four domains (Fig. 16). The northwest-striking Tepustete fault marks the limit between the West and East parts, while the East-West fault is the limit between the North and South parts (Fig. 4). Most of the supergene orebody occupies the northern part of the deposit area. On the Northwest side (Cerro Cinco), the enrichment zone consists chiefly of copper oxides, including chrysocolla, tenorite/neotocite, malachite, brochantite, and minor limonite copper, averaging 0.50% total copper with only traces of chalcocite at depth. In the North-central part, and adjacent to the Tepustete fault within the village area, secondary copper consists of limonite copper, chrysocolla, cuprite, and native copper, which are justapoxed to a chalcocite zone at depth, that averages 0.58% total copper. Two oxidation-enrichment events are observed in this sector. The new episode of oxidation and remobilization of copper oxides was facilitated by the intersection of the Tepustete fault with the east-west major structural zone. East of the Tepustete fault, on the North-east part (Cerro La Cueva) the best chalcocite enrichment was found, averaging 0.50-0.80% total copper. The chalcocite blanket is overlain by small copper-oxide zones within leached cap (Fig. 17). These copper-oxide zones are interpreted as an earlier formed chalcocite blanket. Deep leaching and oxidation along penetrative structures generated limonite copper that is often mixed with minor copper

oxides and remnant chalcocite veins at depth, along the main east-west fault. The chalcocite veins are often high-grade, averaging 3-6% total copper. The origin of these veins may be due to remobilization of chalcocite from a previous enrichment zone to a deeper oxidation zone. South of the Cerro La Cueva (Cerro Ocho), is another chalcocite zone that is hosted in pyritic intrusion breccia, which again supports a strong structural control of supergene enrichment accumulation.

Discussion of the ore distribution

As was explained above, in the western part of the deposit, supergene mineralization is constituted mainly by copper oxides, whereas in the eastern part by chalcocite (Fig. 16). This distribution is due to differences in the mineral composition of the host rocks or by changes in the abundance of sulfides beneath the copper enriched zones. Figure 20 shows a Eh-pH diagram with the most important copper minerals present at Piedras Verdes porphyry copper deposit. Arrows 1 and 2 show the two proposed fluid evolution paths responsible for the formation of secondary copper minerals at Piedras Verdes.

Arrow 1, indicates the evolution path of a fluid enriched in Cu^{++} that moved through a rock that does not consume H^{+}, therefore pH remains constant but Eh changes as the fluids move downward, until the point where they reach the water table and the conditions become more reducing. As a result, chalcocite and covellite are formed, leaving close to the paleosurface only limonites. In Piedras Verdes this type of

mineralization is developed in areas dominated by quartz-sericite and weak potassic alteration (chalcocite zones in the deposit) (Fig.17).

Arrow 2, indicates the paths of a fluid where the conditions of Eh remain almost constant but pH increases. These conditions produce the precipitation of copper as sulfate, oxides, carbonates or silicates. This type of mineralization does not necessarily represent leaching and redeposition of copper minerals with significant movement of copper from its original location. In Piedras Verdes, this type of mineralization is present in the western part of the deposit (Fig. 18). This is where "gneissic" units, containing considerable amount of biotite (60%), are the principal host rocks. When the fluids interact with this potassium-rich rocks, the acidity of the fluid decreases by the consumption of H^+ by minerals like biotite or chlorite.

A second explanation to this supergene distribution is the sulfide amounts of the protore beneath the supergene mineralization. It is notable from mapping and drill core that the content of primary sulfides increases in the east part of the deposit. These conditions allowed for the production of more sulfuric acid, enhanced the leaching of the copper minerals and allowing to the formation of chalcocite blankets (process also indicated by Anderson, 1982). The increment in the amount of sulfides in the eastern part, could be due to the emplacement of the quartz-feldspar porphyry, which introduced more pyrite to the system.

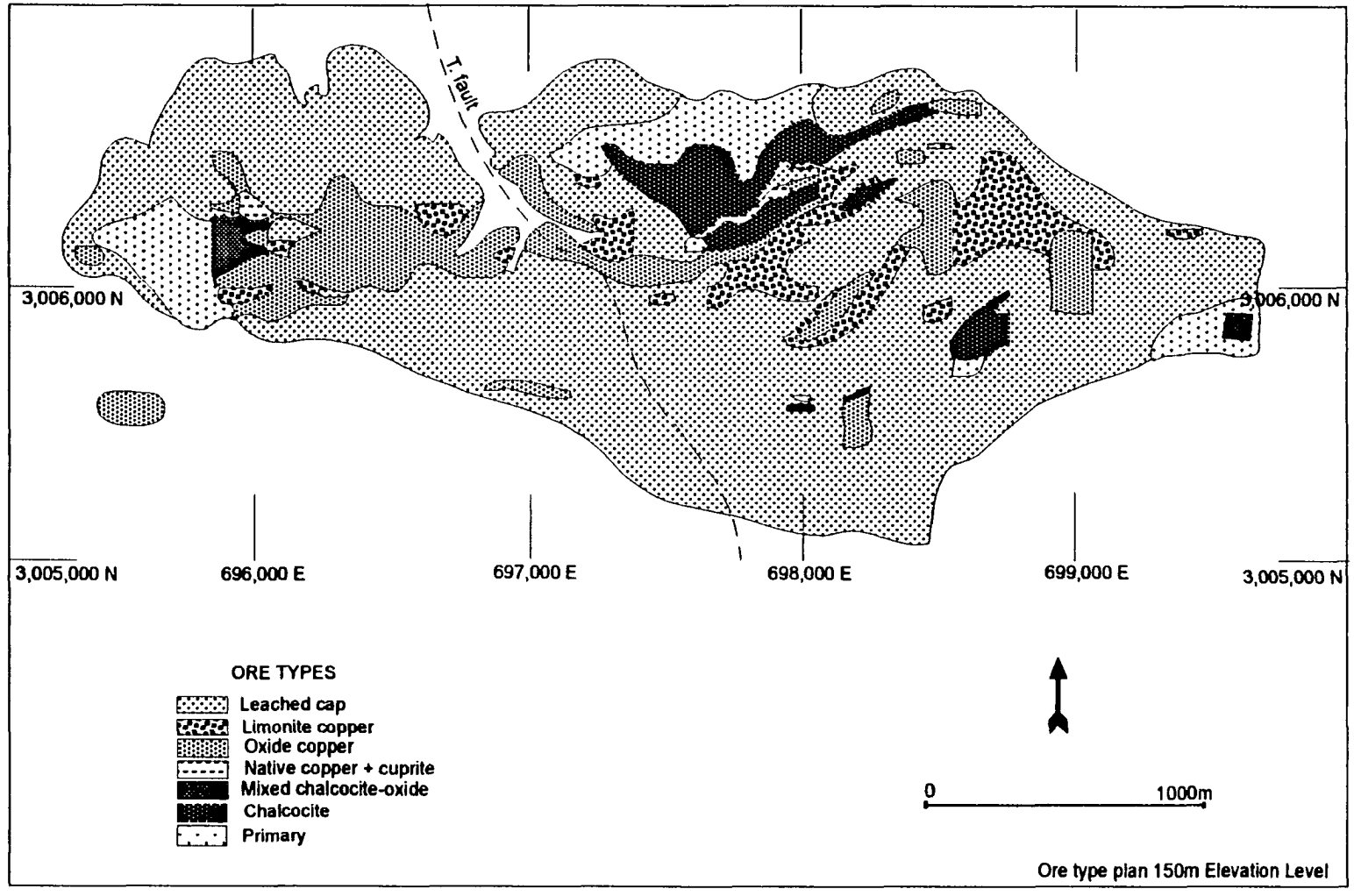

Fig. 16. Ore type plan, 150 m Elevation Level of Piedras Verdes Deposit, Sonora Mex, showing the chalcocite distribution. The West side of the deposit (west part of the Tepustete fault) is mainly copper oxides and the East side is oxides+chalcocite. See text for explanation.

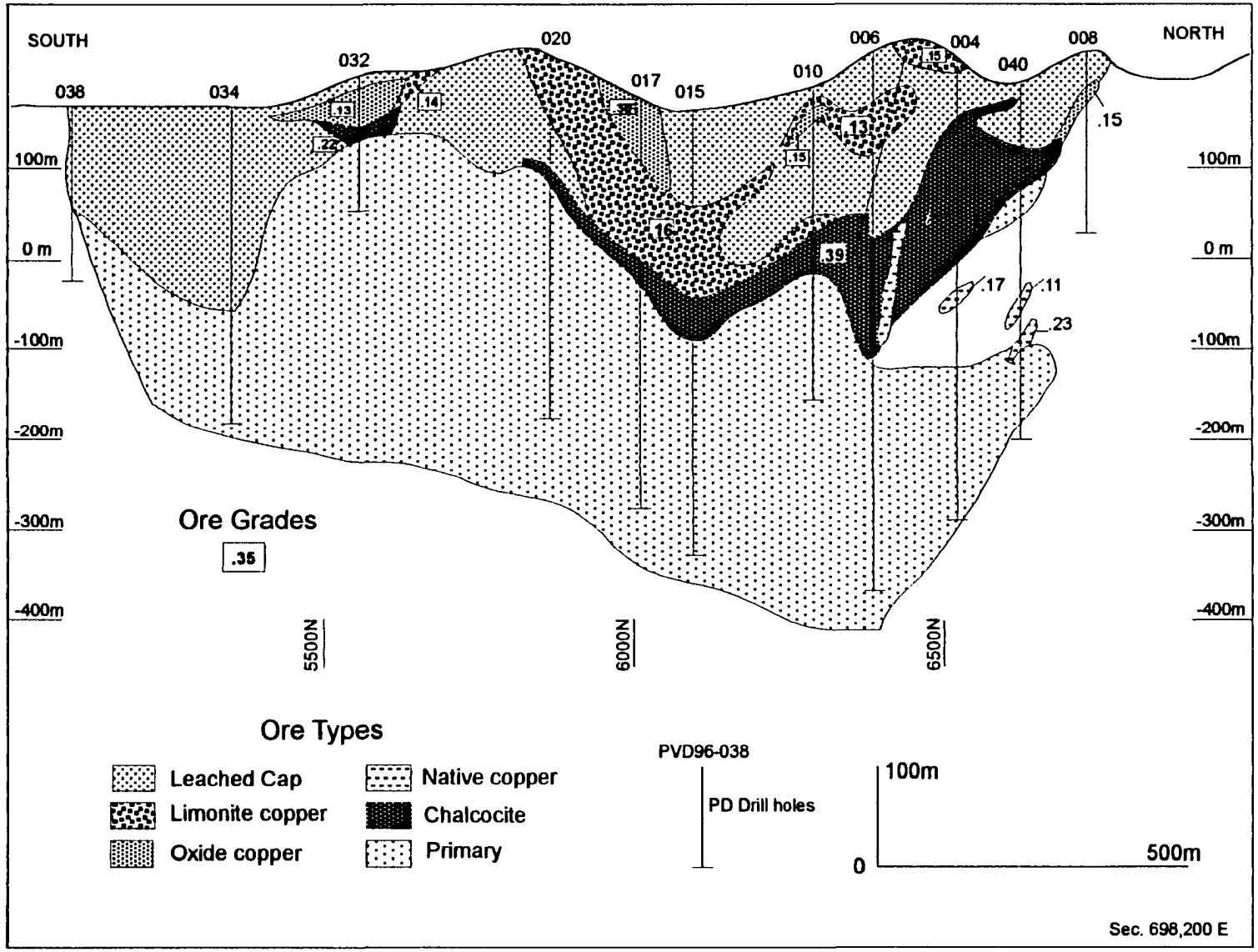

Fig. 17. North-South ore type section, 698,200 E. Typical ore distribution of the eastern side of Piedras Verdes Deposit, Sonora Mexico.

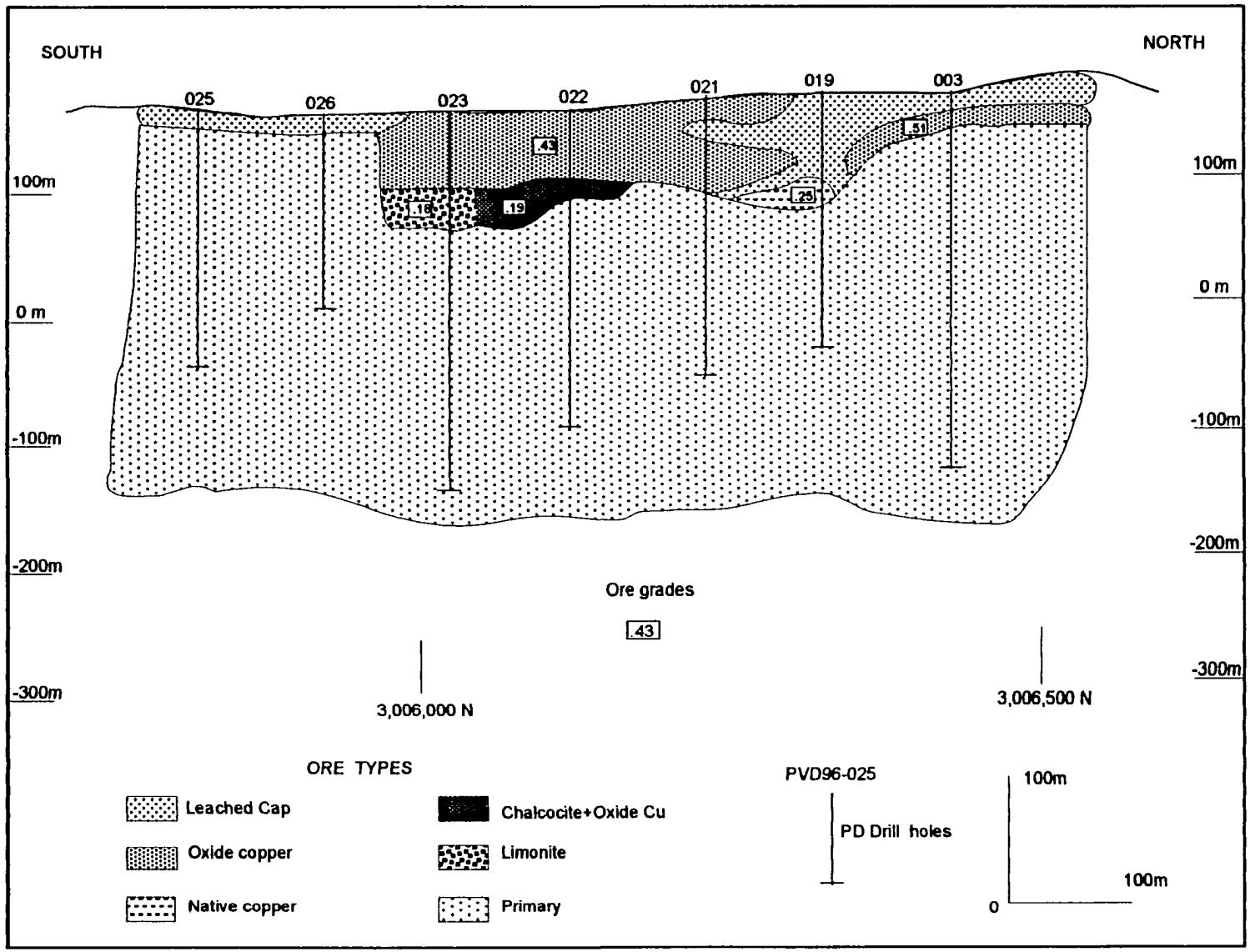

Fig. 18. North-south ore types section, 696,400 E. Typical ore types distribution of the western part of Piedras Verdes deposit, Sonora, Mexico.

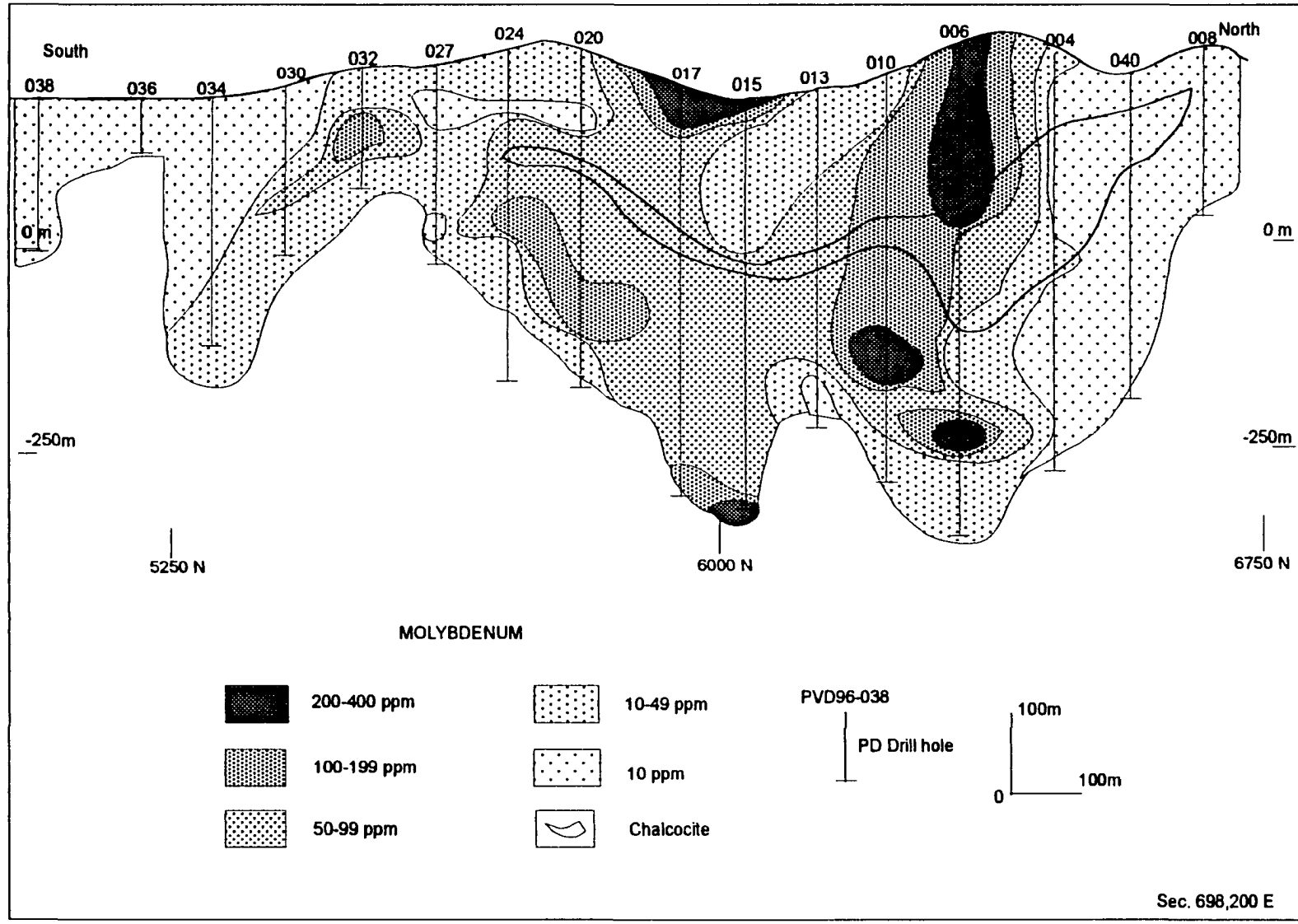

Fig. 19. North-South section, 698,200 E, showing molybdenum distribution of the Piedras Verdes Deposit, Son., Mex.

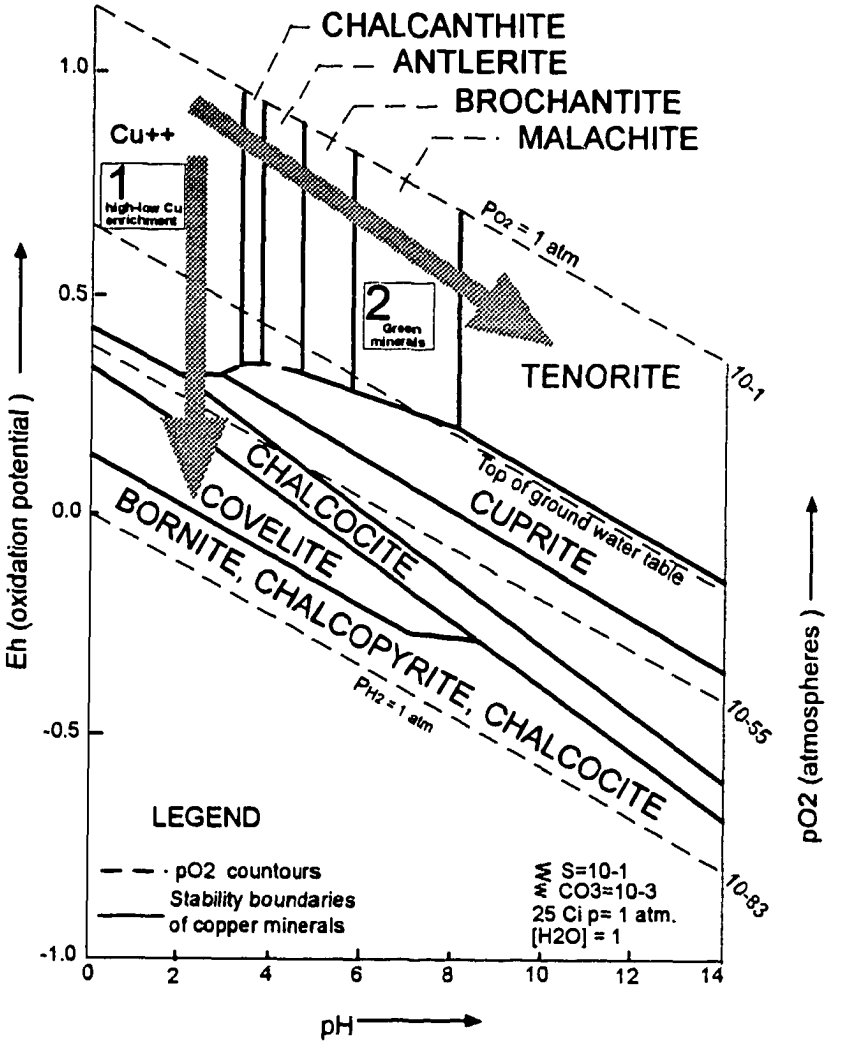

Fig. 20. Eh -pH diagram showing the stability fields of copper minerals in the system Cu-S-H_2O. The arrows represent the path of the fluid that formed high-low enrichment and the green copper mineral assemblages at Piedras Verdes deposit. The area between P_{O_2} and P_{H_2O} limits is the H_2O stability field (From Anderson, 1982).

GEOCHEMISTRY

Sampling and analytical methods

The lithology, location and numbers of the samples used for the geochemical Study presented here, are listed in Table 6. The samples are from drill core and outcrops around and within the project area. All the different intrusive phases of the Piedras Verdes Intrusive Complex were sampled. Some of them belong to the same unit, but have distinct textures. An effort to take samples of rocks, which were not altered or having lesser grades of alteration, was made. This was possible by taking samples from the deepest drill holes and from outcrops outside of the deposit area. However, most of the rocks in the main mineralized area are altered. It is worthy to mention that a sample from the Alamos Batholith granite was taken along the road from the town of Alamos to the Piedras Verdes deposit. This sample correlates with the granodiorite (Kgd) at Piedras Verdes, since they both show very similar geochemical signatures.

The samples were analyzed at XRAL Laboratories in Ontario, Canada. The analytical methods were, for the major elements by X-ray Fluorecence techniques, for the REE elements by ICP-MS and for Hf by Neutron Activation (INAA).

Major elements

Representative chemical analyses and the CIPW norm calculation for the PiedrasVerdes granitoids are listed in table 1. The CIPW norm was calculated to 100%

Table 1. REPRESENTATIVE CHEMICAL AND C.I.P.W. NORMATIVE ANALYSES OF PIEDRAS VERDES INTRUSIVE SUITE

	AlamBatho	Kgd (PV)	Tqd	Tgdptb	GdBuffel	MDChato	MDBuffel	Tqfp	Tgdpx
Wt%									
SiO_2	65.9	63.3	55.7	67.6	65.3	62.5	60.5	70.36	67.1
Al_2O_3	15.6	15.5	17.9	15.5	16	16.3	16.7	12.33	15.6
CaO	4.48	4.56	7.57	3.75	5.39	5.12	6.23	1.55	2.4
MgO	2.14	2.11	3.71	1.55	1.92	2.36	2.99	1.17	1.36
Na_2O	3.65	3.28	3.27	3.61	3.81	3.16	3.17	2.33	3.66
K_2O	2.38	2.86	1.02	2.62	3.03	2.57	2.14	5.4	2.93
Fe_2O_3	4.34	5.09	7.68	3.39	2.63	5.58	6.45	2.68	2.37
MnO	0.06	0.05	0.12	0.03	0.04	0.09	0.1	0.01	0.01
TiO_2	0.569	0.63	0.954	0.463	0.585	0.716	0.819	0.38	0.542
P_2O_5	0.13	0.13	0.22	0.13	0.18	0.18	0.19	0.13	0.1
LOI	0.75	1.05	0.9	0.75	0.65	1	0.2	2.83	2.65
TOTAL	99.999	98.56	99.044	99.393	99.535	99.576	99.489	99.17	98.722
NORMATIVE MINERAL									
Q	23.9875	22.0814	13.4604	26.7916	19.8717	21.035	18.1776	32.4494	28.6868
Or	14.1977	17.3645	6.1493	15.727	18.1411	15.4402	12.761	33.1715	18.065
Ab	31.1193	28.4634	28.1933	30.9673	32.603	27.1255	27.016	20.465	32.2364
An	19.2842	19.5955	31.7361	18.3269	17.788	23.0123	25.1847	7.4463	11.9876
C	0	0	0	0.0955	0	0	0	0.015	202684
Il	0.1293	0.1097	0.2616	0.0651	0.0865	0.1953	0.2154	0.0222	0.0223
Ap	0.3033	0.3087	0.5191	0.3052	0.04215	0.4228	0.4431	0.3125	0.241
En	5.37	5.3892	9.4146	3.9134	3.154	5.9623	7.487	3.0246	3.5256
Rutile	0.1405	0.1578	0.65	0.4351	0	0.3544	0	0.3827	0.5299
Sphene	0.895	1.0565	1.8878	0	1.3399	0.6604	1.7458	0	0
Zr	0.0223	0.032	0.0281	0.0245	0.0309	0.0356	0.0332	0.0213	0.0311
Diopside	0	0	0	0	3.6276	0	0.028	0	0
TOTAL	95.4491	94.5587	92.3003	96.6516	96.68485	94.2438	93.0918	97.3105	97.594

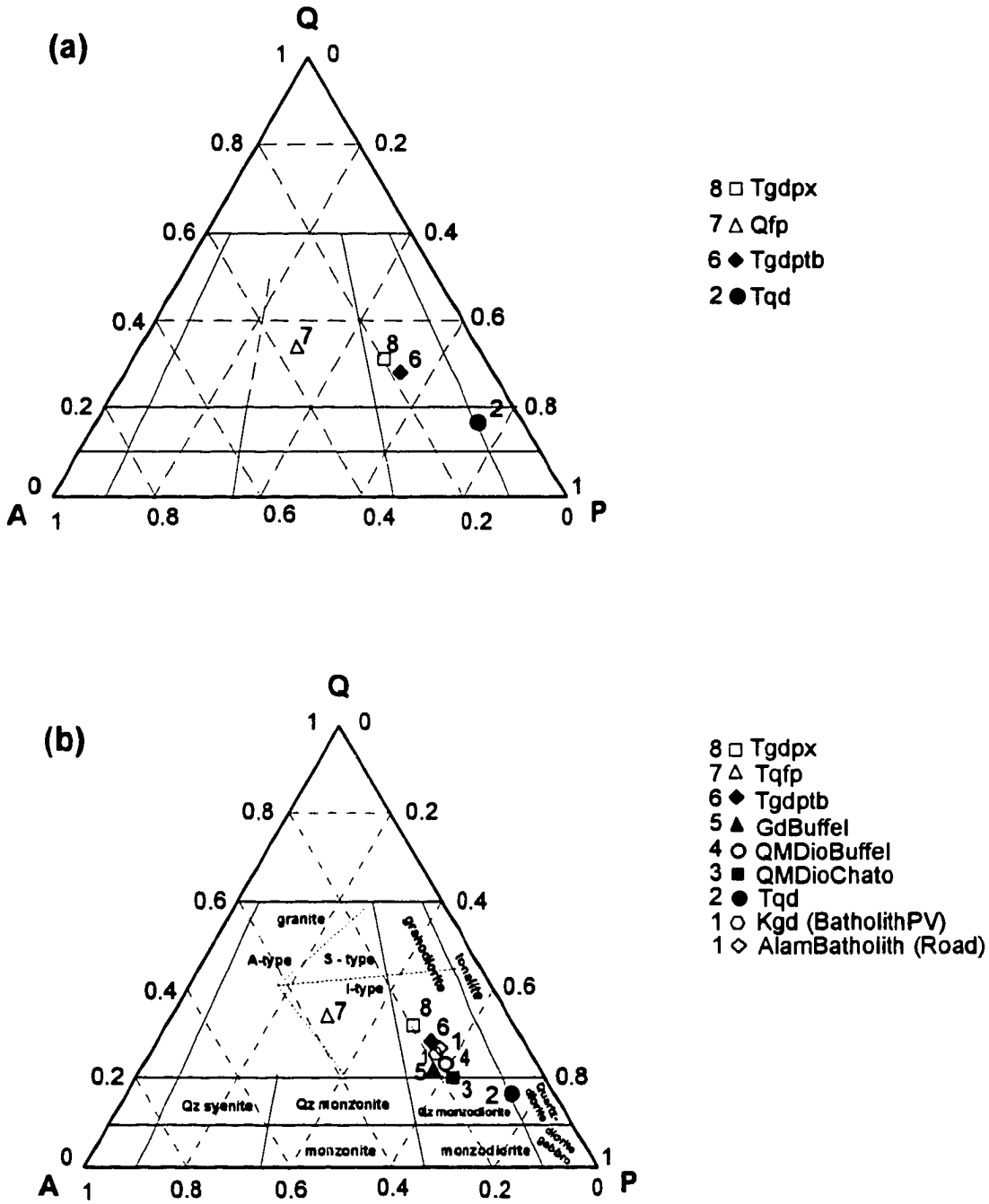

Fig. 21. Composition of the Piedras Verdes intrusive rocks. Modal classification boundaries from Streckeisen (1973) and fields of I-, S-, and A-type granites from Bowden and others (1984). a) shows the composition of the four main porphyry phases and b) shows all the intrusive suite.

anhydrous and used to construct the Streckeisen diagram in the figure 21.

Harker variation diagrams for all the plutonic rocks present at Piedras Verdes are shown in the figure 22. The Alamos Batholith granodiorite (AlamBatholith) is the oldest rock, and the biotite-hornblende granodiorite dikes (Tgdpx) the youngest rocks, excluding the youngest thin andesite dikes at the Piedras Verdes dposit, whose values are not plotted in these diagrams. Fe_2O_3, MgO, TiO_2, CaO, Al_2O, K_2O and Na_2O are plotted in order of increasing silica. TiO_2, MgO, CaO, K_2O, and Na_2O trends for the Piedras Verdes intrusive suite show the expected systematic fractionation trend (Fig. 22). This geochemical behavior indicates that the Piedras Verdes intrusive rocks, beginning with the Tertiary quartz monzodiorite (Tqd), did not fractionated from the Alamos Batholith. The geochemistry of the Tqd phase corresponds to a less evolved magma source than the granodiorite of the Alamos Batholith. The batholith granodiorite (AlamBatholith and Kgd) is more felsic than subsequent quartz monzodiorite event, which indicate that the porphyry suite of Piedras Verdes was not derived from the Alamos Batholith. In addition Harker variation diagrams for the four main intrusive phases show that the biotite-hornblende granodiorite dikes (Tgdpx), did not fractionated from the quartz-diorite (Tqd) to quartz-feldspar porphyry (Tqfp) (Fig.23). This trends show that the "tall" biotite granodiorite (Tgdptb), and (Tqfp) porphyries evolved from the quartz monzodiorite event.

A K_2O versus SiO_2 diagram shows that all the intrusive suits are Medium-K calc-alkaline (fig.24). According to Shand's index they are mainly metaluminous, only

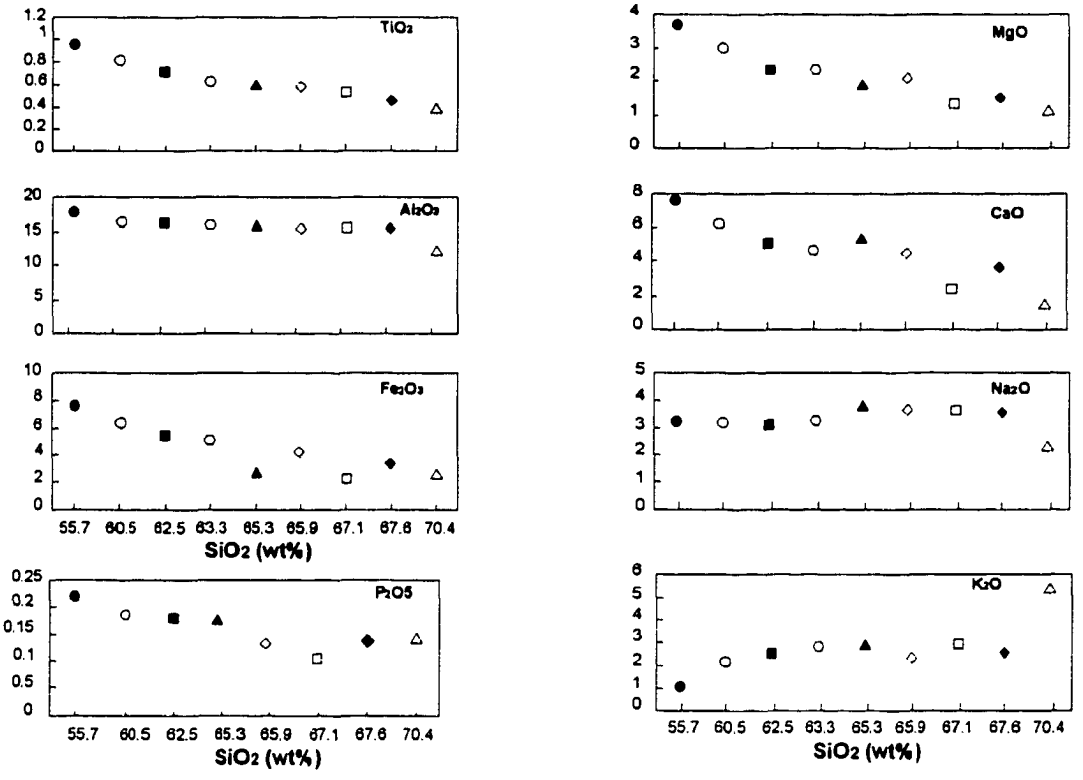

Fig. 22. Harker silica variation diagrams of major elements from all samples of the Piedras Verdes intrusive sequence. Explanation shows the relative age of these intrusive rocks.

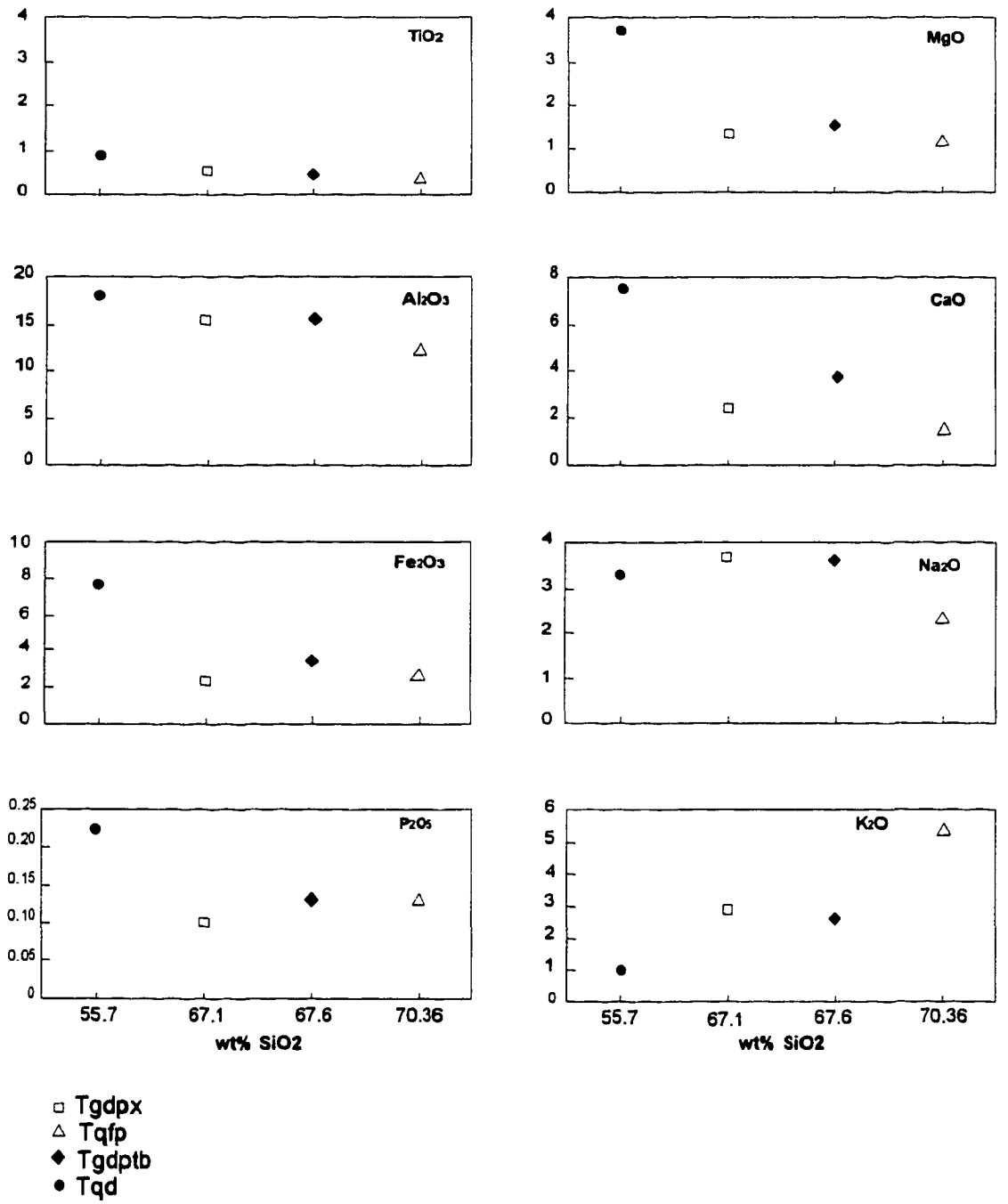

Fig. 23. Harker variation diagrams for the four main intrusive phases of the Piedras Verdes porphyry suite.

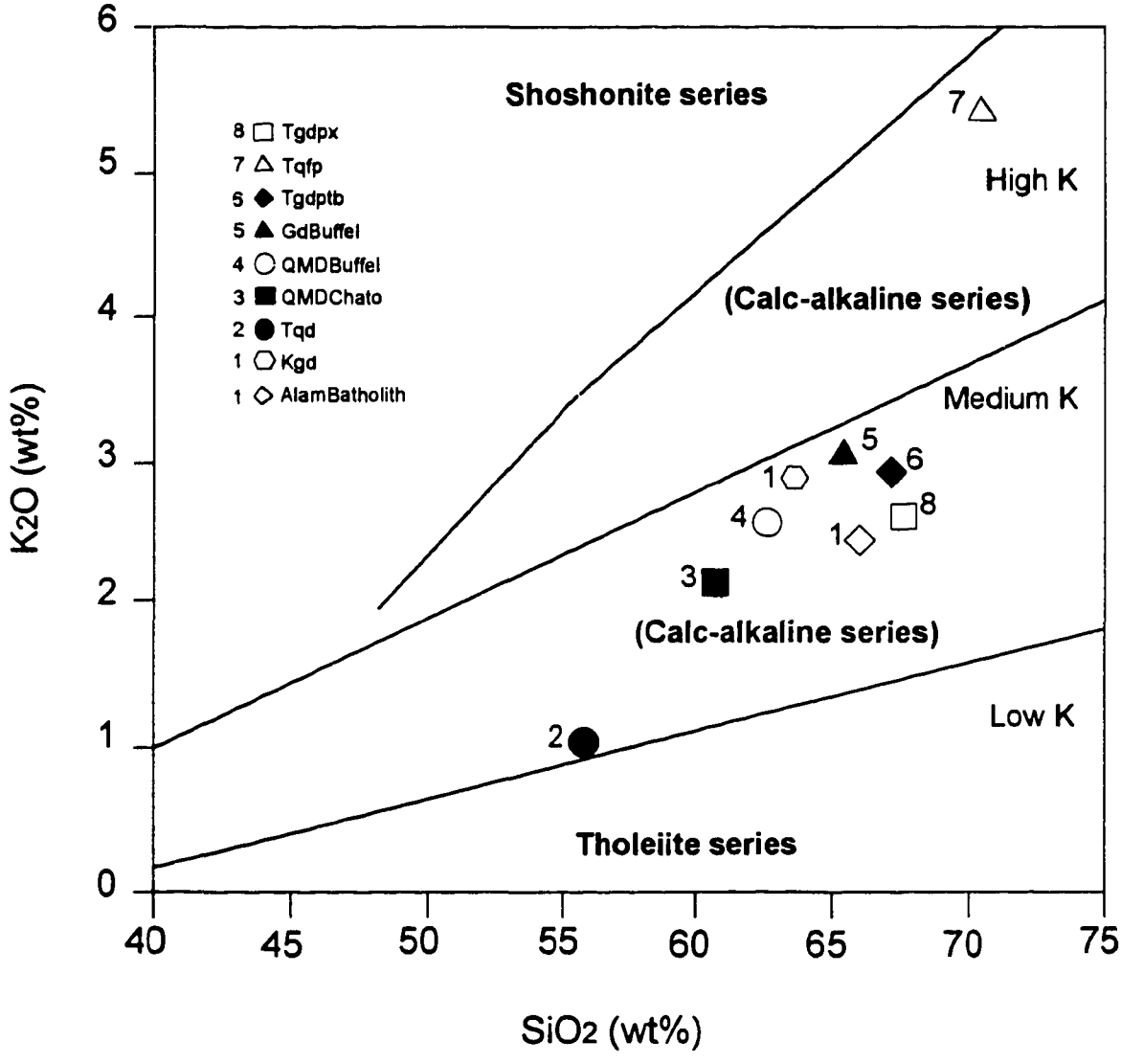

Fig. 24. K_2O versus silica content of the Piedras Verdes intrusive suite. Note that only the Tqfp falls in the hifh-K calc-alkaline series. All of the intrusive rocks of Piedras Verdes intrusive suite fall in the medium-K calc-alkaline series.

one sample Tgdpx falls in the peraluminous field, as it is shown in an Al_2O_3 / (CaO + Na_2O + K_2O) versus Al_2O_3 / (Na_2O + K_2O) (molar) diagram (fig.25). The same diagram shows that the compositions of these intrusive rocks are typical continental granitoids, even though the Piedras Verdes quartz monzodiorite to quartz feldspar porphyry suite exhibits island arc charcteristics.

Figure 26 (Lang, 1995) shows that Piedras Verdes porphyries fall mainly within the High-K calc-alkalic and only one sample, Tqfp, in the calc-alkalic (Arizona calc-alkalic) fields. This suggests that the Arizona porphyries are more evolved than those of Piedras Verdes. The Na_2O/K_2O ratios values indicate that the Piedras Verdes intrusive suit has signature similar to those intrusive rocks of the Cortez terrane (Valencia et al., 1999).

Trace elements

Trace element compositions of the intrusive rocks at Piedras verdes have by Rb, Sr, Y, Nb, Zr and Ba values characteristic of granodiorite-diorite compositions (Hall, 1996) (Fig. 27). The Lu/Hf ratio is 0.068 which is characteristic of continental granitic rocks (Henderson, 1984 and Faure, 1986). The tectonic discrimination as suggested by Pearce et al., 1984, indicates that the granitoids at Piedras Verdes are of volcanic arc (VAG) affinity, as it is shown in the Y + Nb (ppm) versus Rb (ppm) diagram in the figure 28. Likewise, a plot of SiO_2 versus Rb shows that these rocks are arc-related (Fig. 29).

Rare earth elements (REE)

Chondrite normalized REE abundances, are plotted in figure 30 based in Orgueil

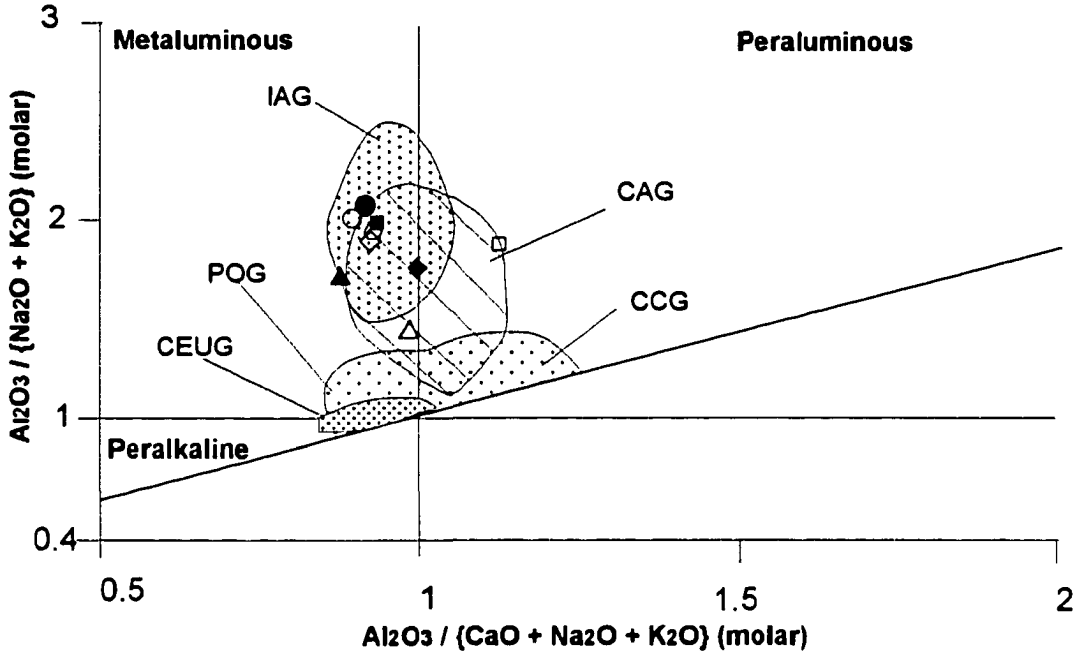

Fig. 25. Shand's index. Characteristics of the Piedras Verdes granitoids. Note the arc affinity of these granitoids. Island arc granitoids (IAG), Continental arc granitoids (CAG), Continental collision granitoids (CCG), Post-orogenic granitoids (POG), Continental epeirogenic uplift granitoids, rift-related granitoids (CEUG).

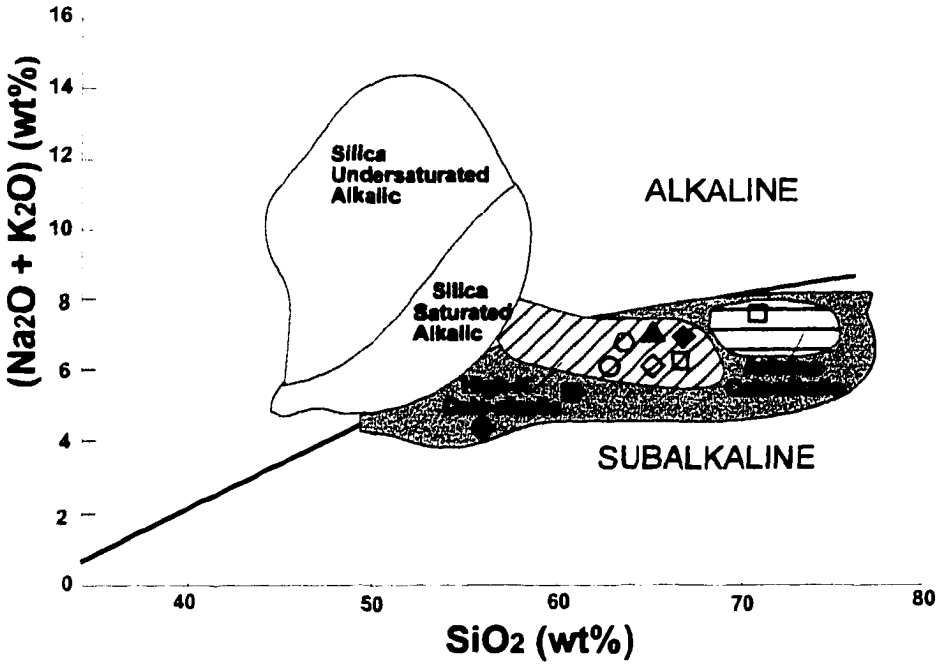

Fig. 26. Alkalis versus silica content of the igneous rocks from Piedras Verdes deposit. Note the high-K affinity of the main porphyries at Piedras Verdes. Only theTqfp falls in the calc-alkalic field similar to some porphyries from Arizona. Lang (1991).

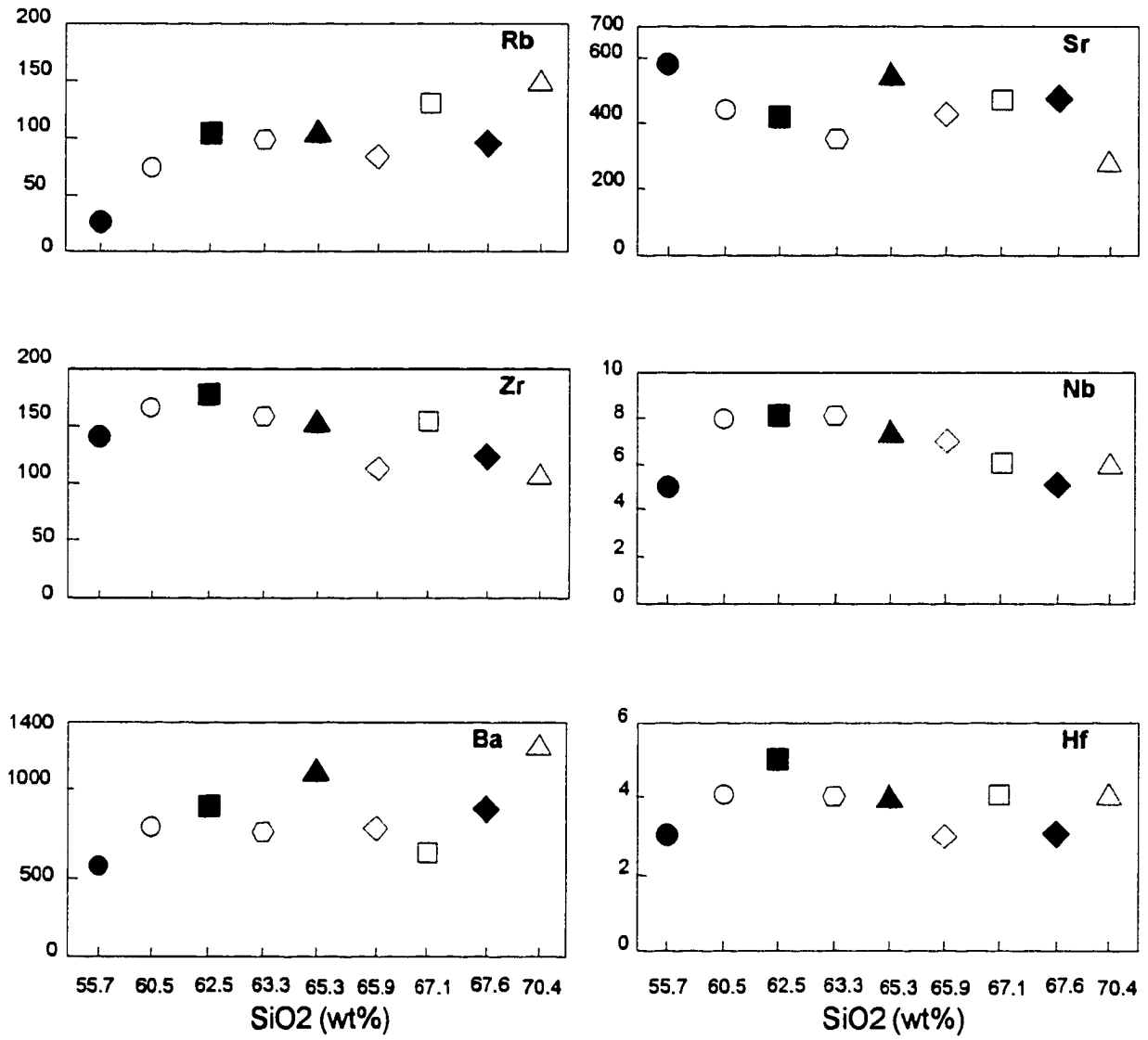

Fig. 27. Harker variation diagrams of some trace elements (ppm) for all the Piedras Verdes intrusive suite. Symbols as in previous figures.

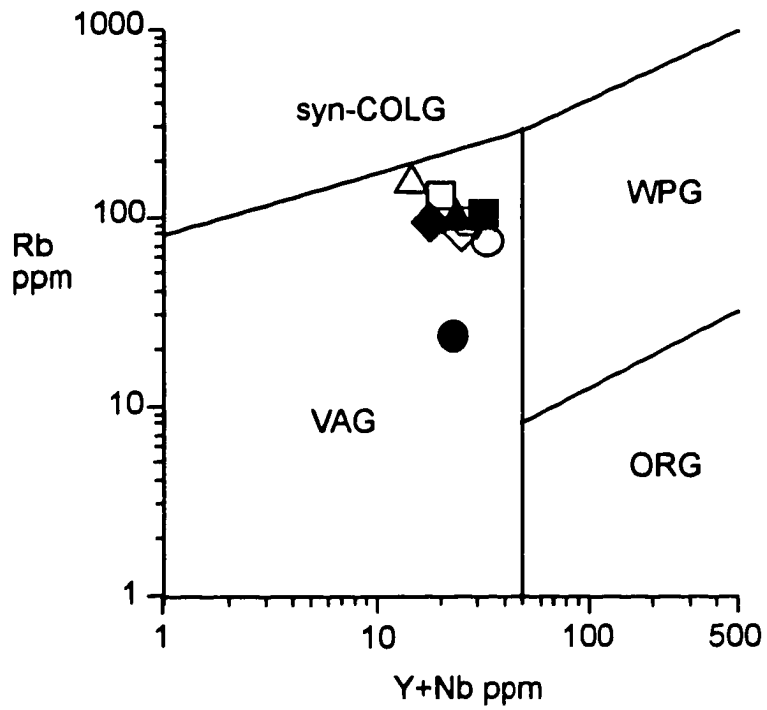

Fig. 28. Rubidium versus Yttrium plus Niobium discrimination diagram for the Piedras Verdes intrusive suite (from Pearce et al., 1984). (VAG) volcanic arc granites -oceanic and continental-, (WPG) within plate granites, (ORG) ocean ridge granites and (COLG) collisional granites.

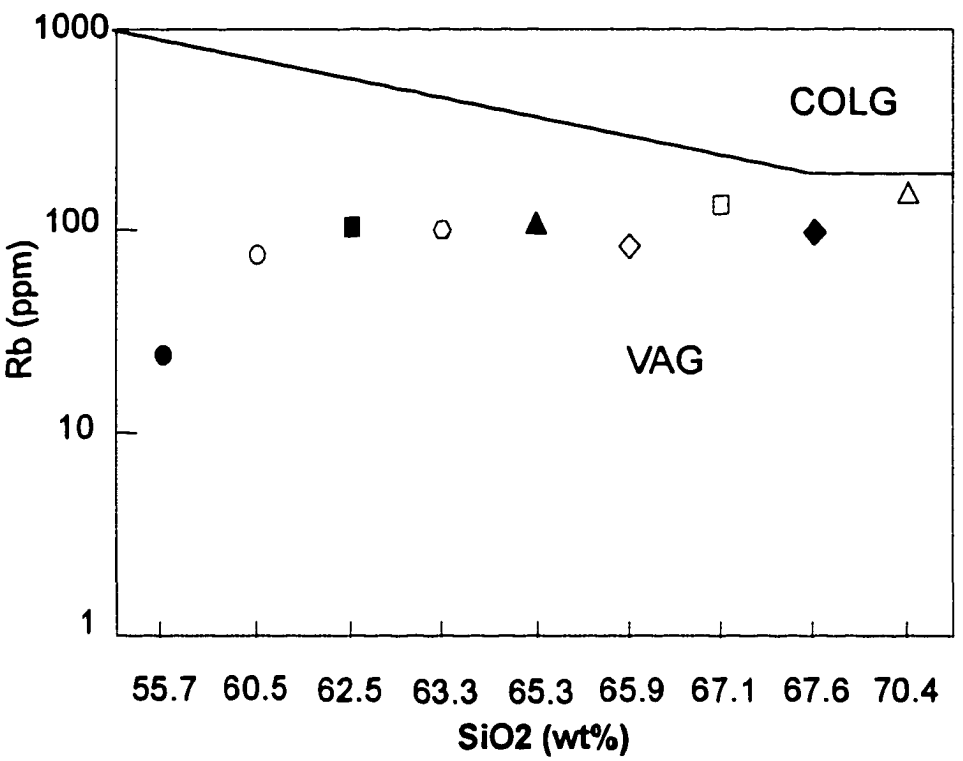

Fig. 29. SiO_2 versus Rb diagram of the Piedras Verdes intrusive sequence. Note the arc affinity of these intrusive rocks. Volcanic arc granitoids (VAG) and Continental collision granitoids (COLG).

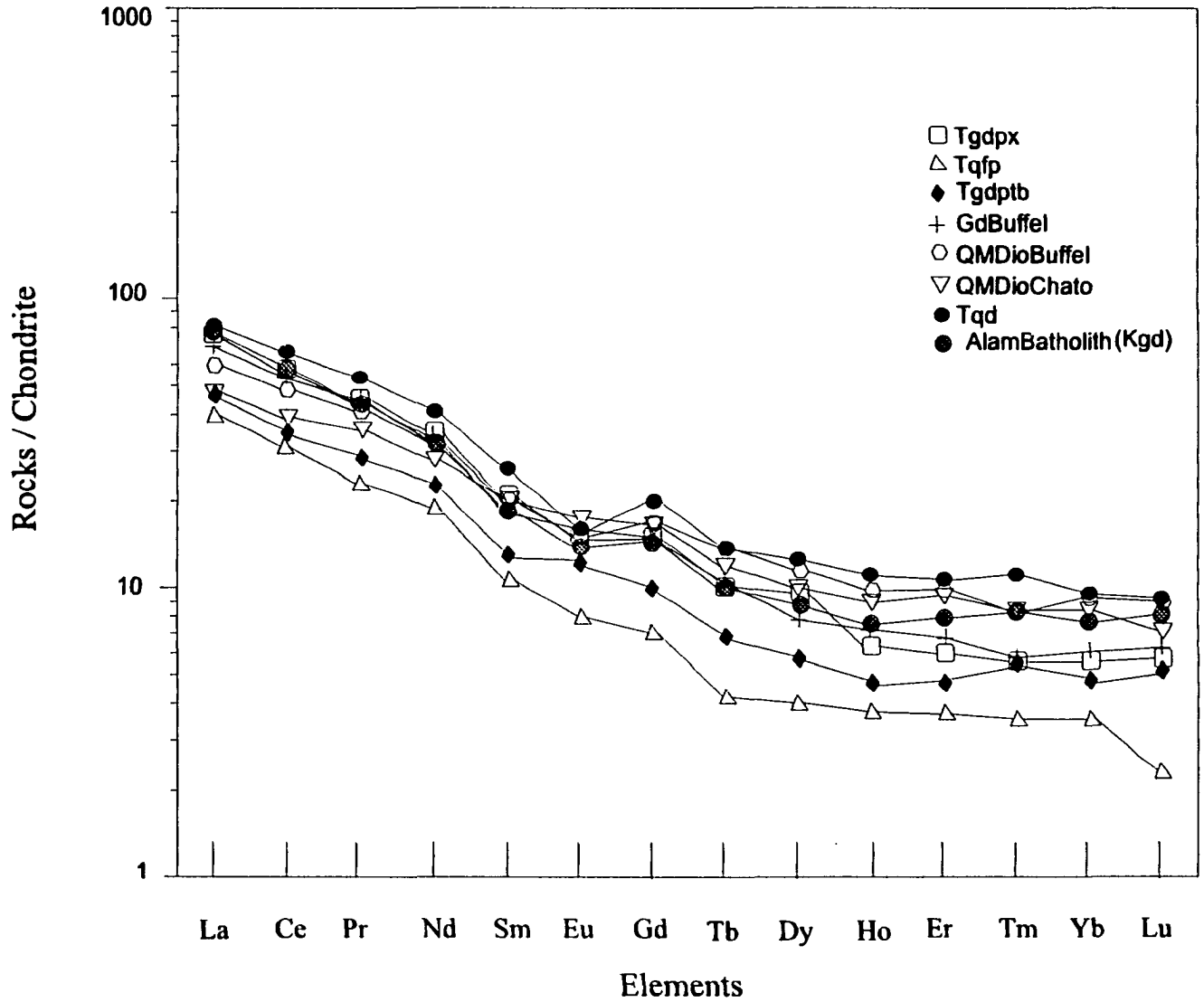

Fig. 30. REE patterns of the Piedras Verdes intrusive suite. See text for explanation. The values for Gd in Tqd, for Lu in Tqfp, and for Tm in Tgdptb are analytical errors.

TABLE 2. REPRESENTATIVE RARE EARTH AND TRACE ELEMENT DATA OF PIEDRAS VERDES INTRUSIVE SUITE

	Tgdptb	Tgdptb2	GdBuffel	Tgdpx	Kgdf-creek	AnddikesAB	Kgd (PV)	AnddikesP	AlamBatho	Tqd	MDioChato	MDioBuffel	Tqfp
La	17.4	22.1	25.4	28.3	40.6	37.3	22.6	14.5	29	30.3	16.8	22.1	15
Ce	33.8	44.2	50.6	54.7	80.2	67.6	43.9	26.9	55.8	63.5	37.3	47.6	30
Pr	3.9	5.1	6.1	6.4	9.1	7.1	5	3.1	6.2	7.4	4.8	5.8	3.22
Nd	16.2	19.5	22.9	25.1	31.5	24.9	19.5	12	23.7	29.4	20.2	22.9	10
Sm	3	3.5	4.3	4.8	6	4.1	3.8	3.2	4.4	6	4.6	4.7	1.7
Eu	1.06	1.23	1.46	1.28	1.2	1.99	1.12	1.07	1.23	1.39	1.5	1.33	1.1
Gd	3.1	3.6	4.5	4.6	6.3	5	4.3	4.1	4.5	6.2	5	5.2	2.8
Tb	0.4	0.4	0.6	0.6	0.8	0.7	0.6	0.7	0.6	0.8	0.7	0.8	0.35
Dy	2.2	2.6	3	3.2	4.8	3.6	3.3	4.4	3.4	4.9	4	4.4	1.55
Ho	0.41	0.48	0.61	0.54	0.93	0.72	0.71	0.88	0.65	0.95	0.77	0.85	0.35
Er	1.2	1.4	1.7	1.5	2.7	2.2	2	2.5	2	2.7	2.4	2.5	0.96
Tm	0.2	0.2	0.2	0.2	0.4	0.3	0.3	0.3	0.3	0.4	0.3	0.3	0.18
Yb	1.2	1.3	1.5	1.4	2.8	2.2	1.9	2.2	1.9	2.4	2.1	2.3	0.93
Lu	0.2	0.2	0.24	0.22	0.42	0.36	0.3	0.3	0.32	0.35	0.27	0.34	0.2
REE	84.27	105.81	123.11	132.84	187.75	158.07	109.33	76.15	134	156.69	100.74	121.12	68.34
$(La/Yb)_N$	9.80	11.49	11.44	13.66	9.80	11.46	8.04	4.45	10.31	8.53	5.41	6.49	10.90
$(La/Lu)_N$	9.03	11.47	10.99	13.35	10.04	10.76	7.82	5.02	9.41	8.99	6.46	6.75	7.79
Eu/Eu*	1.20	1.20	1.14	0.98	0.67	1.40	0.92	0.92	0.96	0.79	1.06	0.90	1.38
Rb	97	81	104	131	154	19	99	362	83	104	24	75	150
Sr	475	507	541	465	306	997	352	141	422	415	575	442	285
Ba	875	950	1120	626	884	184	755	1000	752	890	545	772	1262
Zr	122	131	154	155	150	154	159	157	111	177	140	165	106
Y	13	14	17	14	26	18	19	27	18	24	18	24	9
U	4.7	4.2	3.1	2.1	4.8	13.9	4.9	3.2	3.6	3	0.6	3	3.8
Th	7.3	8.1	9	7.1	29.4	15.6	15.9	8.3	12.1	13.3	0.1	8.4	6.9
Hf	3	3	4	4	5	4	4	4	3	5	3	4	4
Nb	5	7	7	6	9	8	8	5	7	8	5	8	6

Concentration in ppm

X 1.5 of Taylor and McLennan (1993). Light rare earths show an enrichment of light REE of about 50-70 times chondritic composition, with ratios of $(La/Lu)_{CN}$ = 6.4-13 and $Ce/Yb)_{CN}$ = 4.6-10, and total REE contents of 84-134 ppm. Alamos batholith (Kgd), quartz-monzodiorite (Tqd), and biotite-Hornblende granodiorite dikes show a very small negative Eu anomaly (Fig. 30).

The REE patterns show that the Piedras Verdes intrusive sequence did not differentiated from the batholith (Kgd in the Piedras Verdes deposit). This conclusion is based in that the latter contains lower LREE and HREE contents than the Tertiary quartz-monzodiorite, which is more mafic than the batholith.

The REE patterns of the quartz monzodiorite to porphyry suite show the differentiation trend of the Piedras Verdes intrusive suite (Fig. 31). These patterns show that the REE contents decrease in subsequent more felsic phases and that the Lu/La ratios increase systematically. $(La/Yb)_{CN}$ of the Piedras Verdes intrusive suite, (6.5 and 11.5), are similar to those of the Cortez terrane (6.4 to 14.8), but different to the Guerrero terrane (4.3 and 11.6). However, Piedras Verdes exibit non-pronunced Eu anomalies more akin to the Guerrero terrane (Valencia et all.,1999).

Neodymium isotopic data

The four main intrusive rocks of the Piedras verdes magmatic suite were analyzed for Nd. These rocks are: Tertiary quartz-diorite (Tqd), Tertiary "tall"-biotite granodiorite porphyry (Tgdptb), Tertiary quartz-feldspar porphyry (Tqfp), and Tertiary biotite-

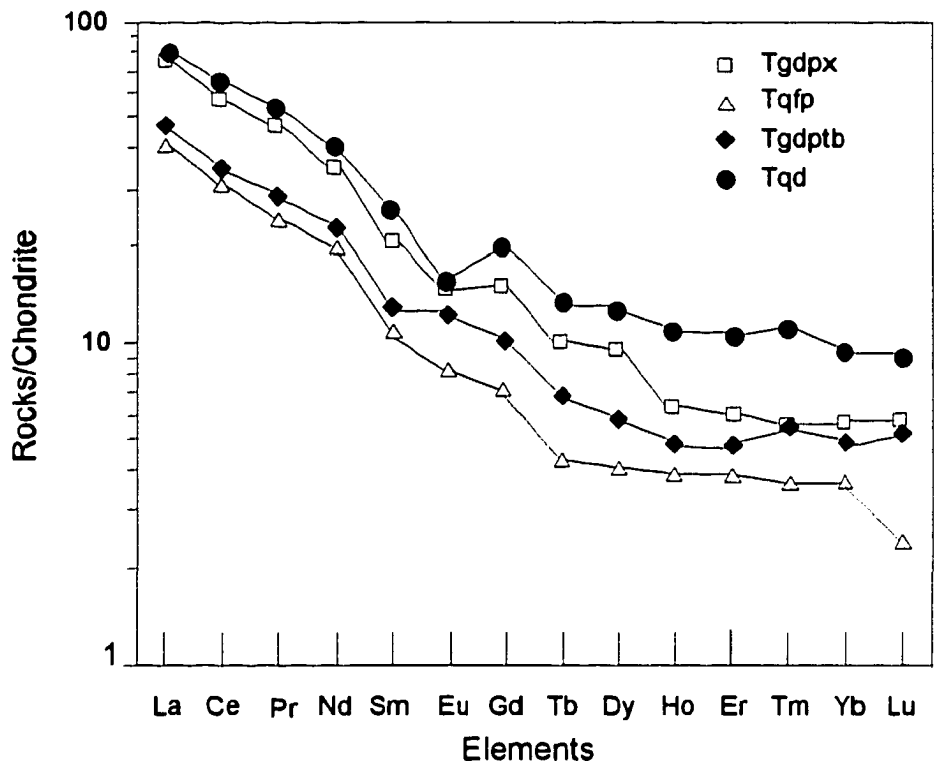

Fig.31. REE patterns of the four main porphyries of Piedras Verdes deposit, showing the crystallization trend from Tqd to Tqfp. Note a negative correlation of Si to REE content. Only the Tqd shows small Eu anomaly. Tgdpx being the younger rocks, show higher REE contents than the Tgdptb and Tqfp, indicating other magmatic event.

hornblende porphyry dikes (Tgdpx). The Nd analyses were performed at the University of Arizona. Analytical techniques are discussed in Patchett and Ruiz (1987). The results are presented in Table 3. Although there is little variation, neodymium isotopic data suggest a progression from less to more evolved signatures, for the quartz monzodiorite, "tall" biotite and quartz-feldspar porphyry (–2.59, -2.87 and –3.82 respectively). The initial neodymium value for the younger biotite-hornblende dike was –2.09, which does not conform to the same evolutionary trend (Fig. 24). The Figure 24 was generated from K/Ar ages for Tqd and Tgdptb and supplemented with relative cross-cutting relations for Tgdpx and Tqfp. The epsilon neodymium values versus age and $^{143}Nd/^{144}Nd$ ratios diagrams show that the Tgdpx does not appear to have originated from the same source area as the porphyry suite (Figs. 32 and 33). The initial epsilon neodymium data is in agreement whit the magmatic sequence derived from field relations, major, trace and REE element results. Negative epsilon neodymium values for the Piedras Verdes main phases also indicate that these rocks could have originated from a mixture of primitive sources with a modest component of continental crust.

The ENd initial values from the Piedras Verdes intrusive sequence corresponds to the ENd initial values of the granitic rocks from the Cortez terrane, that have values around –4 in central and eastern Sonora. In contrast, ENd initial values for granites of the Guerrero terrane are positive (Valencia et al., 1999). Therefore the Piedras Verdes porphyries have higher crustal contamination component than the positive values obtained from the Guerrero terrane. Thus, like the major, trace and REE elements

indicate, also the End values place the Piedras Verdes intrusive sequence within the Cortez terrane. The epsilon neodymium values plotted together with values of other igneous rocks of Arizona and Chile, show that the Piedras Verdes intrusive rocks, fall in the Arizona Laramide andesite-dacite type intrusions (Fig. 34: data from Titley, 1988: Lang, 1991).

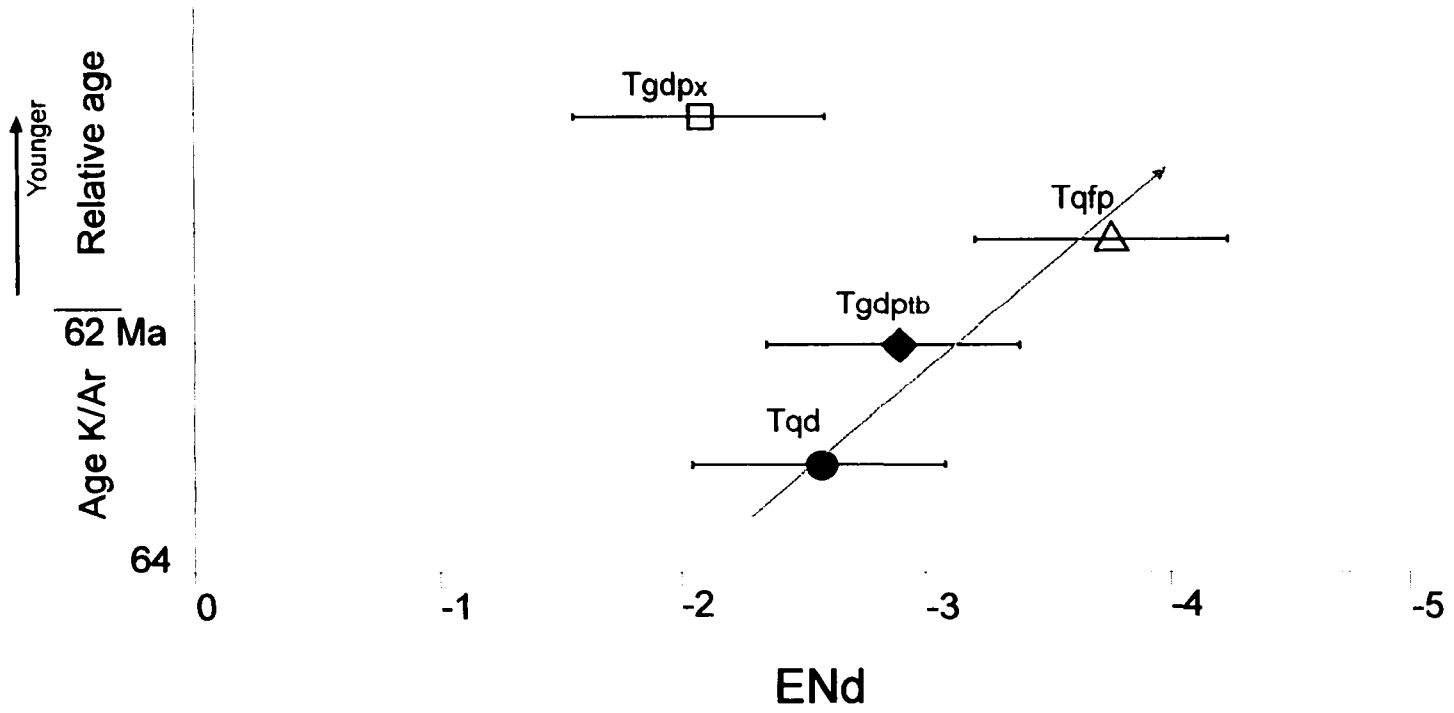

Fig.32. Iinitial ENd versus age diagram, showing the evolution path of the main porphyry phases of the Piedras Verdes deposit. K / Ar ages for Tqd and Tgdptb and relative age for Tqfp and Tgdpx (based in crosscutting evidences). Note that Tgdpx could be originated from remelting of the magma source of Tqd. Horizontal lines = error of +/- 0.5.

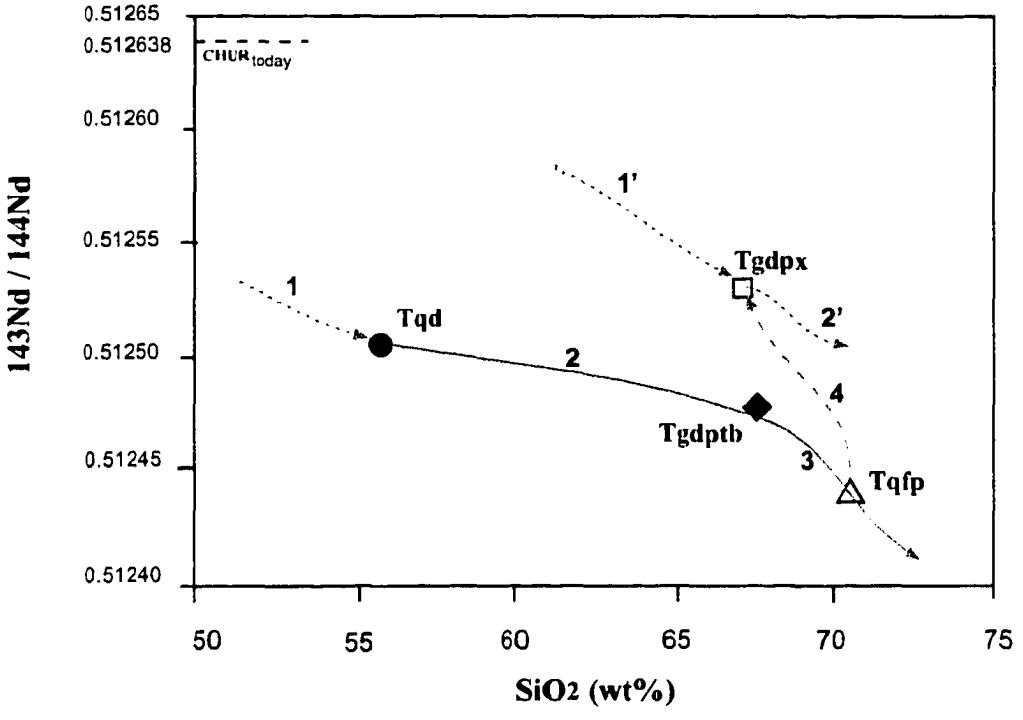

Fig. 33. SiO2 versus 143Nd / 144Nd. Showing the evolution path of the four main porphyries of the Piedras Verdes intrusive suite. Note Tgdpx dikes had a less evolved parent magma indicated by their higher 143Nd / 144Nd ratio. The dashed line 4 was drew just to show that the Tgdpx dikes were formed after crystallization of the Tqfp. This line has not any other meaning. The 1 to 3 line shows the possible evolution from the Tqd to Tqfp and the 1' to 2' dashed line the probable evolution path for the Tgdpx dikes.

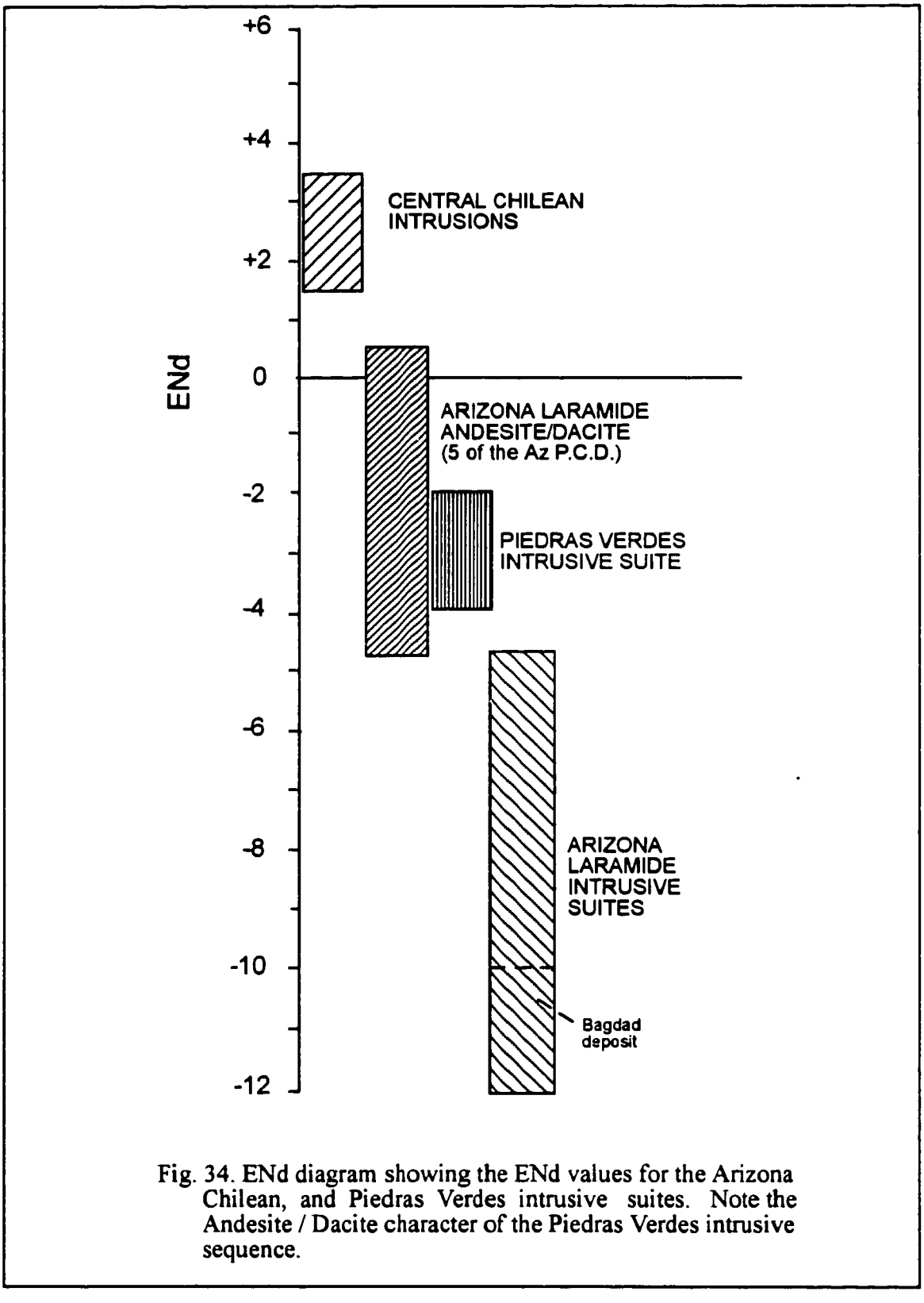

Fig. 34. ENd diagram showing the ENd values for the Arizona Chilean, and Piedras Verdes intrusive suites. Note the Andesite / Dacite character of the Piedras Verdes intrusive sequence.

TABLE 3. WHOLE ROCK Sm-Nd DATA OF PIEDRAS VERDES MAIN INTRUSIVE PHASES

Sample	Litology	Age (Ma)	Sm (ppm)	Nd (ppm)	147Sm/144Nd	143Nd/144Nd measured (b)	Nd present (e, c)	Nd initial (e, c)
Tgdpx	Biotite-hornblende Gd porphyry	ND	5.1817	19.5767	0.160018	0.512531	-1.8	-2.09
Tqfp	Quartz-feldspar porphyry	ND	1.8	8.42	0.129473	0.512442	-3.29	-3.82
$Tgdp_{tb}$	Tall biotite granodiorite porphyry	62.2	2.4888	13.2063	0.113928	0.512491	-2.22	-2.87
Tqd	Quartz diorite-quartz monzodio.	61.7	5.1978	26.3633	0.119192	0.512505	-1.98	-2.59

aUncertainties at 2-sigma are + 0.5%

bRatios normalized to $^{146}Nd/^{144}Nd = 0.7219$ (2-sigma errors reflected in-run precision)

e,c$Nd=10^4 [(^{143}Nd/^{144}Nd(t)CHUR) - 1)]$, using $^{143}Nd/^{144}Nd = 0.512638$ as present day CHUR value, and $^{147}Sm/^{144}NdCHUR = 0.1966$

GEOLOGIC HISTORY OF PIEDRAS VERDES DEPOSIT

Six representative phases of the Piedras Verdes intrusive complex were recognized. Interpretation of their petrological, geochemical, and Nd isotopic data, and crosscutting relationships observed from mapping and core logging, indicates that not all of these intrusive phases originated from the same parent magma. A schematic geologic history of Piedras Verdes deposit is presented in figure 35.

During Paleozoic to early Mesozoic time a sedimentary sequence was deposited in a marginal oceanic environment, that correlates with the deeper (eugeoclinal) rocks deposited outboard of the North American continent (Fig 35a). These eugeoclinal rocks are present in the Cortez terrane, which was originally proposed by Coney and Campa (1987). The eugeoclinal strata deposits of the Cortez terrane were accreted to the shallow-water (miogeocline) rocks of the Caborca terrane and North American continent during the Late Permian to Middle Triassic Sonoran Orogeny, which was produced by north-northwest directed compression (Poole and Madrid, 1990). Although no exposures of Paleozoic rocks have been positively identified in the Piedras Verdes region, King (1939), proposed that a deformed sedimentary sequence which crops out in the vicinity of Presa Mocuzari may be of this age.

During the Late Triassic to Early Jurassic continental clastic and shallow-marine sediments of the Barranca Group, were unconformably deposited in a rift-related basin upon the Paleozoic-early Mesozoic eugeoclinal rocks (Stewart and Roldan

Quintana, 1991) (Fig. 35b). These pull-apart basins may have formed by transtensional faulting within a zone of left-lateral faults that are the precursors (Pindell, 1985) of possible left-lateral faults such as the Mojave-Sonora Megashear in Northern Mexico (Silver and Anderson, 1974). The transtensional regime is associated to the separation of the North America from Gondwana in the Early Jurassic (Pindell, 1985; Stewart, 1988). The meta-sedimentary sequence at Piedras verdes is similar to the Barranca Group, constituted by quartzite, arkose, siltstone, shales, and mudstones. Nevertheless no fossils have been identified to establish its age unequivocally. The presence of graphite at San Bernardo area, located 20 km northeast from Piedras Verdes, was the basis for correlation with the Barranca Fm by King (1939).

During the Middle Jurassic-Late Cretaceous, Nevadan Orogeny, the region was affected by faulting, metamorphism and folding. East-west oriented fold axes in El Fuerte region, 30 km South of Piedras Verdes, indicate a north-south to northeast-southwest compression event (Mullan, 1978). The meta-sedimentary sequence has been affected by regional metamorphism and deformation, akin to this event. Therefore, the meta-sedimentary sequence at Piedras Verdes could be as old as upper Paleozoic (Mullan 1978).

During the Late Cretaceous Laramide Orogeny (Coney, 1977), characterized by a great production of voluminous and continuous plutonism of cal-alkaline composition, the Sinaloa-Sonora Batholith was emplaced. It was part of a well developed volcano-plutonic arc, which is notably broad and well exposed along the central western Pacific

margin of Mexico. This magmatic arc resulted from the subduction of the Farallon plate under the western margin of North America. One of its phases, locally named Alamos Batholith (Kgd) occurs as the oldest magmatic event at Piedras Verdes. The intrusion of this granodioritic batholith (Kgd) produced broad contact metamorphic halos and small skarns, which developed mostly in limy units of the Paleozoic rocks (Fig 35c). At Piedras Verdes, biotite-plagioclase hornfels and localized skarn were generated near the contacts with siltstone-mudstone units.

In Early Tertiary-Eocene time, late stage continental intrusive complexes were emplaced at shallow depths along east-northeast to east-west trending shear zones. One such intrusive suite and shear zone are present at Piedras Verdes. This shear zone is believed to have formed in response to northeast-directed regional compression during Laramide time. Pre-shear regional faults appear to have been partially reactivated and re-oriented. At Piedras Verdes, the western and central parts of the shear zone are intruded by a quartz monzodiorite stock (Tqd) (Fig 35d). The parent source of this rock (Tqd) has not been recognized in the area. Nevertheless geochemical reults indicate that it could not have differentiated from the granodiorite batholith. Contact metamorphic effects associated with the Early Tertiary granitoid intrusions are superimposed on regional metamorphism. The quartz monzodiorite-quartz diorite phase (Tqd) generated small iron skarns and veinlets with subordinate copper.

Following at least, partial consolidation the quartz monzodiorite phases were intruded by small dikes and "fingers" of biotite granodiorite porphyry (Tgdp) (Fig. 35e),

which in aggregated formed the core of the Piedras Verdes intrusive complex. Geochemical results and age relationships show that the subsequent granodiorite porphyry phase (Tgdp), fractionated from the quartz monzodiorite. This porphyry phase (Tgdp) includes the "tall' biotite granodiorite porphyry (Tgdptb) of 62 Ma in age, which forms the central part of this dike-like granodiorite porphyry. It also includes the equigranular feldspar-granodiorite, that forms chiefly the contact between the "tall" biotite granodiorite and the meta-sedimentary units, possibly being the "chilled" margin of the 'tall" biotite granodiorite intrusion. It intruded as an elongated body into the shear zone, generating intrusive breccia on its margins. The first alteration and associated low-grade copper and molybdenite mineralization were introduced during this event.

A quartz-feldspar porphyry phase (tqfp) fractionated shortly after the emplacement of the granodiorite porphyry (Fig. 35f). It is believed that the emplacement of this stock was controlled by the intersection of the NW and NNE striking faults in the central-eastern part of the deposit. A second event of pyrite-molybdenite and minor chalcopyrite mineralization was associated with this porphyry phase. Some of the previous copper mineralization may have been remobilized by the more sulfidized fluids of the quartz-feldspar porphyry intrusion.

Hornblende-biotite porphyry dikes (Tgdpx) were intruded after the emplacement of the quartz-feldspar porphyry (Fig. 35g). Geochemical results suggest that these dikes were generated by a less evolved magma source than the magma that produced the former porphyry phases, which tapped progressively deeper and more primitive sources

as an effect of continuous uplift. They show copper mineralization that was remobilized from the core of the system.

The latest intrusive event at Piedras Verdes is indicated by the emplacement of thin andesitic to trachiandesitic dikes. They have a K/Ar age of 48.4 ± 1.2 Ma. They could be the initial magmatic pulses that led to the formation of the Tertiary andesitic volcanism in the region (Wisser, 1966; Vazquez, 1975). Vazquez, op cit., describes a porphyritic andesitic stock of Early Tertiary age, wich crops out in the central part of the Sierra de Alamos cutting the granodirite batholith. He also, recognized andesitic dikes striking N20-40°W associated with the andesitic stock. Similar attitude and age of these andesitic dikes to those of Piedras Verdes area, probably, indicate a same time of emplacement for these rocks.

These andesitic dikes that are affected by clay alteration along fractures, suggest that the first enrichment event is Middle Eocene in age (Fig. 35h). Erosion, volcanism and renewed uplift, associated to the Oligocene-Miocene Sierra Madre Occidental orogenic event, may have caused renewed downward migration of the enrichment blanket. Oxidation, leaching and faulting in part channeled and disrupted supergene mineralization to high permeability zones (Fig. 35i).

Isolated patches of copper-oxide zones within the leached cap represent relict chalcocite blankets. Eruption of volcanic sequences around the deposit area and possibly over the deposit occurred during some of the faulting, but largely preceded the late Tertiary extensional faulting. These volcanic units have been stripped by erosion at

Piedras Verdes, but may have played an important role in the preservation of supergene enrichment.

EXPLANATION

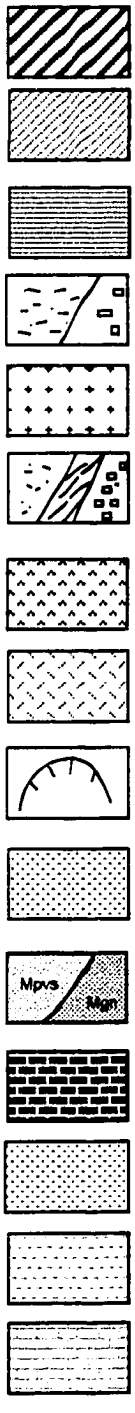

Explanation for the figure 35 (next page).

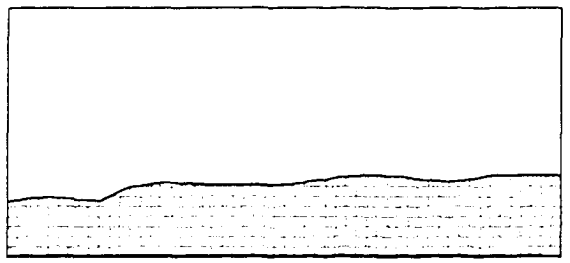

a

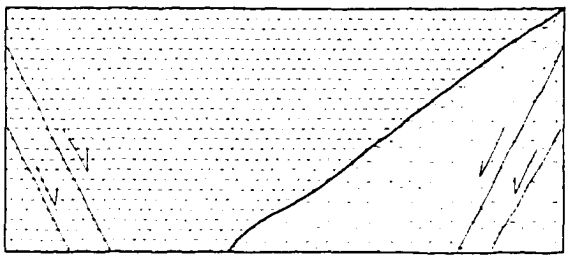

b

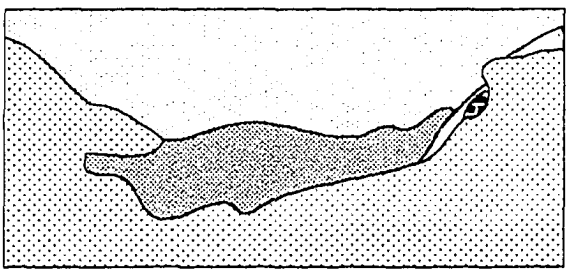

c

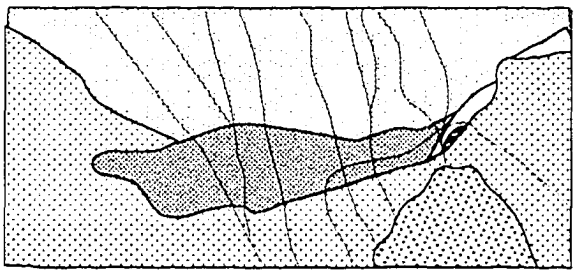

d

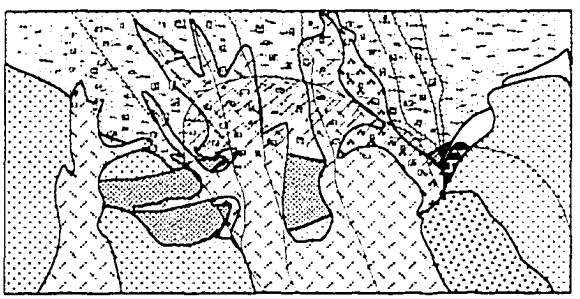

e

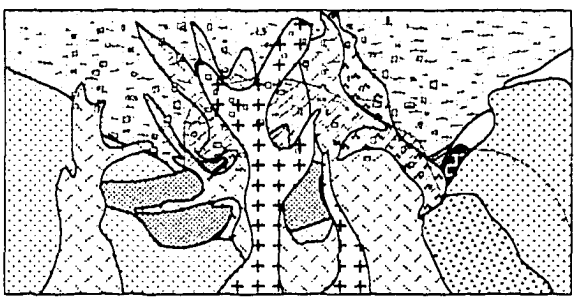

f

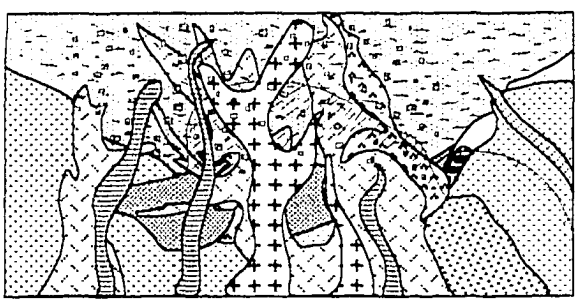

g

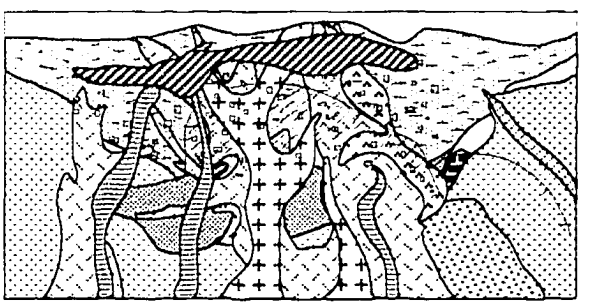

h

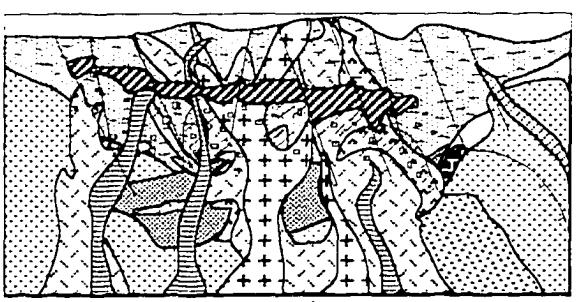

i

RE-OS ISOTOPIC STUDY

The Re-Os isotopic system has become an important tool in the study of ore deposits because it has the potential of directly dating the mineralization instead of associated alteration or magmatic rocks, and of constraining the source of the ore-forming elements (McCandless,1993). Rhenium and osmium are chalcophile elements and therefore concentrated in sulfides.

The source of the ore-forming elements can be constrained because Re is highly incompatible in the mantle relative to Os. The result of this beheivor is that the mantle has evolved to much less radiogenic $^{187}Os/^{188}Os$ ratios than the crust. The main assumption is that Os behaves like Cu.

By measuring the amount of rhenium and osmium within a sample, the age of mineralization can be calculated. Samples need to be examined for alteration before they are run to be sure of the results obtained, as there are no internal checks on the date acquired (McCandless et al., 1993).

As the crust and mantle have been characterized with respect to osmium ratios (Allegre and Luck, 1980, Martin et al., 1991), comparisons can be made between the initial $^{187}Os/^{188}Os$ of porphyry copper-sulfide mineralization to mantle and crustal values. This comparison can then lead to hypotheses regarding the ultimate origin of the copper, as osmium is considered a sensitive tracer of crustal mixing (Johnson et al., 1997).

This chapter attempts to date mineralization of the Piedras Verdes system, and constrain the sources of copper by using molydenite and sulfides samples.

Molybdenite results

Re geochronology of molybdenite was attempted for Piedras Verdes. The Re-Os analyses were performed at the University of Arizona. Analytical techniques are discussed in Martin et al., 1999 and Ruiz and Martin, 1999. Four samples of molybdenite veins from drill core (Table 4) were analyzed by electron microprobe and XRD in order to determine if the molybdenites were suitable for dating or had evidence of alteration which would alter the original Re concentration by either Re loss or gain (McCandless et al., 1993). The electromicroprobe elemental maps for Re show that the molybdenites are altered and that a Re-rich silicate coexists with the samples (Figs.37,38,39). Thus the samples were suspect before the Re-Os analyses were done. The molybdenite samples from Piedras Verdes have Re concentrations that range from 57 to 135 ppm. All of the samples yielded unreasonably old ages around 80 Ma (Table 4). The old ages are probably the result of Re loss due to the hydrothermal alteration in the Piedras Verdes system. Another sample from Suaqui Verde, which is a nearby project with similar style of mineralization than Piedras Verdes, contains molybdenite without clear alteration signs, higher Re content (ca. 490 ppm) and yields a more reasonable age, based on tectonic interpretations of ca. 60 Ma (Fig. 40).

Pyrite and Chalcopyrite results

Re and Os values were also obtained for pyrite and chalcopyrite samples from the deposit. Re concentrations range from 0.8 to13 ppb. Because of the low Re content in the sulfide samples, no age was obtained for them. It is assumed, like the molybdenite samples, that the sulfides suffered Re loss during alteration after primary mineralization.

Table 4. Re-Os DATA ON MOLYBDENITE

Sample	Re(ppm)	$^{187}Os/^{190}Os$	Os %1sigma	$^{187}Re/^{185}Re$	Re %1sigma	%radiogenic Os	Age my(+/-.5%2sigma)
PV1	116.19	0.976125	0.0095	0.12484	0.0559	99.75	78.382
PV2	134.37	0.48907	0.0047	0.0796	0.0107	97.72	78.716
PV3	57.761	0.247236	0.0351	0.06344	0.3913	100.46	79.812
SV1	488.85	1.122324	0.0033	0.1966	0.0365	100.12	60.3

PV1 = PV-DH-96-22: 156.50m depth
PV2 = PV-DH-96-23: 280m depth
PV3 = PV-DH-96-22: 161.30m depth
SV1 = Surface; hand sample.

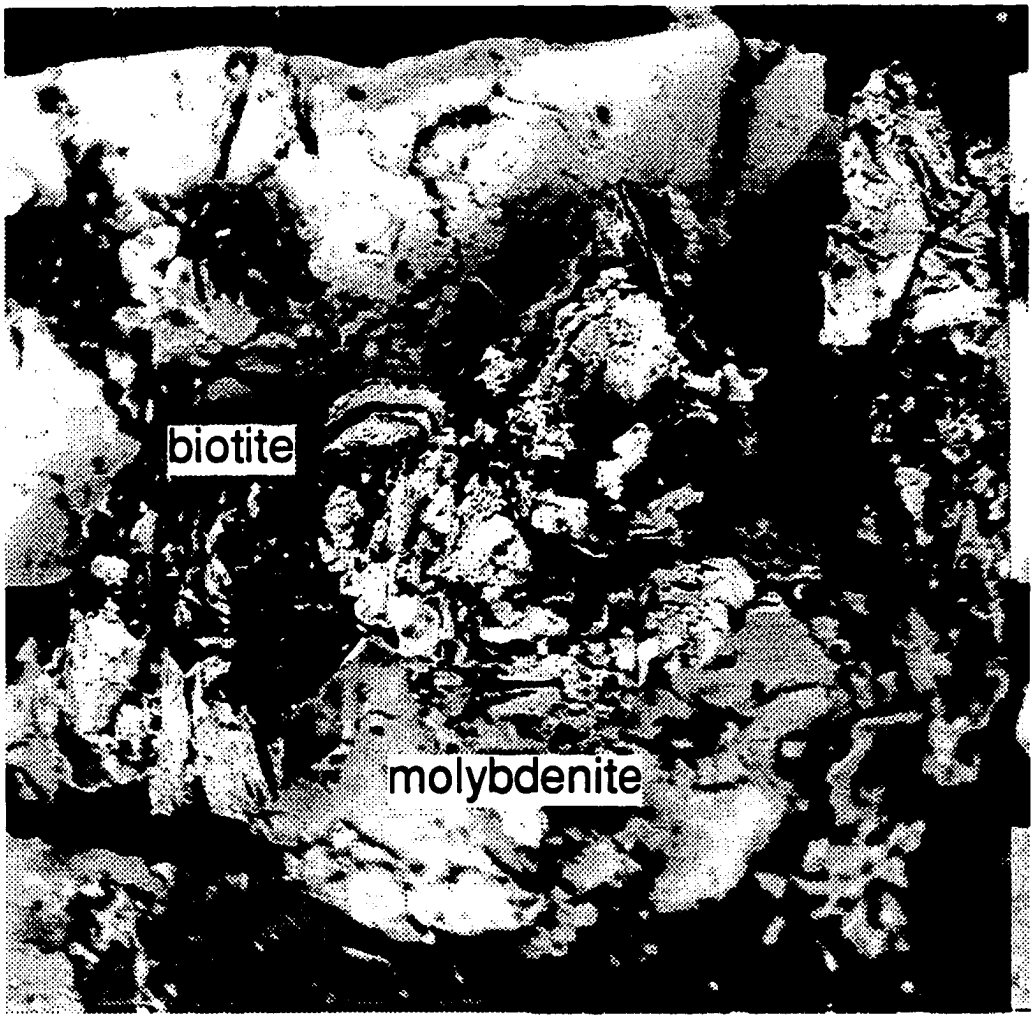

Figure 36. Sample PV1. Molybdenite with hydrothermal biotite. Note the intimate association of the biotite and molybdenite. WOF= 1000 microns.

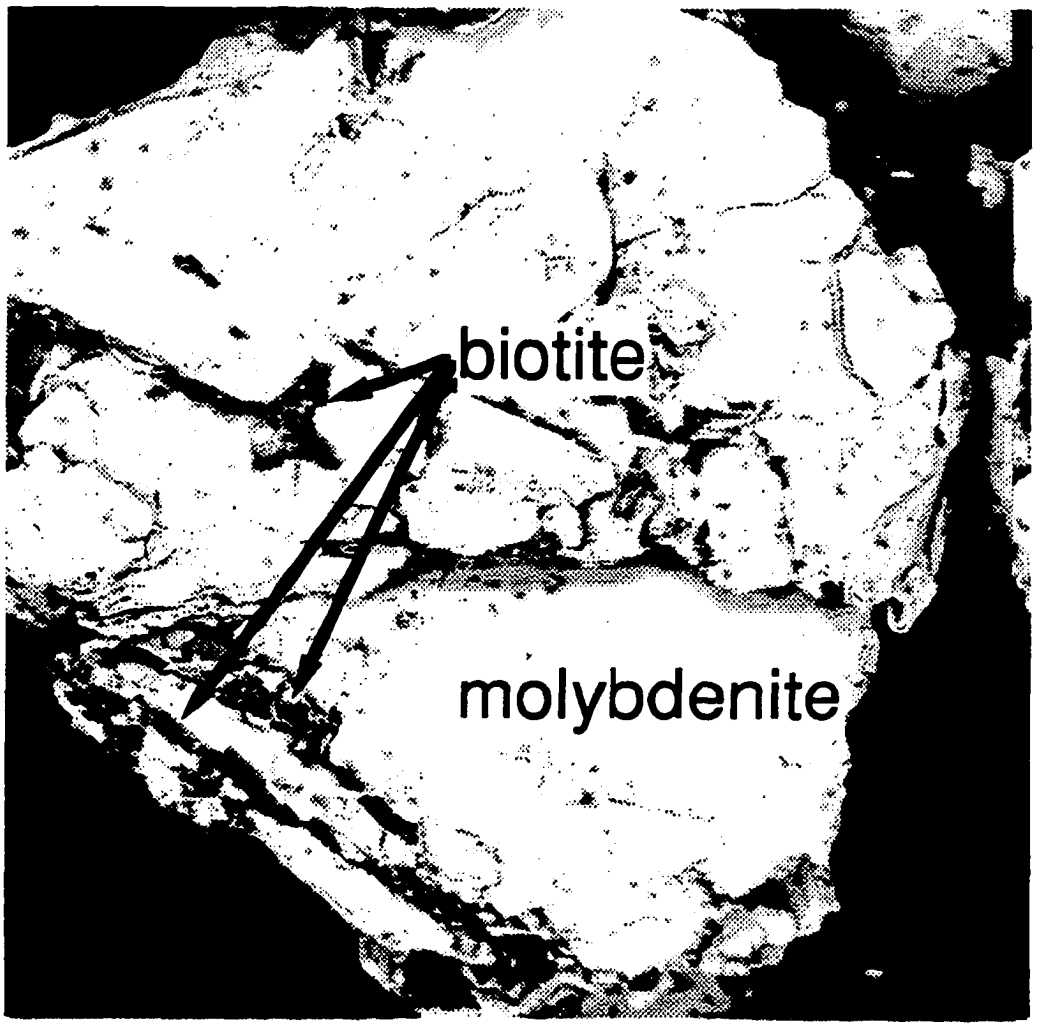

Figure 37. Sample PV2. Single molybdenite crystal, looking down on the (0001) surface. Note the apparent occurrence of hydrothermal biotite (arrows) parallel to the cleavage planes of the molybdenite. WOF = 1000 microns.

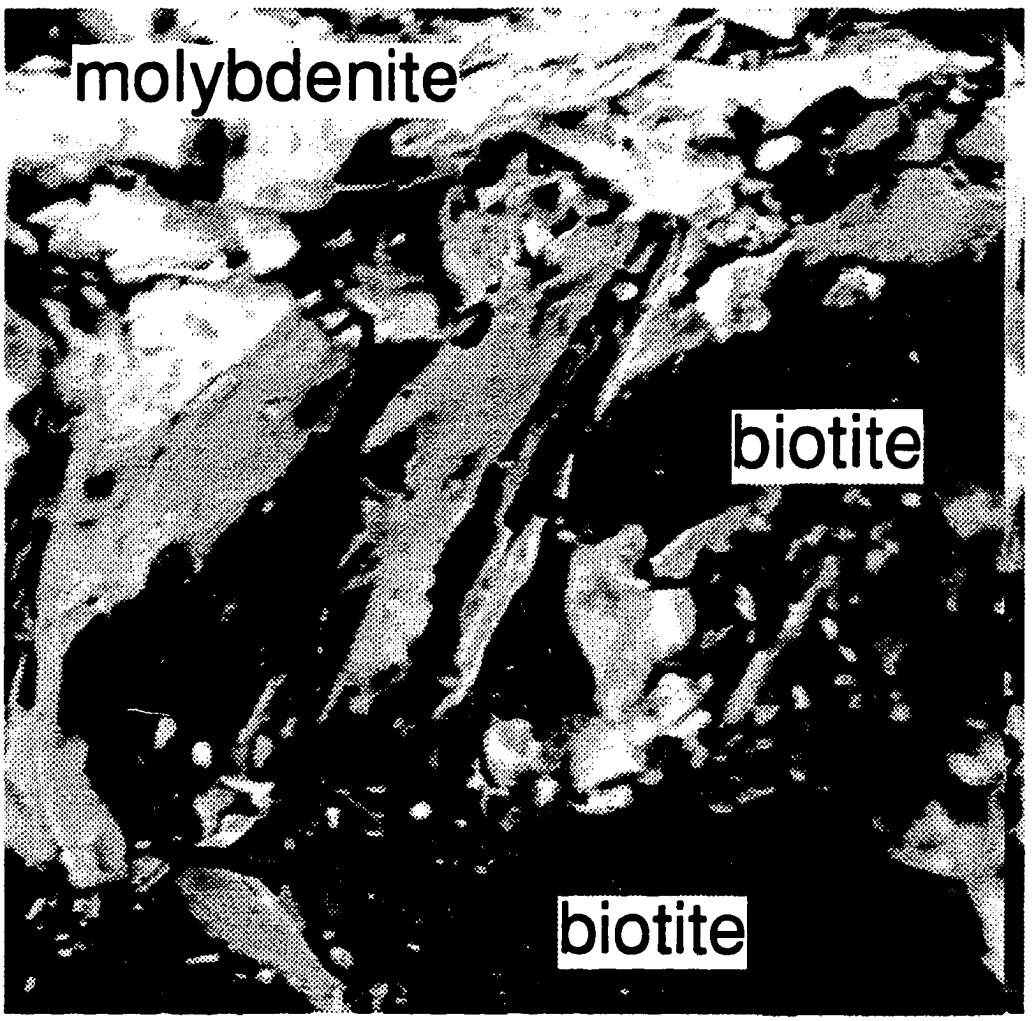

Figure 38. Sample PV3. Intimately intergrown association of molybdenite and biotite. Note that the hydrothermal biotite in the center of the image is clearly growing parallel with the cleavage planes of the molybdenite (arrow). WOF = 450 microns.

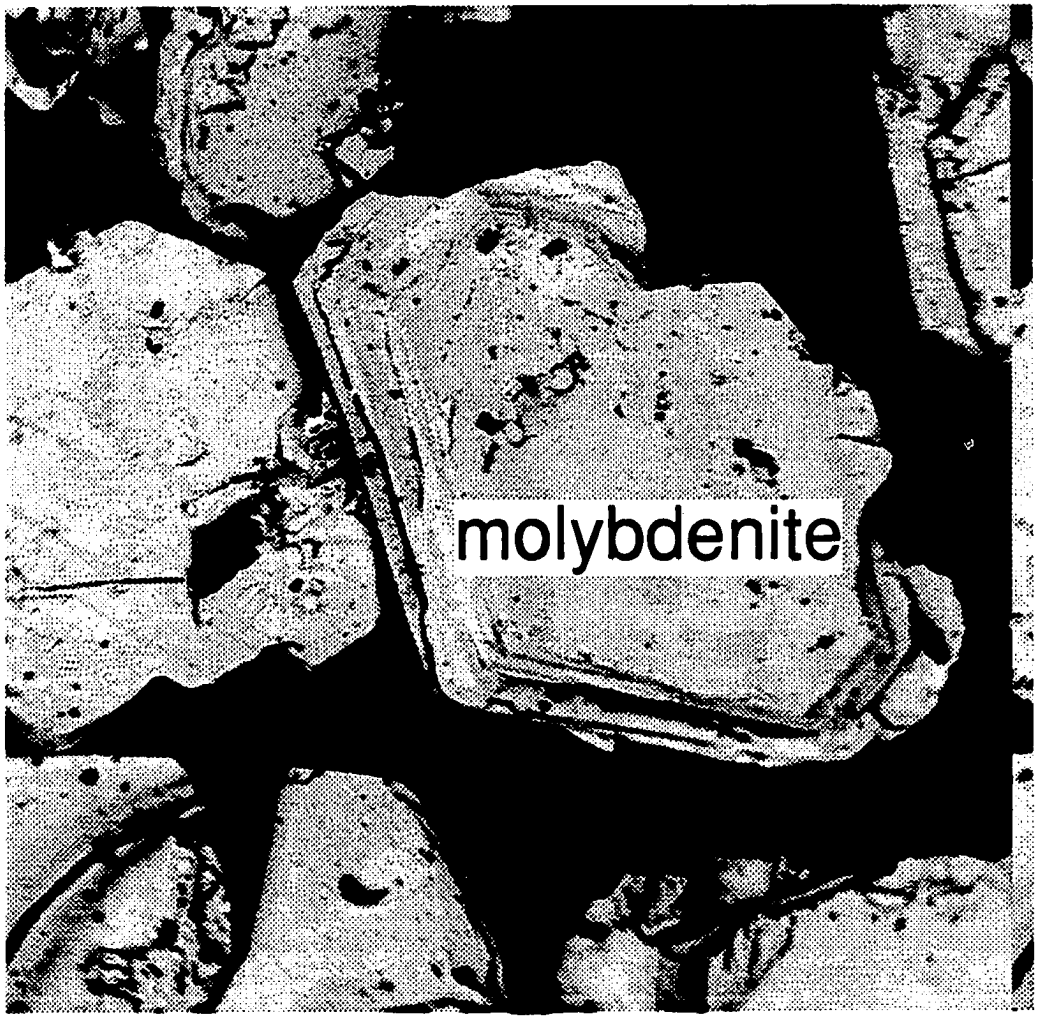

Figure 39 . Sample SV1. Euhedral molybdenite crystals from a single hand sample. The molybdenite crystals were disseminated in quartz-sericite altered rock from Suaqui Verde area. Note the clean, inclusion-free appearance of the molybdenite crystals. WOF = 1000 microns.

CONCLUSIONS

Piedras Verdes is a structurally controlled supergenic-enriched porphyry copper deposit. Isolated patches of low grade alternating with high grade copper zones as copper oxides, and with the remains of primary sulfides, indicate that multiple stages of supergene activity formed the chalcocite blanket of the Piedras Verdes deposit. Supergene minerals are a mixed assemblage dominated by chalcocite with subordinate covellite on hypogene chalcopyrite. The K/Ar age for andesite dikes, which have been affected by clay alteration, suggests that the first supergene cicle could be as older as Middle Eocene time, similar to those of America Southwest. Tertiary volcanic covers, up lift, erosion and strong faulting events enhanced the subsequent supergene cicles, since Middle Eocene to Recent time. The leached primary sulfides originated from two principal events of copper mineralization. They were associated with granodiorite and quartz-feldspar porphyries. The age of the first pulse of mineralization is constrained by the K/Ar age of 62 $\pm$ 1.6 Ma for the granodiorite porphyry related with this event of copper mineralization. This pulse introduced principally chalcopyrite-pyrite-molybdenite veinlets, intimately associated with secondary biotite. Shortly after the first pulse, the second event of copper mineralization, associated with a quartz-feldspar porphyry took place, introducing quartz-pyrite-molybdenite and minor chalcopyrite veins. Six representative phases of the Piedras Verdes intrusive complex were recognized. Interpretation of their petrological, geochemical, and neodimium isotopic data, and field relationships, indicates that the main four intrusive phases, which are: quartz monzodiorite to quartz diorite, "tall" biotite granodiorite, quartz-feldspar and hornblende-

biotite porphyries, were not fractionated from the Sinaloa-Sonora batholith. Neodimium isotope data, indicate that the Piedras Verdes intrusive suite formed by a mixture of primitive and crustal materials. Analytical results of major and trace element suggest that these intrusive rocks are arc related I type granitoids and range from quartz-monzodiorite to granodiorite in composition. Re-Os for molybdenite and sulfides were not consistent with the K/Ar age for the 'tall" biotite granodiorite porphyry associated with the first mineralizing pulse. A first interpretation of these unreasonably ages is that the molybdenite and sulfides suffered Re loss by alteration after primary mineralization. However, it is necessary to analyze more samples of these minerals in order to find non altered samples. At the time of the writing of this thesis, all the best samples of molybdenite and sulfides found in drill core were studied.

COMMENTS

Although in this study the metasedimentary sequence at Piedras Verdes was correlated with the metasedimentary units of the Barranca group, no any fossils were found to corroborate this assumption. However, the presence of, possibly, graphite in one of the samples, could be indication that graphite was present in the units of the Piedras Verdes sequence, similar to the graphite content in some units of the Barranca group. The correlation with the Barranca group was based on two relevant observations. A first one is that no rhyolitic beds were found within the Piedras Verdes metasedimentary sequence, as they were found in similar units in the Fuerte Formation of Paleozoic age in northern Sinaloa. The second one is that laterally variable deposits of the Piedras Verdes sequence reflects deposition chiefly by streams, similarly to the Barranca Group deposits of upper

Triassic age. However, Quintana et al., 1991, reports thin layers of tuff within the units of the Barranca Group, which has not been found at Piedras Verdes. Therefore detailed studies of the Piedras Verdes meta-sediments are necessary to define if they could be correlated with the Barranca Group or the Fuerte Formation or they are a different sedimentary sequence, which has not been reported until now. Therefore, the meta-sediments of the Piedras Verdes sequence could be as old as Paleozoic.

Structure mapping, in order to constrain the timing of the different faulting events and better understand the structural complexity of the Piedras Verdes area, is recommended. Dating of the Piedras Verdes porphyries by the Pb/Pb method to constrain the age of the mineralization of the Piedras Verdes deposit, is also recommended. Additionally, the possibility that the K/Ar age for the granodiorite porphyry related to the mineralization is reset by hydrothermal alteration could be known by using the Pb/Pb method, which is comparatively resistent to metamorphic and hydrothermal re-setting.

APPENDIX A

Metasedimentary units petrographic description

The following descriptions are a summary of a total petrographic studies of 257 thin sections performed by several geologists involved in the Piedras Verdes Project. These are very general descriptions. Nevertheless, locally numerous variations in mineral content and textures, due to the strong hydrothermal alteration associated with the mineralization, exist in the Piedras Verdes meta-sediments.

Arkose: It was not described in thin section. It is limited in aerial extent but form bold outcrops. It is constituted mainly by feldspar and quartz.

Quartzite: These rocks present a fine to medium grained granoblastic texture with a clay-hematitic matrix. They are constituted by 70 to 90%, polygonal unstrained quartz, most grains from 0.3 to 1.5 mm in size; 30% K feldspar maximum, secondary?, minor to 1 mm in size, mainly as interestitial to quartz grains, and very irregular patchy distribution; in some places 100% anhedral quartz grains, 5 mm in size. Very few larger quartz grains show strain. < 2% disseminated pyrite when it is present. Minor sericite along fractures. Not or very weak foliated.

Chlorite/biotite silstone: these units are constitued by 20 to 90% quartz, 0.1-0.6 mm grains, in irregular streaks; 15% K feldspar; very fine grained (< 0.25 mm) biotite unoriented flakes; 4-5% fine grained chlorite. In some of the thin sections this rock shows 2% corroded pyrite, and some times very fine grained (<0.1 mm) sericite with maximum of 25% contained. Calcite <2% in fractures. They show not preferred mineral

orientation.

Mudstone: The mudstone is a downward continuation of the silstone unit, but with a minor grained size and preferred orientation of the minerals. Extremely fine grained (< 20-50 um) sericite>quartz. Few very fine grains of disseminated pyrite. In one thin section; 60% quartz, 40% sericite, < 4% pyrite.

Biotite to sericite/muscovite schist: these units show poorly to moderate developed foliation oblicue and parallel to banding, showing by sericite/muscovite – quartz-biotite irregular compositional bands. They are formed by 40 to 80% quartz (0.1-0.5 mm grains) some flattened/elongated; rutile neddles common; 5-10%, rarely 30% anhedral K feldspar (20-50 um to <0.1 mm) along quartz edges or disseminated within quartz crystalls; 5-20% biotite, mostly < 0.25 mm, interestitial to quartz; 10% muscovite; *sericite/muscovite schist*: 25-30% sericite/muscovite, sericite from 0.5 to 2 mm, occasionally >50% sericite from few-micron sericite size to 2 mm. This unit contains 2-4% disseminated fine grained to 0.5 mm anhedral pyrite.

Hornfels-Gneiss: Irregular mm scale (occacionaly cm) bands of quartz and biotite or quartz and muscovite dominant mineralogy. They varie from: *a*)quartz-biotite-sericite, *b*) quartz-biotite-muscovite, and *c*) quartz-muscovite-sericite gneissic units. *a*) 30-60% quartz, tipically 0.1 to 0.8 mm grains, polygonal with little or no strain, indistintic flattening fabric; 15-30% biotite, usually < 0.5 mm, pale reddish-brown color, in part may be altered to phlogopite; 25-40% sericite/clay surrounding and invading quartz streaks, and predominant within biotitic streaks, in parts associated with K feldspar; 2-4% rectangular to corroded pyrite. *b*) 40-50% quartz, polygonal, unstrained 0.1 to 0.6

mm grains; 10-15% unoriented biotite, 0.3- 0.6 (rarely) mm grains, in parts plogophite; 15-30% anhedral to 0.6 mm (rare 2 mm) muscovite flakes, not oriented; 5-15% very fine grained anhedral K feldspar, 25-30% fine grained sericite/muscovite groundmass. *c*) where 30-40% of the thin sections are irregular 1-4 cm bands of polygonal little strained quartz, and the rest of the section is 25-70% quartz, 30-75 sericite/muscovite bands-streaks or 70% sericite/muscovite and30% quartz, some with 10-20% 0.3 to 0.5 mm muscovite flakes .

The honrfels-gneissic unit includes a ***quartz-andalucite schist*** (hornfels) when they contain 10% andalucite as anhedral grains < 1 mm, occacionally > 40% very fine grained combained quartz-biotite-andalucite groundmass, 25-30% quartz, as irregular-discontinuous polycrystalline streaks, 10-30% K feldspar associated with quartz streaks, 15% biotite, 10%- rarely >50% muscovite as grounmass. Not prefered mineral orientation; and a ***quartz-tremolite schist*** (hornfels)*:* 30-35% quartz (<0.5 mm); 55-60% tremolite (<0.1 mm, some to 0.3 mm); 5-6% chloritized biotite (<0.25 mm); 3-4% epidote. 2% finely disseminated pyrite.

Table 5. LOCATION OF THE PIEDRAS VERDES INTRUSIVE UNITS USED FOR GEOCHEMICAL STUDY

Sample	Ubication	Lithology	Comments
And	698650E-3005940N	Andesite dikes	48.2+/- 1.6 Ma K/Ar age
Tgdpx	DH-97-130, 47m depth	Hornblende-biotite granodiorite dikes.	Post-mnt'n grd dikes
Tqfp	DH-96-24, 342m depth	Quartz-feldspar porphyry	Related to the 2nd Cu Mnt'n event
Tgdptb	DH-96-25,25m depth	Tall biotite granodiorite porphyry	Related to the 1rst Cu mnt'n evnt. Weak to very weak alt'n
GdBuffel	697175E-3005150N	Equigranular granodiorite	South limit of PV area
MDBuffel	697200E-3005200N	Fine-grained granodiorite	South limit of PV area
MDChato	694840E-3005645N	Qtz-monzodiorite to gd.	600m west of PV deposit
Tqd	DH-96-11, 66m depth	Quartz monzodiorite to quartz diorite.	Wpart of PVdeposit,sec N50^{0}E
Anddikes AlaBat	701150E-3002500N	Lamprophyre-Andesite	Dikes intruding the Alam batho.
Kgd (PV)	DH-96-04,300mdepth		Cretaceous gd batholith at Piedras Verdes area
AlamoBatho	701150E-3002500N	Granodiorite	Cretaceous gd batholith, over the Alamos-El Tabelo Road

TABLE 6. LOCATION AND CHARACTERISTICS OF THE SAMPLES USED FOR THE MINERAL PARAGENESIS STUDY. (They are samples that better represent the forms of the mineralization at Piedras Verdes deposit. However they were taken from a few drill holes and may not show all types of mineralization emplacemet of the all deposit).

Sample No.	Drill hole No.	Depth (m)	Section No.	Host rocks
PVPS-1	96-6	419	698,200 E	Mgn (Py-po vein)
PVPS-2	96-6	450	698,200 E	Mgn-Tgdp contact (Po)
PVPS-3	96-6	426	698,200 E	Mgn (Py-cp-po-Mo vein)
PVPS-4	96-16	310.90	696,300 E	Mgn (Py-cp-sph-bn vein)
PVPS-5	96-14	298	695,900 E	Mgn/Tgdp (Py>cp-bio v.)
PVPS-6	96-48	88-93	697,500 E	Mpvs/Mgn contact (Py-Cc)
PVPS-7	97-194	61	696,550 E	Tgdptb (Qtz-Mo vein)
PVPS-8	97-194	60	696,550 E	"
PVPS-9	97-194	62	696,550 E	"
PVPS-10	96-22	154	696,400 E	Mgn (Cp-py-Mo-bio vein)
PVPS-11	96-22	157	696,400 E	Mgn (Cp-py-Mo-bio vein)
PVPS-12	96-22	159	696,400 E	Mgn (cp-po-sph-Mo-bio v.)
PVPS-13	96-22	160	696,400 E	Mgn (Cp-py-sph-po-Mo v.)
PVPS-14	96-6	419	698,200 E	Mgn (Mt-cp-po-sph-Mo-py)
PVPS-15	96-22	161.30	696,400 E	Mgn "
PVPS-16	96-10	169.30	698,200 E	Mpvs close Tgdp(cp-cc-py)
PVPS-17	96-10	390	698,200 E	Mgn/Tgdp (py-cp-po v.)
PVPS-18	96-48	169	697,500 E	Tgdp (Py-cp-po-Mo vein)
PVPS-19	96-48	169	697,500 E	Tgdp (Py-po-cp vein)
PVPS-20	96-25	153.40	696,400 E	Tgdp (Py-mt-po-cp vein.)
PVPS-21	96-10	185	698,200 E	Mpvs /Tgdp (py-sph-cp-po)

REFERENCES

Allegre, J.C., and Luck, J.M., 1980, Osmium Isotopes as Petrogenic and Geologic Tracers: Earth Planetary Science Letters, v.48, p. 148-154.

Anderson, J.A., 1983, Characteristics of Leached Capping and Techniques of Appraisal: in Titley, S.R. ed., Advances in Geology of the Porphyry Copper Deposits, Southwestern North America, Arizona, p. 275-296.

Cardenas-Vargas, J., ed., 1993, Monografia Geologico-Minera del Estado de Sonora: Pachuca, Hidalgo, Mexico, Consejo de Recursos Minerales, 220 p.

Cojan, I., and Potter, P., 1991, Depositional environment, petrology, and provenance of the Santa Clara Formation, Upper Triassic Barranca Group, eastern Sonora, Mexico, in Perez-Segura, E. and Jacques-Ayala, C. eds.: Studies fo Sonoran Geology, Geological Society of America, Special Paper 254, p. 37-50.

Cox, K.G. and Bell, J.D., 1979, The Interpretation of Igneous Rocks, George Allen & Unwin Ltd, London, 450 pages.

Coney, P.J., 1977, Mesozoic-Cenosoic Cordilleran Plate Tectonics: Geological Society of America, Memori 152, p. 33-50.

Coney, P.J., 1983, Un Modelo Tectonico de Mexico y sus Relaciones con America del Norte, America del Sur y el Caribe: Revista del Instituto Mexicano del Petroleo, v.15, p. 6-15.

Cook, S.S., 1994, The Geologic History of Supergene Enrichment in the Porphyry Copper Deposits of Southwestern North America: University of Arizona Ph.D Thesis, Tucson, Arizona, 163 pages.

Cullers, R.L., and Graf, J.L., 1984, Rare Earth Elements in igneous Rocks of the Continental Crust: Intermediate and Silicic Rocks- Ore Petrogenesis, in Henderson, P. ed., Rare Earth Geochemistry, Elsevier Science Publishers B. V., p. 275-316.

Damon, P.E., Shafiqullah, M., and Clark, K.F., 1983, Geochronology of the Porphyry Copper Deposits and Related Mineralization of Mexico: Canadian Journal of Earth Sciences, v. 20, No. 6, p. 1052-1071.

Davis, G.H., and Reynolds, S.J. 1996, Structural Geology of Rocks and regions, John Wiley & Sons Inc., New York, 776 p.

Dreir, J.E., and Braun, E.R., 1995, Piedras Verdes, Sonora, Mexico: A Structurally Controlled Porphyry Copper Deposit: Arizona Geological Survey Digest, v. 20, p. 535- 543.

Faure, G., 1986, Principles of Isotope Geology, Second Edition, John Willey & Sons, In., 589 pages.

Hall, A., 1996, Igneous Petrology, Second Edition, Longman Group Limited, 551 pages.

Hawkesworth, C.J., and Van-Calsteren P.W.C., 1984, Radiogenic Isotopes-Some Geological Applications, in Henderson, P. ed., Rare Earth Geochemestry, Elsevier Science Publishers B. V., p. 375-421.

King, R.E., 1939, Geological Reconnaissance in Northern Sierra Madre Occidental of Mexico: Geological Society of America Bulletin, v. 50, p. 1625-1722.

Krauskopf, K.B., and Bird, D.K., 1995, Introduction to Geochemistry, Third edition, McGraw Hill, 647 pages.

Lang, J.R., 1995, Porphyry Copper-Gold Deposits Related to Alkalic Igneous Rocks in the Triassic-Jurassic Arc Terranes of British Columbia: Arizona Geological Survey Digest, v. 20, p. 219-236.

Maniar, P.D., and Piccoli, P.M., 1989, Tectonic Discrimination of Granitoids: Geological Society of America Bulletin, v. 101, p. 635-643.

McCandless, T.E., Ruiz, J., and Campbell, A.R., 1993, Rhenium Behavior in Molybdenite in Hypogene and Near-Surface environments: Implications for Re-Os geochemistry: Geochemica et Cosmochimica Acta, v. 57, p. 889-905

McCandless, T.E., and Ruiz, J., 1993, Rhenium-Osmium Evidence for Regional Mineralization in Southwestern North America: Science, v. 261, p. 1282-1286.

McCandless, T.E., 1994, Evaluation of the Molybdenite Rhenium-Osmium Geochronometer, and Its Implications to Base Metal Porphyry Mineralization: University of Arizona Ph.D Thesis, 92 pages.

Mullan, H.S., 1978, Evolution of Part of the Nevadan Orogen in Northwestern Mexico: Geological Society of America Bulletin, v. 89, p. 1175-1188.

Patchett, P.J., and Ruiz, J., 1987, Nd isotopic ages of crust formation and metamorphism in the Precambrian of eastern and southern Mexico: Contributions to Mineralogy and Petrology, v. 96, p.523-528.

Pearce, S.L., 1910, Piedras Verdes Disseminated-Copper Zone (Alamos District, Sonora, Mexico): Enginnering and Mining Journal, v. 89, p. 920.

Pearce, J.A., Harris, N.B.W., and Tindle, A.G., 1984, Trace Element Discrimination Diagrams for the Tectonic Interpretation of Granitic Rocks: Journal of Petrology, v. 25, p. 956-983.

Rollinson, H., 1993, Using geochemical data; evaluation, presentation, interpretation, Longman Group UK Limited, 352 pages.

Rosas, S.A., 1991, Gochico Mineral Deposit; Geology, Enviroment of Formation, and Tectonics, in Salas, G. P., ed., Economic Geology, Mexico: Boulder, Colorado, Geological Society of America, The Geology of North America, v P-3, p. 205-214.

Sillitoe, R.H., 1976, A Reconnaissance of the Mexican Porphyry Copper Belt: Institution of Mining and Metallurgy Transactions, section B-85, p. 170-189.

Stewart, J.H., and Roldan, Q.J., 1991, Upper Triassic Barranca Group; Nonmarine and Shallow-marine Rift-Basin deposits of Northwestern Mexico, in Perez-Segura, E. and Jacques-Ayala, C. eds.: Studies of Sonoran Geology, Geological Society of America, Special Paper 254, p. 19-36.

Stewart, J.H., 1992, Late Proterozoic and Paleozoic Southern Margin of North America in Northern Mexico, in Clark, K.F., Quintana, J.R., and Schmidt, R.H. eds., Geology and Mineral Resources of Northern Sierra Madre Occidental, Mexico, Guide book for the 1992 Field Conference: El Paso Geological Society, p. 291-299.

Titley, S.R., 1995, Geological Summary and Prespective of Porphyry Copper Deposits in Southwestern North America: Arizona Geological Survey Digest, v. 20, p. 6-20.

Valencia,-Moreno, M.A., et al., 1999, Geochemistry of Laramide Granitoids in NW Mexico, University of Arizona, Ph.D Thesis.

Vazquez-Perez, A., 1975, Economic Geology of the Alamos Mining District, Sonora, Mexico: University of Arizona Master's Thesis, Tucson, Arizona, 170 pages.

Whalen, J.B., 1990, The Topsails igneous suite, western Newfoundland; Fractionation and magma mixing in an "orogenic" A type granite suite, in Stein H.J. and Hannah, J.L. eds.: Ore Bearing Granite Systems; Petrogenesis and Mineralizing Processes: Geological Society of America, Special Paper 246, p. 287-289.